Vestigial Side Band Demultiplexing for High Spectral Efficiency WDM systems

by

Chidambaram Pavanasam

B.E (Electronics and Communications Engineering),

Anna University, Chennai, India, 2000

Submitted to the Department of Electrical Engineering and Computer Science and the Faculty of the Graduate School of the University of Kansas in partial fulfillment of the requirements for the degree of Master of Science.

_____

Professor in Charge

_____

Committee Members

_____

Date thesis accepted

Dedicated to my loving parents and brothers

Acknowledgements

I wish to express my sincere and heartfelt thanks to Dr. Kenneth Demarest, my faculty advisor and thesis committee chair, for his encouragement, guidance and support throughout the course of this thesis work. His suggestions and comments have been of great help for me in completing this work. I thank Dr. Ronqing Hui for his valuable suggestions during my research work and for serving on my committee. I would also like to thank Dr. Chris Allen for serving on my committee and for reviewing my thesis work. I am thankful to my team member Minnan Fei for her help during my research.

I would like to thank all my friends at KU who have made my stay here memorable and enjoyable.

I am especially thankful to my parents for their blessings, love and support throughout my life. I would also like to thank my brothers for their encouragement and support.

Abstract

The current emphasis on lightwave systems is on increasing the spectral efficiency of WDM systems. One of the techniques that is used for achieving high spectral efficiency in WDM systems is vestigial side band demultiplexing. This thesis reports the modeling and analysis of an experimental 40 Gbit/s WDM system, which used vestigial side band demultiplexing. The modeling and analysis is carried out using FiberSim, the fiber optic simulator developed at Information and Telecommunication Technology Center, University of Kansas. The 40 Gbit/s experimental WDM system used vestigial side band demultiplexing to achieve a spectral efficiency of 0.64 bit/s/Hz and 5 Tbit/s capacity over 1200 km of Teralight Ultra fiber. Simulations are performed to find the pump powers used in the experimental system and a fiber-EDFA equivalent for the Raman amplification used in the experimental system is also developed. Analyses on various optical parameters like channel launch power, dispersion compensation scheme etc is carried out to find their significance on the system performance.

In addition, a 10 Gbit/s WDM system using vestigial side band demultiplexing to achieve a spectral efficiency of 0.8 bit/s/Hz is designed and analyzed. This system uses standard SMF for transmission and achieves amplification using EDFA, as used in many legacy WDM systems. The design involves finding the optimal channel spacing scheme, demultiplexer optical filter parameters, channel launch power etc.

Table of contents

List of figures

List of tables

1.   Introduction

Over the years, many forms of communication systems have been developed. The basic motivation behind each development was either to improve the transmission fidelity, to increase the capacity, or to increase the transmission distance. The use of light for communication dates back to antiquity, when most civilizations used mirrors, fire beacons or smoke signals to convey single piece of information. The same idea was used till the end of eighteenth century through signaling lamps, flags and other semaphore devices. The effective bit rate of such systems was less than 1 bit/s.

A commonly used figure of merit for the communication systems is the bit rate-distance product BL, where B is the transmission bit rate and L is the transmission distance, which indicates the transmission capacity of the system. The advent of telegraphy in the 1830s replaced the use of light by electricity, where the bit rate could be increased to approximately 10 bit/s. The invention of telephone in 1876 brought a major change in the way electric signals were transmitted in analog form through a continuously varying electric current. The use of coaxial cable in place of wire pairs increased system capacity considerably. But the bandwidth of such systems was limited by the frequency dependent cable losses, which increased rapidly for frequencies beyond 10 MHz. This led to the

development of microwave communication systems in which an electromagnetic carrier wave with frequencies in the range of 1-10 GHz is used to transmit the signal by using suitable modulation techniques. Microwave communication systems generally allow for larger repeater spacing, but their bit rates are also limited by the carrier frequencies. By the second half of twentieth century it was realized that the transmission capacity could be increased by several orders of magnitude if optical waves were used as the carrier. Such systems are called the lightwave systems. Figure 1.1 shows the increase the transmission capacity over the last two centuries.
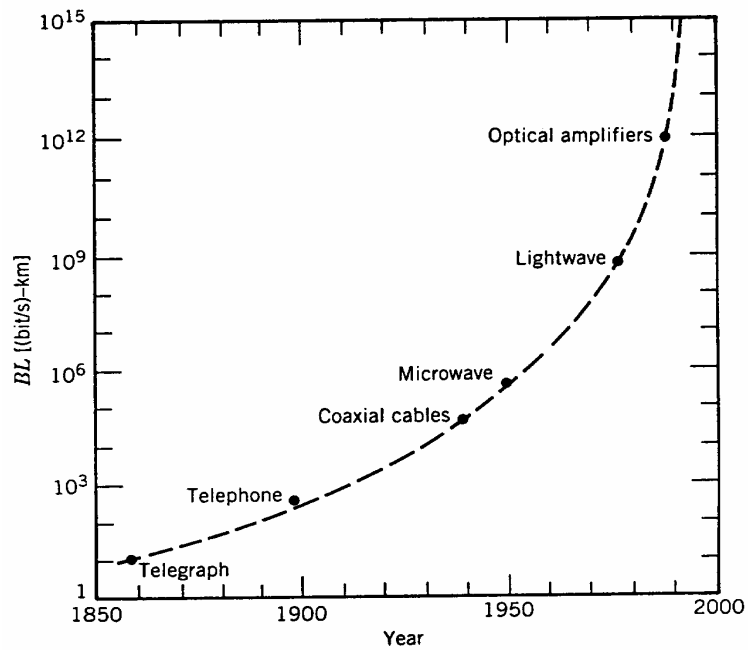
Figure 1.1: Increase in transmission capacity over the last two centuries [Ref. 1]

The first generation of lightwave systems operated near the 800 nm wavelength and used GaAs semiconductor lasers. They operated at bit rates of 45 Mbit/s and allowed repeater spacing of up to 10 km. By the 1970s it was found that operating in the 1300 nm wavelength region, in which fiber has lower loss (less than 1 dB/km) and minimum dispersion, could increase repeater spacing. Also, the introduction of single-mode fibers led to increase in bit rates, which were earlier limited by the dispersion in the multi-mode fibers. Thus, the second generation of lightwave systems operated near the 1300 nm, had bit rates of up to 1.5 Gbit/s, and repeater spacing of about 50 km. It is during the second generation of lightwave systems that commercial systems were introduced.

Losses of silica fibers are smallest near 1550 nm. But, the introduction of third-generation lightwave systems operating at 1550 nm was considerably delayed by the large fiber dispersion near 1550 nm. The dispersion problem was overcome either by using dispersion-shifted fibers, or by limiting the laser spectrum to a single longitudinal mode. The third generation lightwave systems, operating at 2.5 Gbit/s, became available commercially in 1990. A drawback of the third generation 1550 nm lightwave systems were that the signal had to be regenerated periodically by using electronic repeaters spaced apart typically by 60-70 km. This problem was overcome by the advent of fiber amplifiers in 1989.

The fourth generation of lightwave systems made use of optical amplification for increasing the repeater spacing and wavelength-division multiplexing (WDM) for increasing the capacity. The basis of WDM is to use multiple optical sources operating at slightly different wavelengths to transmit several independent information streams over the same fiber. The development of Erbium doped fiber amplifier (EDFA) revolutionized the lightwave systems by replacing the electronic repeaters. Typical fourth generation WDM systems can operate at 40 Gbit/s with 100s of channels and can transmit data without regeneration over a distance of a few thousands of kilometers. Figure 1.2 shows the increase in capacity of the lightwave system spanned over the last 25 years.
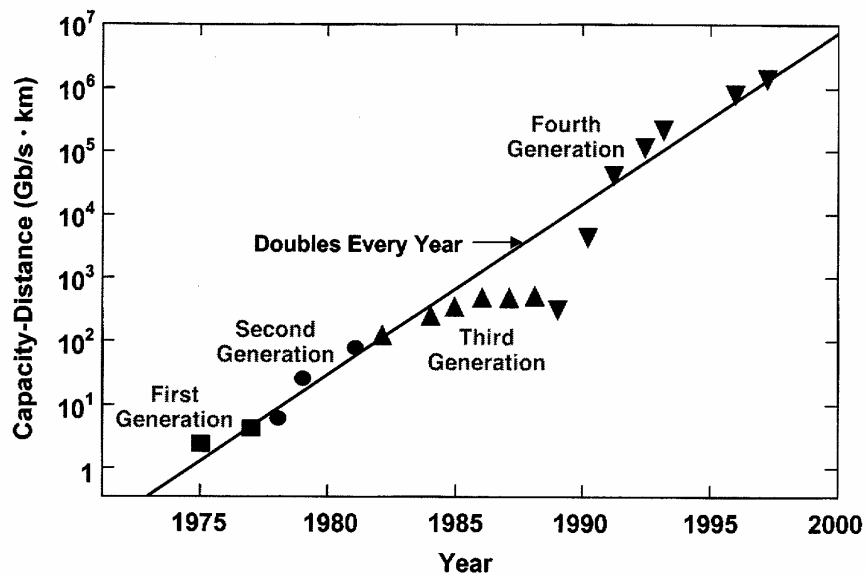
Figure 1.2: Increase in capacity of lightwave systems over the last 25 years [Ref. 1]

The current emphasis on WDM lightwave systems in on increasing system capacity by transmitting more and more channels through the WDM technique. This can be achieved by either extending the wavelength range of operation to include the L (long-) and S (short-) bands along with the conventional C band or by decreasing the spacing between the channels, thereby increasing spectral efficiency. Spectral efficiency is defined as the ratio of average channel bit rate to the average channel spacing, expressed in terms of bit/s/Hz. Thus, the fifth generation of lightwave systems deal with the wavelength range over which a WDM system can operate simultaneously and increasing spectral efficiency.

The technologies used in lightwave systems for the past 25 years have been growing steadily to meet the bandwidth demand. With growing bit rates and increasing channel capacities in WDM systems, dispersion and nonlinear effects present in the optical fiber become more prominent and lead to degradation of system performance. System performance evaluation and predictions for WDM systems where the dispersion and nonlinear effects are significant is critical for system design and installation. Experiments can be performed to do the evaluation, but the complexity and the high cost of optical components prohibit a thorough exploration in many systems. This led to the development of numerical simulation models, which offer a cost effective and time efficient method to investigate and optimize the optical systems. For a full understanding of a system design, the optical components in lightwave systems must be modeled in

sufficient detail. By using simulations, it is easy to explore new ideas or schemes for system design and installment. Simulations can offer insights regarding which effects are significant and which are not in a particular system. Therefore, even though simulation has the drawback of complexity in modeling and calculation, the numerical simulation becomes a critical tool for system design.

A numerical simulations based fiber optical simulator named "FiberSim" has been developed at the Lightwave communications systems laboratory of Information and Telecommunication Technology Center, University of Kansas. FiberSim is capable of modeling all major fiber properties, including nonlinearity and polarization characteristics. FiberSim can be used to model Wavelength Division Multiplexing (WDM) systems and to study the effects of various fiber properties on a transmitted signal. It offers solution for questions like the choice of fiber type, modulation type, channel power level on photonic system design etc. FiberSim verifies link designs at a sampled-signal level to identify cost savings and investigate novel technologies.

In this thesis, various techniques that can be used to increase the spectral efficiency of WDM systems are explored. These techniques include polarization interleave multiplexing and modulation formats, including vestigial side band (VSB) demultiplexing. The first part of this thesis deals with the modeling and analysis of a reported experimental system using FiberSim. The 40 Gbit/s

experimental WDM system chosen used the vestigial side band demultiplexing technique to achieve high spectral efficiency [Ref. 2] of 0.64 bit/s/Hz and 5 Tbit/s capacity over 1200 km of Teralight Ultra fiber. This experimental system was modeled using the FiberSim simulator and analysis of the effects of various simulation parameters on the system performance is reported. The simulation parameters on which analyses are performed include amplifier gain tilt, dispersion slope compensation, residual dispersion per span, and channel launch power.

The modeling and analysis of the experimental system is followed by design and analysis of a new VSB demultiplexing WDM model with 0.8 bit/s/Hz spectral efficiency. Unlike the experimental system, which used channel bit rates of 40 Gbit/s this new WDM system utilized lower bit rates per channel (10 Gbit/s) but achieved higher spectral efficiency. Also, the new WDM system used standard SMF for transmission and used EDFA for optical amplification. This design involved finding the optimal channel spacing, demultiplexer optical filter parameters and channel launch power.

The outline of this thesis is as follows. Chapter 2 discusses the various fiber properties and the propagation of optical signal through a fiber, since optical fibers form the heart of any lightwave system. Chapter 3 gives an introduction to FiberSim and describes the various optical components in it. This is followed by the description of the various techniques that can be used to increase the spectral

efficiency in WDM systems in chapter 4. Chapter 5 deals with the modeling and analysis of an experimental system using FiberSim and comparison of the simulation results with the reported experimental results. This is followed with the design of a 0.8 bit/s/Hz spectral efficiency WDM system using vestigial side band (VSB) demultiplexing technique. The final chapter includes conclusions and suggestions for future work.

2.   Signal Propagation in Optical Fibers

2.1.   Introduction

The core of any optical communication systems is the optical fiber, which is used to carry signals from one point to another. An optical signal that is launched into fiber from a light source, usually a laser, is affected by the properties of the fiber. The properties of the optical fiber lead to degradation of the optical signal as it propagates through it. Therefore, it becomes necessary to know about the various characteristics of optical fiber.

2.2.   Fiber Characteristics and Nonlinearities

An optical fiber consists of a central core, surrounded by a cladding layer whose refractive index is slightly lower than that of the core. Optical fiber acts as a dielectric waveguide to confine light within its surfaces and guides the light in a direction parallel to its axis. This confinement of light is achieved using the phenomenon called as total internal reflection. Total internal reflection is achieved when the angle of incidence of light is greater than the critical angle.

Like any other transmission medium, signal loss and distortion in optical fiber are important degradation factors. The loss of signal is attributed to *attenuation* in the fiber as the signal propagates through it. The distortion of signal is due to

dispersion in fiber that causes optical signal pulses to broaden as they travel along a fiber.

Along with attenuation and dispersion, fibers also add *nonlinear effects*. Fiber nonlinearities can be classified into two categories based on their origin. One category of nonlinearities arises from Kerr effect, which is the intensity-dependent variation in the refractive index of fiber. This produces effects such as *self-phase modulation* (SPM*), cross-phase modulation* (XPM) and *four-wave mixing* (FWM). The other category arises from the nonlinear inelastic scattering processes. These are *stimulated Raman scattering* (SRS) and *stimulated Brillouin scattering* (SBS).

2.2.1. Fiber Attenuation

As light propagates along a fiber, its power decreases exponentially with distance due to fiber attenuation. It can be mathematically represented as follows:

$$P(z) = P(0)\, e^{-\alpha_p z} \qquad\qquad ...\,(2.2.1)$$

where *P(z)* is optical power at distance *z*, *P(0)* is optical power at the start of the fiber (z = 0), and α_p is fiber attenuation coefficient .

In general fiber attenuation is expressed in decibels per km (dB/km) and can be obtained as follows [Ref. 3]:

$$\alpha(dB/km) = \frac{10}{z}\log\left[\frac{P(0)}{P(z)}\right] = 4.343\alpha_p (km^{-1}) \qquad \text{... (2.2.2)}$$

Attenuation in a fiber occurs due to absorption, scattering and radiative losses of the optical energy. Absorption losses are caused by atomic defects in the glass composition, intrinsic absorption by atomic resonance of fiber material and extrinsic absorption by the atomic resonance of external particles (like OH ion) in the fiber. Scattering losses in fiber arise from microscopic variations in the material density and from structural inhomogeneities. There are four kinds of scattering losses in optical fibers namely Rayleigh, Mie, Brillouin and Raman scattering. Radiative losses occur in an optical fiber at bends and curves because of evanescent modes generated. Also attenuation in a fiber is a function of the wavelength as illustrated by the general attenuation curve given in figure 2.1.
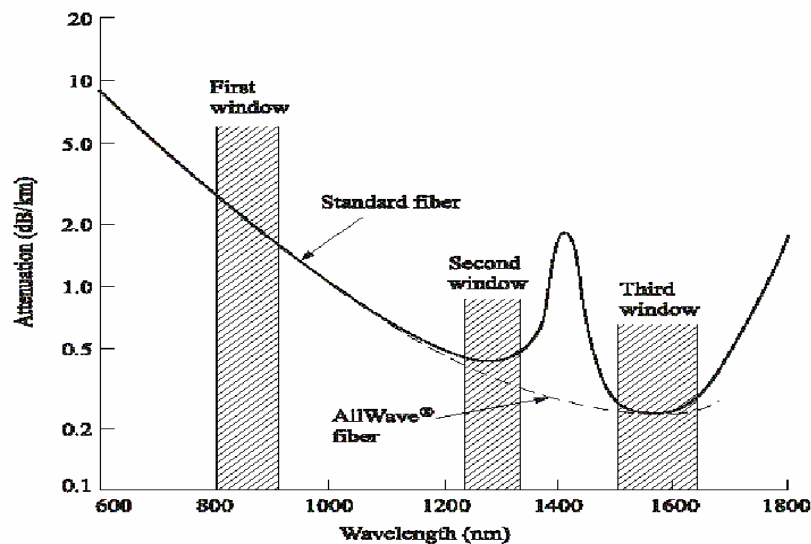
Figure 2.1: Optical fiber attenuation as a function of wavelength [Ref. 3]

2.2.2. Fiber Dispersion

An optical signal propagating through a fiber usually consists of components at different frequencies and different propagation modes. The propagation delays from these components will lead to pulse broadening, which is called as dispersion. Fiber dispersion can be classified into three kinds: *material or chromatic dispersion*, *waveguide dispersion* and *modal dispersion*. Chromatic and waveguide dispersion are results of group velocity being a function of wavelength. Hence this phenomenon is also known as *group velocity dispersion* (*GVD*). Group velocity is the speed at which energy in a particular mode travels along a fiber. Modal dispersion is the result of group velocity being different for different propagation modes. Modal dispersion is not an issue in single mode fibers.

The GVD manifests itself through the frequency dependence of the refractive index *n(ω)* and, hence, that of the wave propagation factor *β(ω)*. Expanding *β(ω)* in a Taylor series about the center frequency *ω₀* [Ref. 4]

$$\beta(\omega) = n(\omega)\frac{\omega}{c} = \beta_0 + \beta_1(\omega - \omega_0) + \frac{1}{2}\beta_2(\omega - \omega_0)^2 + \frac{1}{6}\beta_3(\omega - \omega_0)^3 ....$$

where $\quad \beta_m = \left[\frac{d^m\beta}{d\omega^m}\right]_{\omega=\omega_0} \quad (m = 0,1,2...)$ ... (2.2.3)

β_1 is the inverse of group velocity v_g, β_2 is the first-order dispersion and β_3 is the second-order dispersion. The higher order terms are generally negligible if the signal spectral width $\Delta\omega$ is much less than the center frequency ω_0.

Fiber dispersion is generally expressed in the form of dispersion parameter D, which is related to β_1 and β_2 by

$$D = \frac{d\beta_1}{d\lambda} = -\frac{2\pi c}{\lambda^2}\beta_2 \qquad \text{... (2.2.4)}$$

A typical dispersion versus wavelength plot for a single mode fiber is as given in figure 2.2.
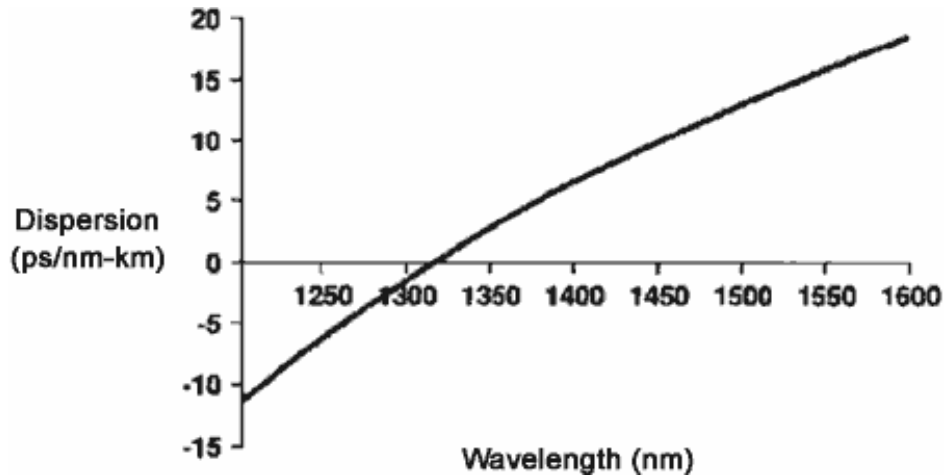
Figure 2.2: Typical dispersion vs. wavelength plot

Apart from GVD and modal dispersion, there exists another kind of pulse broadening in fiber called *Polarization Mode Dispersion* (PMD). PMD is the consequence of birefringence in a fiber, which is defined as the difference in refractive indices of a pair of orthogonal polarization states. A varying birefringence along the fiber length will cause each polarization mode to travel at

a slightly different velocity and the polarization orientation will rotate with distance. The resulting difference in propagation times between the two orthogonal polarization modes will result in pulse spreading. In contrast to GVD, which is a relatively stable phenomenon along a fiber, PMD varies randomly along a fiber.

2.2.3. Self Phase Modulation and Cross Phase Modulation

The refractive index of a fiber has a weak dependence on optical signal intensity and it can be represented as [Ref. 4]

$$n = n_0 + n_2 \frac{P}{A_{eff}} = n_0 + n_2 I \qquad \text{... (2.2.5)}$$

where I is the optical signal intensity, n_0 is the ordinary refractive index of the fiber and n_2 is the nonlinear index coefficient.

Self phase modulation (SPM) and cross phase modulation (XPM) are the result of intensity dependence of the refractive index of the fiber. SPM refers to the self-induced phase shift experienced by an optical pulse during its propagation in optical fibers. The magnitude of SPM can be obtained from the phase change of the optical signal. If the length of the fiber is L, the phase of the signal is given by

$$\phi = (n_0 + n_2 I)k_0 L \qquad \text{... (2.2.6)}$$

where $k_0 = 2\pi/\lambda$. Then the phase shift due to SPM is given by $\phi_{NL} = n_2 k_0 L I$

XPM refers to the nonlinear phase shift of an optical signal induced by the co-propagating signals at different wavelengths. When we consider two optical signals with intensities I_1 and I_2, the total nonlinear phase shift experienced by the first signal is given by [Ref. 4]

$$\phi_{NL} = n_2 k_0 L(I_1 + 2I_2) \qquad \dots (2.2.7)$$

which includes both SPM and XPM. From the above expression it can be observed that for equally intense optical signals, the contribution of XPM to the nonlinear phase shift is twice compared with that of SPM. XPM leads to asymmetric spectral broadening of co- propagating optical pulses.

Since the phase fluctuations introduced by SPM and XPM are intensity dependent, different parts of a pulse undergo different phase shifts. This leads to *frequency chirping*, in which the rising edge of the pulse experiences a red shift in frequency (toward higher frequencies), whereas the trailing edge of the pulse experiences a blue shift in frequency (toward lower frequencies).

2.2.4. Four-Wave Mixing

Four-wave mixing (*FWM*) is a type of optical Kerr effect and occurs when light of two or more different wavelengths is launched into a fiber. Generally, when optical signals are located near the zero-dispersion point, three optical frequencies (f_i, f_j, f_k) will mix to produce a fourth intermodulation product f_{ijk} given by

$$f_{ijk} = f_i + f_j - f_k \qquad \text{with } i, j \neq k \qquad \qquad ...\ (2.2.8)$$

f₁ f₂ sidebands diagram
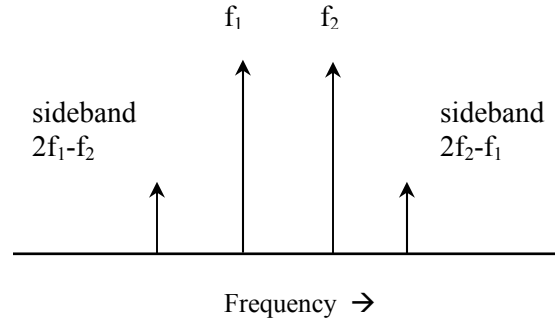
Figure 2.3: Two optical waves at frequencies f_1 and f_2 mix to generate two third-order sidebands

As shown above in figure 2.3 two optical signals of frequencies f_1 and f_2 co-propagating along a fiber mix and generate sidebands at *2f₁-f₂* and *2f₂-f₁*. In general, for *N* wavelengths launched into a fiber, the number of sidebands *M* generated is

$$M = \frac{1}{2}(N^3 - N^2) \qquad \qquad …\ (2.2.9)$$

The efficiency of FWM depends on fiber dispersion and the channel spacing. Dispersion, being a function of wavelength, leads to a group velocity mismatch in the signal and generated sidebands. This destroys the phase matching of the interacting waves and lowers the efficiency at which power is transferred to newly generated sidebands. Hence, FWM is inversely proportional to dispersion and channel spacing.

2.2.5. Stimulated Raman Scattering

Stimulated Raman Scattering (*SRS*) results from interaction between light waves and the vibration modes of the silica molecules in fiber. When an optical signal of energy hf_1 is injected into a fiber whose molecules have some vibration frequency, its photons gets scattered, thereby attaining a lower energy hf_2 and a corresponding lower frequency f_2. The modified signal is called the *Stokes signal* and the optical signal that is injected into a fiber is called the *pump signal*, since it supplies power for the generated signal.

SRS can occur both in the forward and backward direction in optical fibers. The interference of the pump light with the scattered light creates a frequency component at the beat frequency ω_p-ω_s, which acts as a source that drives molecular oscillations. Since the amplitude of the scattered wave increases in response to these oscillations, a positive feedback loop is created. In the forward direction, the feedback process is described by the following set of coupled rate equations [Ref. 4]

$$\frac{dI_s}{dz} = g_R I_p I_s - \alpha_s I_s$$

$$\frac{dI_p}{dz} = -\frac{\omega_p}{\omega_s} g_R I_p I_s - \alpha_p I_p \qquad \text{... (2.2.10)}$$

where I_p and I_s are the stokes intensity and pump intensity respectively, α_s and α_p are signal and pump attenuation, g_R is the Raman gain coefficient. The Raman gain coefficient is related to the cross section of spontaneous Raman scattering, an experimentally measurable quantity and has a distribution as shown in figure 2.4.

The most significant feature of the Raman gain in silica fibers is that g_R extends over a large frequency range (up to 40 THz). The peak of the Raman gain occurs at when the Raman shift $\Omega_R = \omega_p - \omega_s$ is about 13 THz. The peak value of the Raman gain, g_R is about 1.0×10^{-13} m/W at $\lambda = 1.55$ μm.
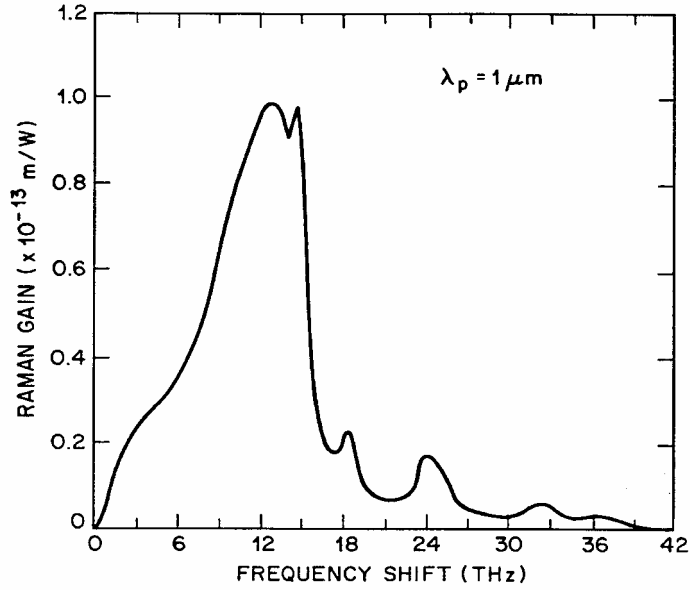
Figure 2.4: Measured Raman gain spectrum [Ref. 4]

The coupled rate equations mentioned above could be solved easily with the assumption that pump depletion is negligible in the fiber to obtain

$$I_s(L) = I_s(0)\exp(g_R I_0 L_{eff} - \alpha_s L)$$

where,
$$L_{eff} = \frac{1}{\alpha_p}[1 - \exp(-\alpha_p L)] \qquad \text{... (2.2.11)}$$

Here I_0 is the pump intensity at z=0. Also the threshold power level for SRS, which is defined as the input pump power at which the Stokes power becomes equal to the pump power at the fiber output, satisfies the condition

$$\frac{g_R P_{th} L_{eff}}{A_{eff}} \approx 16 \qquad \qquad ...\,(2.2.12)$$

where A_{eff} is the effective core area of the fiber.

2.3. The Nonlinear Schrödinger Wave Equation

The nonlinear Schrödinger wave equation is a mathematical representation for the nonlinear propagation of light signal through a fiber. From Maxwell's equations, one can derive [Ref. 4],

$$\nabla^2 E - \frac{1}{c^2}\frac{\partial^2 E}{\partial t^2} = \mu_0 \frac{\partial^2 P_L}{\partial t^2} + \mu_0 \frac{\partial^2 P_{NL}}{\partial t^2} \qquad ...\,(2.3.1)$$

where E is the rapidly varying electric field, P_L is the linear polarization induced by electric field and P_{NL} is the nonlinear polarization induced by electric field

The electric field E consists of a rapidly varying carrier component (with frequency ω_0) and a slowly varying envelope component $\{E_s(z,t)\}$. For simplification, just consider the x-polarized signals. This can be represented as

$$E(z,t) = \frac{1}{2}\hat{x}\{E_s(z,t)\exp(-i\omega_0 t) + c.c\} \qquad ...\,(2.3.2)$$

The polarization components can also be expressed in a similar way,

$$P_L(z,t) = \frac{1}{2}\hat{x}\{P_{sL}(z,t)\exp(-i\omega_0 t) + c.c\}$$

$$P_{NL}(z,t) = \frac{1}{2}\hat{x}\{P_{sNL}(z,t)\exp(-i\omega_0 t) + c.c\} \qquad ...\,(2.3.3)$$

The linear polarization component is induced by the first order susceptibility term $\chi^{(1)}$ whereas the nonlinear polarization component is induced by the third order susceptibility $\chi^{(3)}$. For simplicity, we will for the moment assume that the nonlinear response to be instantaneous only.

$$P_{SL}(z,t) = \varepsilon_0 \chi^{(1)}(t-t')E_s(z,t) = \varepsilon_0 \int_{-\infty}^{\infty} \tilde{\chi}^{(1)}(\omega)E_s(z,\omega-\omega_0)\exp[-i(\omega-\omega_0)t]d\omega$$

... (2.3.4)

$$P_{SNl} = \varepsilon_0 \varepsilon_{NL} E_s(z,t) \quad \text{where,} \quad \varepsilon_{NL} = \frac{3}{4}\chi^{(3)}|E_s(z,t)|^2$$ ... (2.3.5)

Taking Fourier transform of equation 2.3.1 and using the equations 2.3.2 to 2.3.5 we obtain

$$\nabla^2 \tilde{E}_s + \varepsilon(\omega)k_0^2 \tilde{E}_s = 0$$ ... (2.3.6)

$$\varepsilon(\omega) = 1 + \tilde{\chi}^{(1)}(\omega) + \varepsilon_{NL}$$

where

$$k_0 = \frac{\omega}{c}$$ ... (2.3.7)

Equation 2.3.6 can be solved using the method of separation of variables. If we assume a solution of the form:

$$\tilde{E}_s(z,\omega-\omega_0) = F(x,y)\tilde{A}(z,\omega-\omega_0)\exp(-i\beta_0 z)$$ ... (2.3.8)

where $A(z,\omega)$ is the slowly varying envelope spectrum of the signal. The inverse Fourier transform of $A(z,\omega)$ gives the pulse amplitude A, which is assumed to be normalized such that $|A|^2$ represents the optical power. Using 2.3.8 equation 2.3.6 reduces to

$$\frac{1}{F}\left(\frac{\partial^2 F}{\partial x^2}+\frac{\partial^2 F}{\partial y^2}\right)+\frac{1}{\widetilde{A}}\left(2i\beta_0\frac{\partial\widetilde{A}}{\partial z}-\beta_0^2\widetilde{A}\right)+\varepsilon(\omega)k_0^2=0 \quad \text{... (2.3.9)}$$

Solving the above equation, we obtain

$$\frac{\partial^2 F}{\partial x^2}+\frac{\partial^2 F}{\partial y^2}+\left[\varepsilon(\omega)k_0^2-\widetilde{\beta}^2\right]F=0$$

$$\text{... (2.3.10)}$$

$$2i\beta_0\frac{\partial\widetilde{A}}{\partial z}+\left(\widetilde{\beta}^2-\beta_0^2\right)\widetilde{A}=0$$

The dielectric constant $\varepsilon(\omega)$ can be expressed in terms of refractive index n as

$$\varepsilon=(n+\Delta n)^2\approx n^2+2n\Delta n \qquad \text{where } \Delta n=n_2|E|^2+\frac{i\alpha}{2k_0} \quad \text{... (2.3.11)}$$

Also the mode propagation constant can be expressed as

$$\widetilde{\beta}=\beta(\omega)+\Delta\beta \qquad\qquad \text{... (2.3.12)}$$

$$\beta(\omega)=n(\omega)\frac{\omega}{c}=\beta_0+\beta_1(\omega-\omega_0)+\frac{1}{2}\beta_2(\omega-\omega_0)^2+\frac{1}{6}\beta_3(\omega-\omega_0)^3........ \qquad \text{... (2.3.13)}$$

Using equations 2.3.11 to 2.3.13 in 2.3.10 and taking the inverse Fourier transform, we obtain

$$\frac{\partial A}{\partial z}+\beta_1\frac{\partial A}{\partial t}+\frac{i}{2}\beta_2\frac{\partial^2 A}{\partial t^2}-\frac{1}{6}\beta_3\frac{\partial^3 A}{\partial t^3}+\frac{\alpha}{2}A=i\gamma|A|^2 A \qquad \text{... (2.3.14)}$$

where nonlinearity coefficient $\gamma=\dfrac{n_2\,\omega_0}{c\,A_{eff}}$. Equation 2.3.14 is called the generalized Schrödinger equation. When the moving frame (retarded frame) time variable T is used, which is related to the real time variable t through,

$$T=t-z/v_g=t-\beta_1 z \qquad\qquad \text{... (2.3.15)}$$

where v_g is the group velocity of the light in the fiber, equation 2.3.14 modifies to

$$\frac{\partial A}{\partial z} + \frac{i}{2}\beta_2 \frac{\partial^2 A}{\partial T^2} - \frac{1}{6}\beta_3 \frac{\partial^3 A}{\partial T^3} + \frac{\alpha}{2}A = i\gamma|A|^2 A \qquad \text{... (2.3.16)}$$

If we include the delayed and cross-polarized components in nonlinear response in addition to instantaneous components, equation 2.3.16 becomes [Ref. 5]

$$\frac{\partial A_i}{\partial z} + \frac{1}{2}j\beta_2 \frac{\partial^2 A_i}{\partial T^2} - \frac{1}{6}\beta_3 \frac{\partial^3 A_i}{\partial T^3} + \frac{\alpha}{2}A_i$$

$$= j(1-f_R)\gamma(|A_i|^2 + \frac{2}{3}|A_{3-i}|^2)A_i + \frac{1}{3}j(1-f_R)\gamma A_i^* A_{3-i}^2 \exp(-j2\Delta\beta z)$$

$$+ jf_R\gamma A_i(t)\int_0^\infty |A_i(t-s)|^2 h_r(s)ds$$

$$+ \frac{1}{3}jf_R\gamma A_i(t)\int_0^\infty |A_{3-i}(t-s)|^2 h_r(s)ds$$

$$+ \frac{1}{3}jf_R\gamma A_{3-i}(t)\int_0^\infty A_i(t-s)A_{3-i}^*(t-s)h_r(s)ds$$

$$+ \frac{1}{3}jf_R\gamma A_{3-i}(t)\exp[-j2\Delta\beta z]\int_0^\infty A_i^*(t-s)A_{3-i}(t-s)h_r(s)ds \quad \text{... (2.3.17)}$$

where $i=1,2$ represent the x-polarized and y-polarized components, f_R is the Raman delay fraction with a typical value of 0.18 and $h_r(t)$ is the Raman response function. The Raman response function can be expressed in terms of the Raman oscillation constant τ_1 and Raman decay constant τ_2 as [Ref. 4]

$$h_r(t) = \frac{\tau_1^2 + \tau_2^2}{\tau_1 \tau_2^2} \exp\left(-\frac{t}{\tau_2}\right)\sin\left(\frac{t}{\tau_1}\right) \qquad \text{... (2.3.18)}$$

The typical values for τ_1 and τ_2 are 12.2 fs and 32.0 fs respectively. Figure 2.5 depicts the temporal variations of $h_r(t)$ obtained using the experimentally measured Raman gain spectrum.
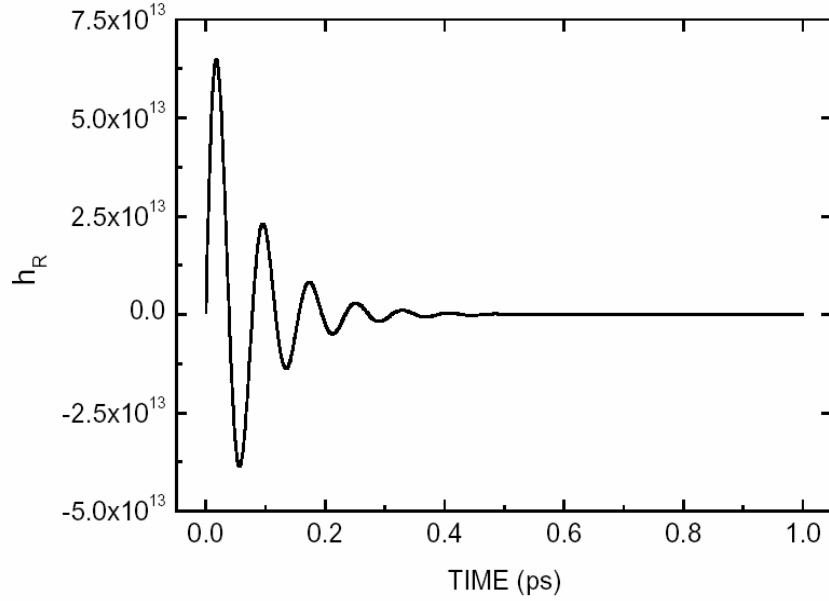
Figure 2.5: Temporal variation of the Raman response function $h_r(t)$

Equation 2.3.17 represents the propagation equation with instantaneous and delayed nonlinear components, along with self-polarized and cross-polarized terms. The description of the individual terms on the right-hand side of the equation is as follows:

$$j(1-f_R)\gamma |A_i|^2 A_i \qquad\qquad \text{: Instantaneous SPM}$$

$$j(1-f_R)\gamma \frac{2}{3}|A_{3-i}|^2 A_i \qquad\qquad \text{: Instantaneous XPM}$$

$$\frac{1}{3}j(1-f_R)\gamma A_i^* A_{3-i}^2 \exp(-j2\Delta\beta z) \qquad\qquad \text{: Instantaneous FWM}$$

$$jf_R \gamma \, A_i(t) \int_0^\infty \left| A_i(t-s) \right|^2 h_r(s)\,ds \qquad : \text{Delayed Self-Polarization Modulation}$$

$$\frac{1}{3} jf_R \gamma \, A_i(t) \int_0^\infty \left| A_{3-i}(t-s) \right|^2 h_r(s)\,ds \qquad : \text{Delayed Cross-Polarization Modulation}$$

$$\frac{1}{3} jf_R \gamma \, A_{3-i}(t) \int_0^\infty A_i(t-s) A_{3-i}^*(t-s) h_r(s)\,ds \qquad : \text{Delayed Cross-Polarization Modulation}$$

$$\frac{1}{3} jf_R \gamma \, A_{3-i}(t) \exp[-j2\Delta\beta z] \int_0^\infty A_i^*(t-s) A_{3-i}(t-s) h_r(s)\,ds \qquad : \text{Delayed FWM}$$

2.4. Split-Step Fourier Transform method

The propagation equation 2.3.17 is a nonlinear partial differential equation, which in general does not have an analytical solution. Hence, a numerical approach is necessary to solve the propagation equation. The split-step Fourier transform method is often used to solve the pulse-propagation problem in nonlinear dispersive media.

The propagation equation is of the form [Ref. 4]

$$\frac{\partial A}{\partial z} = \left(D_s + N_s \right) A \qquad\qquad \text{... (2.4.1)}$$

where D_s is a differential operator that includes dispersion and loss in a linear medium and N_s is a nonlinear operator that includes the effects of fiber nonlinearities.

$$D_s = -\frac{i}{2}\beta_2 \frac{\partial^2}{\partial T^2} + \frac{1}{6}\beta_3 \frac{\partial^3}{\partial T^3} - \frac{\alpha}{2}$$

... (2.4.2)

$$N_s = i\gamma|A|^2$$

An approximate solution for equation 2.4.1 can be obtained by treating that the dispersive and nonlinear effects act independently on the signal propagating over small distance h. When we consider dispersion, N_s is set to zero and when we consider nonlinearities, D_s is set to zero. This leads to

$$A(z+h,T) \cong \exp(hD_s).\exp(hN_s).A(z,T) \qquad ... (2.4.3)$$

The evaluation of the differential operator, which accounts for dispersion, is carried out in the frequency domain, whereas the evaluation of the nonlinear operator is carried out in the time domain.

The accuracy of the split step method can further be improved adopting a symmetric form of exponential operator. This would modify the equation 2.4.3 to

$$A(z+h,T) \cong \exp\left(\frac{h}{2}D_s\right)\exp\left(\int_z^{z+h} N_s(z')dz'\right)\exp\left(\frac{h}{2}D_s\right)A(z,T) \ ... (2.4.4)$$

In this approach, the effect of nonlinearity is included in the middle of the segment rather than at the end of the segment. Since we use symmetric form of exponential operators, it is also called as symmetrized split-step Fourier method. This approach can be diagrammatically represented as shown in the figure 2.6.
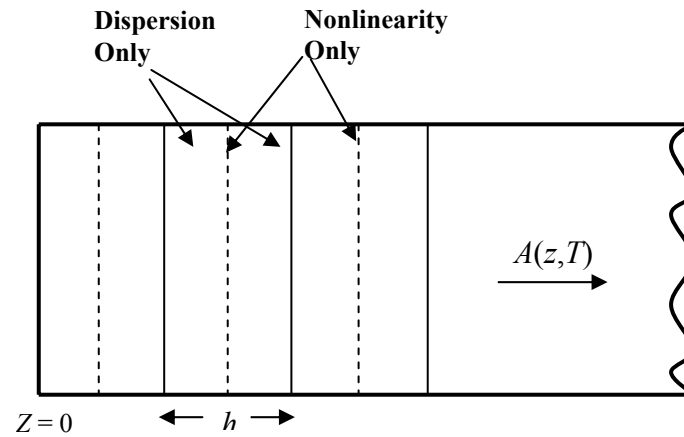
Figure 2.6: Symmetrized split-step Fourier method [Ref. 4]

The optical field *A(z, T)* is first propagated for a distance *h/2* with dispersion only using the FFT algorithm for frequency domain transformation. At the distance *z+h/2*, the field is multiplied by a nonlinear term in time domain that represents the effect of nonlinearity over the whole segment length *h*. Finally, the field is propagated the remaining *h/2* distance with dispersion only to obtain *A(z+h, T)*.

3.   FiberSim – Fiber Optic Simulator

3.1.   Introduction

FiberSim is a Fiber Optic Simulator developed at the Lightwave Communications Systems Laboratory of Information and Telecommunication Technology Center (ITTC), University of Kansas. FiberSim can be used to model Wavelength Division Multiplexing (WDM) systems and to study the effects of various fiber properties on the transmitted signal. The simulator provides a cost effective method to analyze and study the behavior of different WDM system models.

The modules in FiberSim can be broadly divided into a transmitter, a receiver, and an intermediate transmission media. The transmitter of FiberSim consists of a data generator, an optical source (laser), an optical modulator (Mach-Zehnder), and an optical multiplexer. The receiver consists of an optical demultiplexer, an optical receiver (photodiode), and optical & electrical filters. The transmission media consists of fiber and optical amplifier. The core of any WDM system and hence that of FiberSim is the optical fiber, which is used to carry the signal.

In a WDM system, signals pass through different optical and electronic components like modulators, filters, detectors, fibers etc. and are affected by the characteristics of these components. Therefore, FiberSim includes the modeling

of the different optical and electronic components, and the description of these components is carried out in section 3.3.

3.2. Using FiberSim

FiberSim has a user-friendly graphical user interface (GUI), developed using java. Using the various optical components displayed on top of the FiberSim window, one can assemble a wide variety of WDM system. In this section we will have a brief overview of FiberSim GUI and its result formats. Further information on how to use FiberSim can be obtained from the FiberSim user manual [Ref. 8].

A snapshot of the simulator GUI that shows its navigational and menu bar is as shown in figure 3.1.
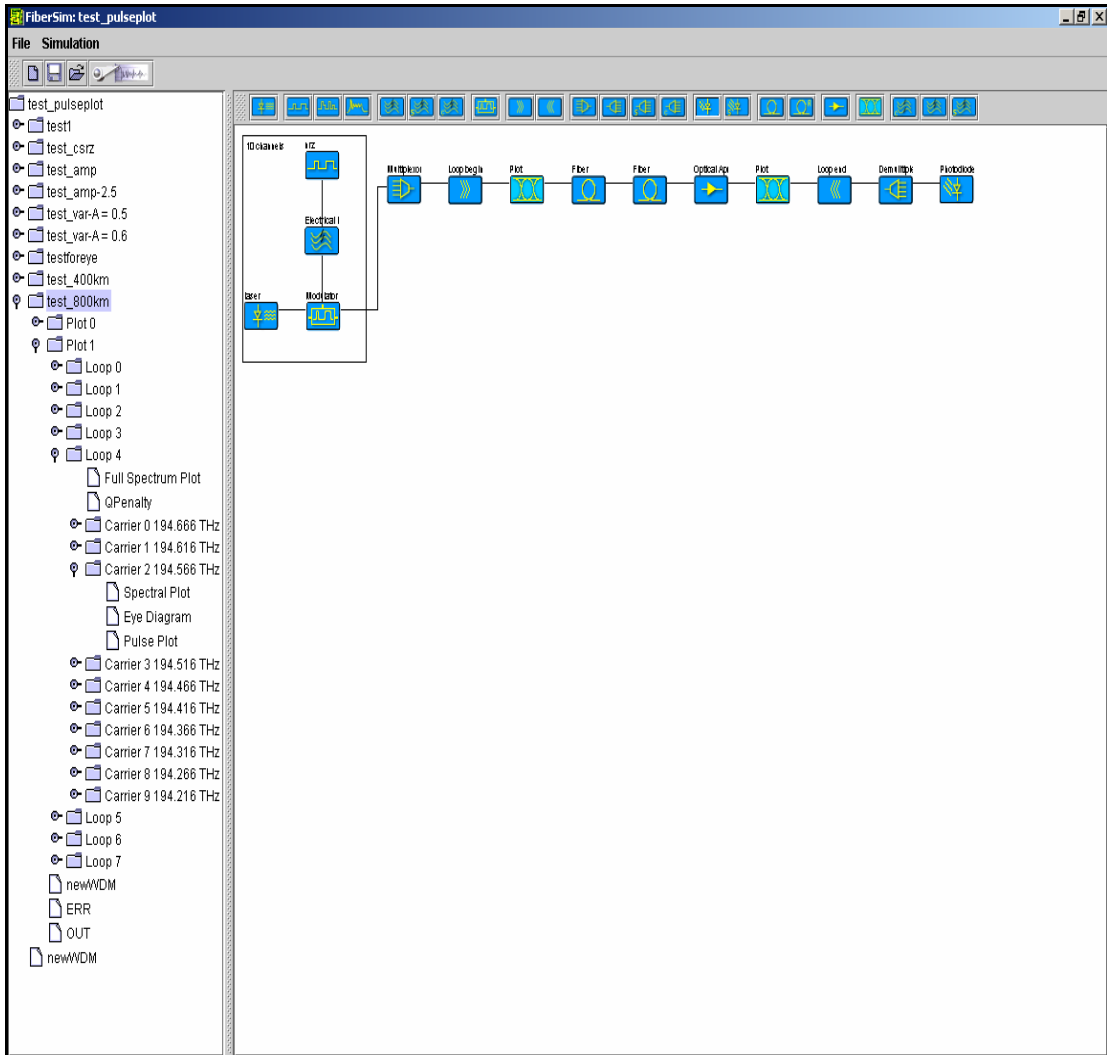
Figure 3.1: Snapshot of FiberSim

The navigational bar, which appears on the left side of the display, can be used to view the various simulation results. The menu bar on the top left corner of the display can be used for opening a new or previously saved model and also to start a simulation. One can assemble a WDM system using the various optical displayed on the top center of the display. Once a system is assembled, the parameters of the optical components are set. Then, the simulation is started and

the results are stored using the name specified by the user for the simulation. On completion of a simulation, the results can be viewed in the form of Eye diagrams or pulse plots for any channel. FiberSim can also display the spectral plot of the entire transmitted spectrum or any single channel. The Q-factors and bit error rate (BER) for any channel in the WDM system can also be displayed. The definitions for Q-factor and BER can be found in section 3.4.
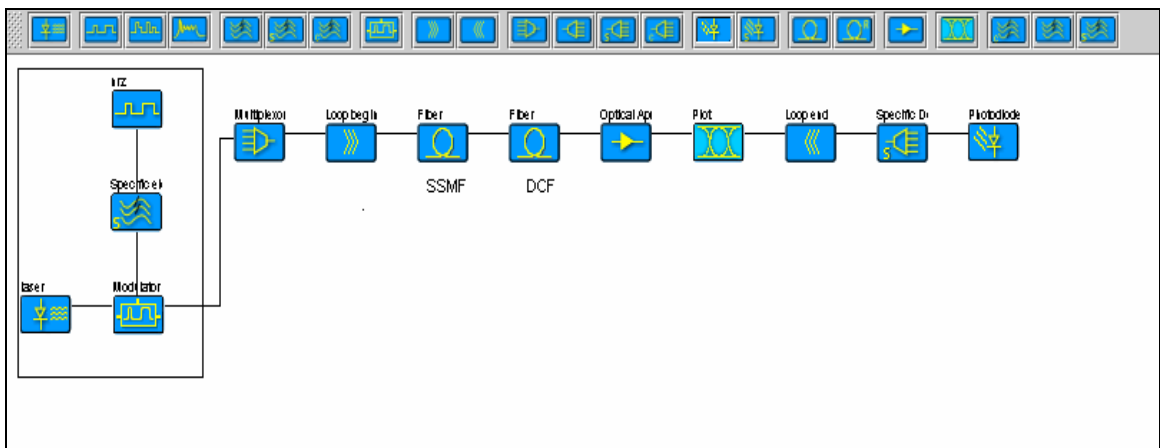
Figure 3.2: WDM system assembled using FiberSim

Figure 3.2 shows the FiberSim GUI for a typical WDM system. The transmitter, as shown in a box on the left side of the figure, consists of a data generator, an electrical filter, a laser and an optical modulator, followed by multiplexer. The multiplexer is followed by a fiber section, a DCF section, an amplifier, and a 'plot' component. Optical components that are to be repeated successively throughout a system are placed between 'Loop begin' and 'Loop end' components. The number of loops can be set in 'Loop begin' component to any number, and the components between 'Loop begin' and 'Loop end' are

repeated that many times. The receiver in this figure consists of a demultiplexer and a photodiode. This particular WDM system consists of 10 channels with 10 Gbit/s data rates, spaced 50 GHz apart. The fiber parameters are set to model standard SMF, and the DCF sections are used to compensate for SMF dispersion.

The results of FiberSim simulations can be viewed in the form of eye diagrams, pulse plots, or spectral plots. FiberSim also calculates the Q, BER and average channel power values of any channel. Figure 3.3 shows the eye diagram of channel 4 of the 10-channel WDM system described above at the end of 600 km of transmission. Figure 3.4 shows the pulse plot of channel number 4 at the end of 600 km. Figure 3.5 shows the full spectral plot i.e. the spectral plot of all the 10 channels and figure 3.6 shows the spectrum of channel 4 at the end of 600 km of fiber transmission.
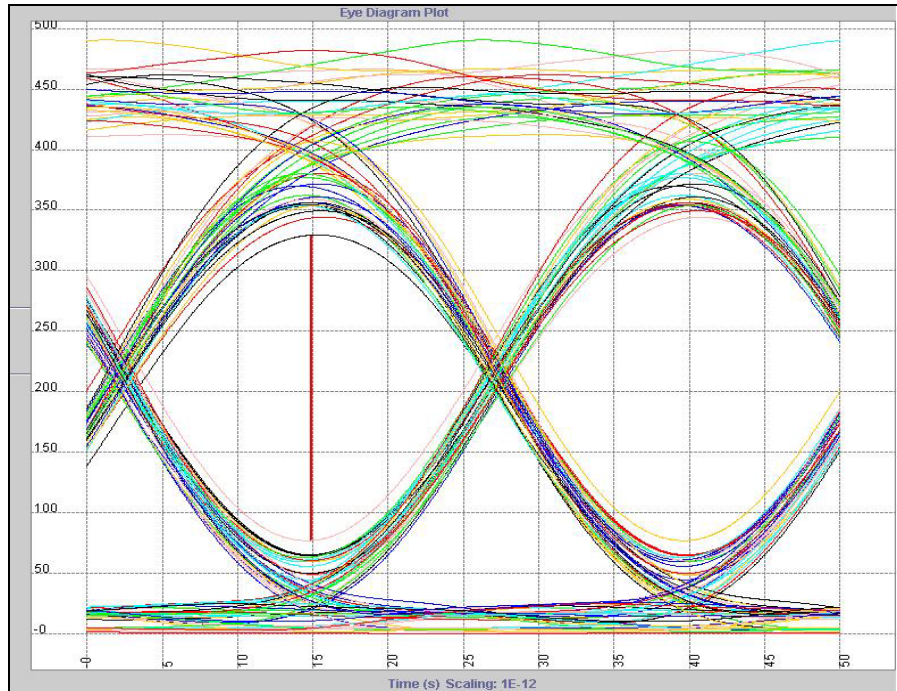
Figure 3.3: Eyediagram of a particular channel
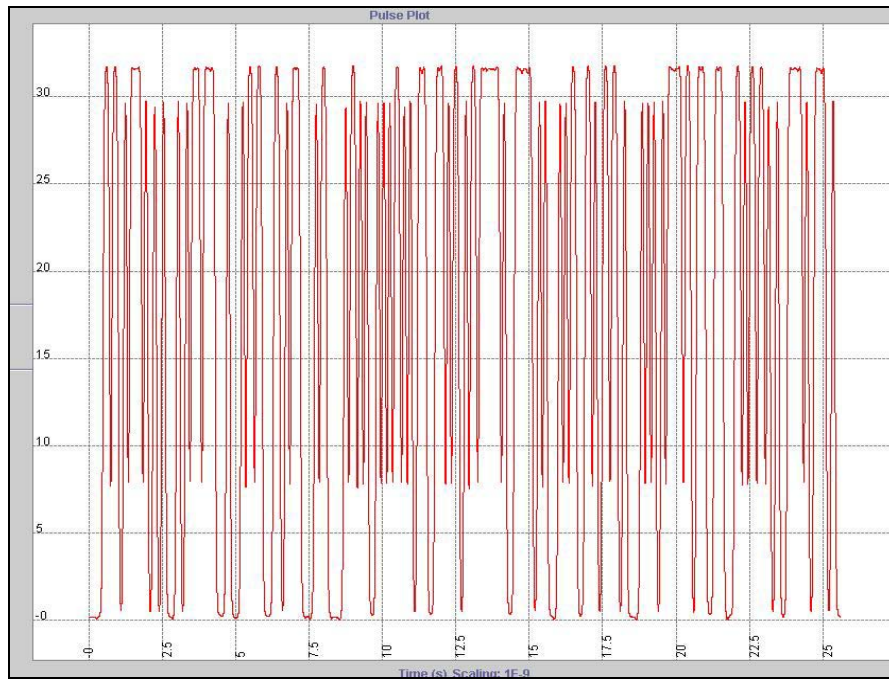
Figure 3.4: Pulse plot of a particular channel
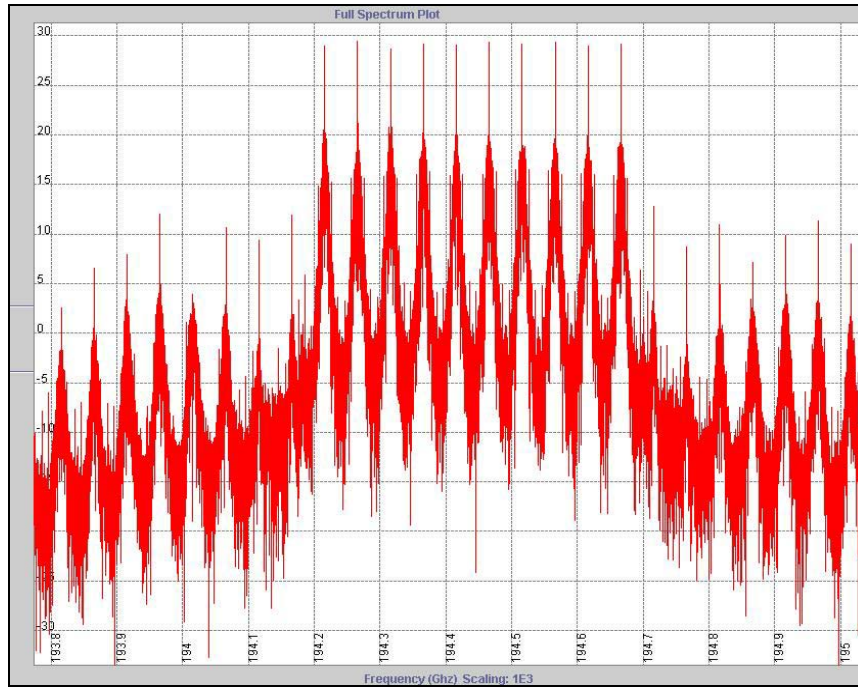
Figure 3.5: Full Spectral plot of a WDM system
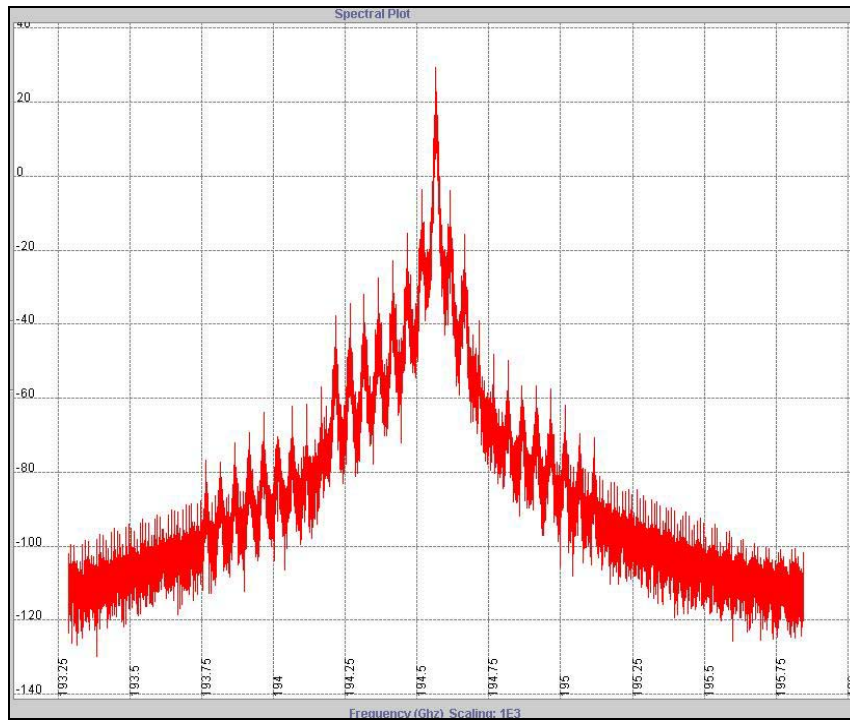
Figure 3.6: Spectral plot of a particular channel

3.3. Description of Optical Components modeled in FiberSim

Descriptions of the various optical components included in FiberSim are given in this section. In FiberSim, the effects of the different optical and electronic components in a WDM system on the signal envelope *A(t)* is evaluated and applied, i.e. the simulator keeps track of the envelope of a composite signal as it passes through the different optical components in a WDM system. The effects of the different optical components on the signal envelope *A(t)* is also discussed in this section. The optical components dealt with are: data generators, electrical filters, optical sources, optical modulators, optical multiplexers and demultiplexers, optical fibers, optical amplifiers, optical filters and photodetectors.

3.3.1. Data Generators

The data (bits) generator in FiberSim is used to build the data streams to be carried by individual channels in the form of bits of ones and zeros. A random seed number can be set to produce different random sequences of data. The data can be in the form of Non-return to zero (NRZ), return to zero (RZ) or carrier suppressed return to zero (CS-RZ).

NRZ is the most widely used data format, in which a pulse of light filling an entire bit period is used to represent a '1' and no pulse is transmitted to represent

a '0'. The bandwidth requirement with NRZ coding is the minimal. In RZ data, a '1' is represented by a half period optical pulse than can occur in either the first half or second half of the bit period and a '0' is represented by no signal during the bit period.
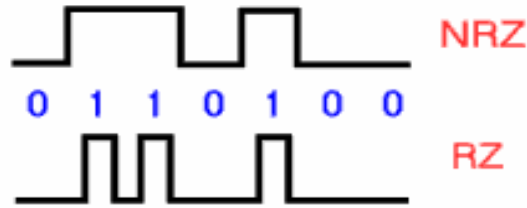
Figure 3.7: Data formats

3.3.2. Electrical Filters

An electrical filter can be used to filter the data before sending it to the optical modulator, or after the photo-detector to suppress noise. The electrical filter types available in FiberSim are Ideal, Bessel, Butterworth and Notch filters. Butterworth filters have a flat response in the frequency domain, which leads to jitters in time domain. For most electrical filters, the bandwidth is usually chosen to be 0.6 ~ 0.8 times the bit rate at both the transmitter and the receiver.

The transfer function of a Nth order Bessel filter is given by,

$$H(\omega) = \frac{1}{\sum\limits_{k=o}^{N} a_k (j\omega)^k} \qquad \qquad \text{... (3.2.1)}$$

where, $\qquad a_k = \dfrac{(2N-k)!}{2^{N-k} k!(N-k)!} \qquad \qquad k = 0,1,2,\ldots,N \qquad \qquad \text{... (3.2.2)}$

The transfer function of an Nth order Butterworth filter is given by

$$H(\omega) = \frac{1}{\sqrt{1 + \left(\dfrac{\omega}{\omega_c}\right)^{2N}}} \qquad \text{... (3.2.3)}$$

where ω_c is the 3dB cut off frequency.

In FiberSim, filtering is performed in frequency domain and an inverse Fourier transform is performed to obtain the output time-domain signal. This can be represented as follows,

$$A_{out}(t) = FFT^{-1}\{A_{in}(\omega) * H(\omega)\} \qquad \text{... (3.2.4)}$$

where $A_{in}(\omega)$ is the envelope signal spectrum at the input of the filter and $A_{out}(t)$ is the envelope signal at the output of the filter.
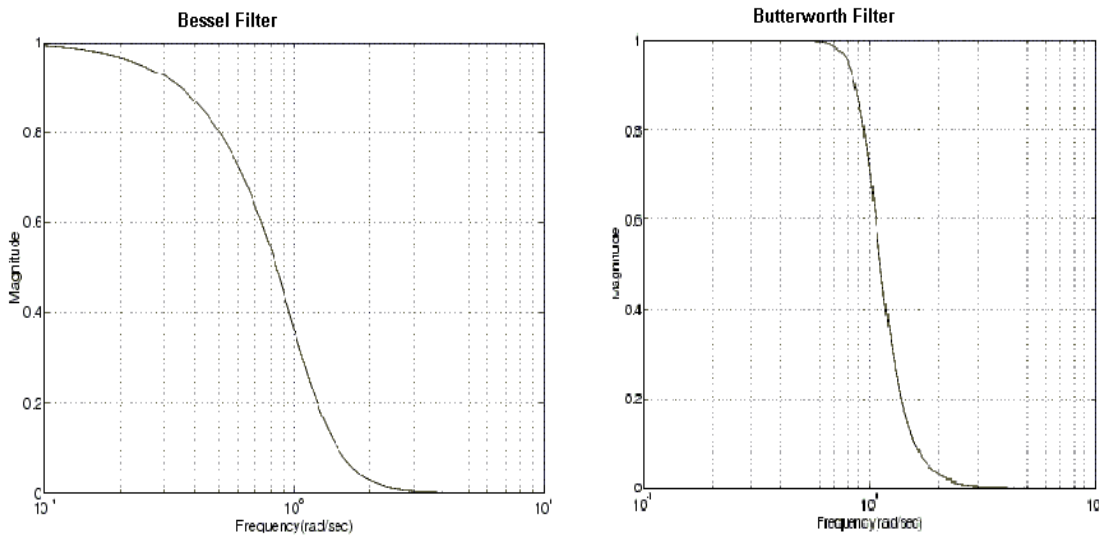
Figure 3.8: Magnitude Response of Bessel and Butterworth filters

3.3.3. Optical Sources

An optical source, typically a laser in an optical transmission system, is the carrier of the transmitted data. In FiberSim, lasers are modeled as a continuous wave (CW) sources with zero linewidths.

Each channel in the WDM system formed using FiberSim can be specified in terms of its wavelength or frequency, launch power and polarization. WDM system with equal channel spacing can be specified in terms of the starting wavelength and the spacing between the channels.

3.3.4. Optical Modulators

An optical modulator is a device that modulates a baseband electrical signal onto an optical carrier. In WDM systems, the modulation can be done on the optical source i.e. laser itself, called as direct modulation, or using an external modulator.

The FiberSim modulator module is an external modulator. In FiberSim, the modulator can be modeled as either an ideal modulator or as a Mach-Zehnder modulator with a pre-chirp. Mach-Zehnder modulators are constructed using Mach-Zehnder interferometers, which use the interference between two light beams with different optical path lengths, as explained in Appendix-A.

The signal output of the ideal modulator in FiberSim is proportional to the square root of the signal voltage and is given by the expression:

$$A_i(t) = \sqrt{P_i}\,\sqrt{v_i(t)}\,\exp\{-j(\omega_c - \omega_i)t\} \qquad \text{... (3.2.5)}$$

where P_i is the laser power of the ith channel, $v_i(t)$ is the filtered data of the ith channel (NRZ/RZ data bits passed through an electrical filter), ω_c is the center wavelength of the composite channel (i.e. all the multiplexed channels put together) and ω_i is the modulated wavelength of the ith channel.

In case of Mach-Zehnder modulator the modulated signal output is given by:

$$A_i(t) = \sqrt{P_i}\,\exp\left\{-jv_i(t)\frac{\pi\alpha}{2v_\pi}\right\}\sin\left[\frac{\pi|v(t)|}{2v_\pi}\right]\exp\{-j(\omega_c - \omega_i)t\} \;\text{... (3.2.6)}$$

where α is the chirp parameter and v_π denotes the voltage bias swing that brings the output from full off to full on. The derivation of equation 3.2.6 can be found in Appendix-A.

As it can be noted from equations 3.2.5 and 3.2.6, the channels are modulated from baseband to the frequency $(\omega_c\text{-}\omega_i)$. ω_c is the center wavelength of the composite channel and ω_i is the modulated wavelength of the ith channel. The concept of optical modulation and multiplexing as used in FiberSim can be schematically represented as shown in figure 3.9.
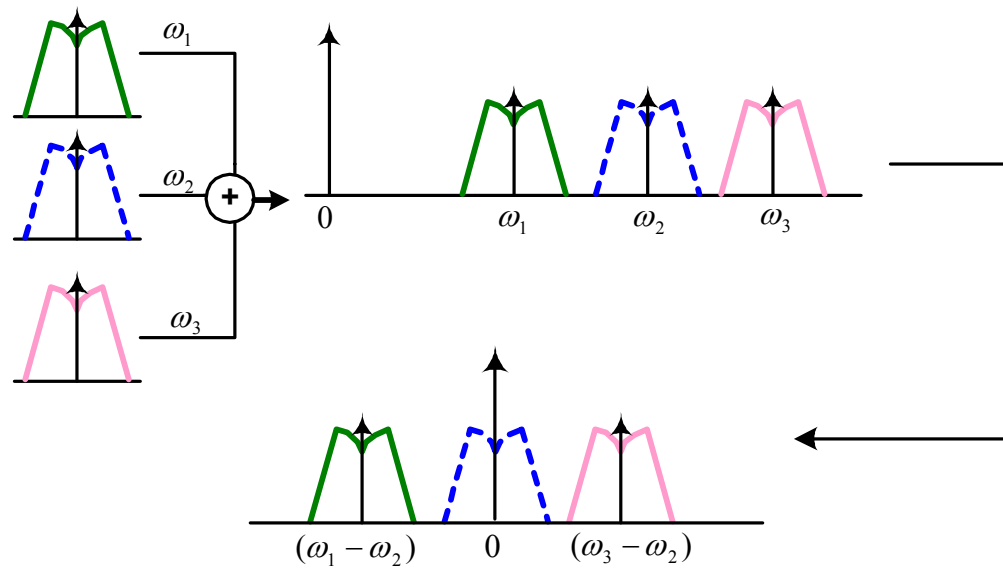
Figure 3.9: Optical modulation and multiplexing in FiberSim

3.3.5. Optical Multiplexers

The optical multiplexer module in FiberSim is used to add the individual channels as a single entity before being launched onto a fiber. The various channels multiplexed together to obtain a single composite signal can be expressed as

$$A_{mux}(t) = \sum_{i=1}^{N} A_i(t) \qquad \ldots (3.2.7)$$

where N represents the total number of channels that are multiplexed. The concept of optical multiplexing is as shown in figure 3.9.

3.3.6. Optical Fibers

An optical signal propagating through a fiber undergoes attenuation, dispersion and nonlinear effects. The optical fiber module in FiberSim evaluates and applies the linear and nonlinear effects encountered by a signal during its propagation to the signal envelope.

The propagation equation 2.3.17 gives a mathematical representation for the nonlinear propagation of light signal through an optical fiber. The solution for the propagation equation cannot be obtained analytically, but can be obtained numerically using split-step Fourier transforms method. As described in the split-step Fourier transform method in section 2.4, the fiber is broken down into smaller sections with step size of say Δz. The signal is propagated through a distance of $\Delta z/2$ with dispersion and loss only. At the end of $\Delta z/2$ the nonlinearities for the entire step size Δz is applied to the signal and the rest of the step size is propagated with dispersion and loss only. The linear effects such as attenuation and dispersion are applied to the optical signal envelope as discussed below.

If the loss in the fiber is α nepers/m, then the loss applied to the envelope signal for propagation a distance of $\Delta z/2$ is,

$$A_{out}(t) = A_{in}(t) \, \exp\left(-\frac{1}{4}\alpha\,\Delta z\right) \qquad\qquad \text{... (3.2.8)}$$

The effect of dispersion for a propagation distance of $\Delta z/2$ is applied to the envelope signal in the frequency domain and is given by

$$\tilde{A}_{out}(f) = \tilde{A}_{in}(f) \exp\left\{ j\beta_2 (\pi f)^2 \Delta z - \frac{2}{3}\beta_3 (\pi f)^3 \Delta z \right\} \qquad \text{... (3.2.9)}$$

where,
$$\beta_2 = -D \frac{\lambda^2}{2\pi c}$$

$$\beta_3 = D \frac{2\lambda^3}{(2\pi c)^2} + D_{slope} \frac{\lambda^4}{(2\pi c)^2} \qquad \text{... (3.2.10)}$$

where D is the dispersion and D_{slope} is the dispersion slope parameter of the fiber specified in ps/nm.km and ps/nm^2.km respectively.

The amount of pulse broadening due to PMD can be given by [Ref. 6]

$$\sigma_t = \frac{1}{\Delta V}\sqrt{2Ll_c} \qquad \text{... (3.2.11)}$$

where σ_t is the root mean square broadening, l_c is the correlation or coupling length, ΔV is the differential group velocity of the two-waveguide modes (x-polarized & y-polarized) and L is the length of the fiber. The differential group velocity in terms of x-polarized group velocity V_x and y-polarized group velocity V_y is given by

$$\Delta V = \frac{1}{\dfrac{1}{V_x} - \dfrac{1}{V_y}} \qquad \text{... (3.2.12)}$$

The amount of PMD in a fiber is expressed in terms of the PMD coefficient with $ps/\sqrt{km}$ units and by definition is given by

$$PMDcoeff = \frac{\sigma_t}{\sqrt{L}} = \frac{1}{\Delta V}\sqrt{2l_c} \qquad \text{... (3.2.13)}$$

In FiberSim, for systems with PMD we are required to use a constant step size Δz for simulation. Hence the amount of differential group velocity induced by a propagation of $\Delta z/2$ in a fiber is

$$\Delta V = \frac{1}{PMDcoeff}\sqrt{\Delta z}$$

... (3.2.14)

The relation between the differential group velocity and differential group delay is as follows

$$\Delta t = l \frac{1}{\Delta V}$$

... (3.2.15)

where l is the section length. The amount of differential group delay induced by a propagation of $\Delta z/2$ in a fiber due to PMD is evaluated and the delay Δt is applied in the form of $+\Delta t/2$ and $-\Delta t/2$.

$$\frac{\Delta t}{2} = \frac{1}{2}\frac{\Delta z}{2}\frac{PMDcoeff}{\sqrt{\Delta z}} = \frac{PMDcoeff}{4}\Delta z$$

... (3.2.16)

Also in FiberSim, the differential group velocity can be evaluated from the birefringence of the fiber (which is the result of different refractive indices for the x-polarized and y-polarized modes). The birefringence in the fiber is expressed in terms of the birefringence coefficients with ps/km units. The evaluated differential group velocity is then applied to the envelope.

The evaluation nonlinear effects such as SPM, XPM, FWM etc is more complex than the effects of attenuation and dispersion. The propagation equation

2.3.17 contains both instantaneous and delayed nonlinear response components. The evaluation of instantaneous components is straight forward, as it does not involve any integrals or the fast varying Raman response function $h_r(t)$. The calculation of the delayed nonlinear response involves a number of integrals. These integrals have a common convolution term of the form

$$\int_0^\infty f(t - \tau) h_r(\tau) \, d\tau \qquad \qquad ... (3.2.17)$$

where $f(t)$ is typically a slowly varying function and $h_r(t)$ is the fast varying Raman response function. The various methods used in FiberSim to numerically compute the above convolution integral are direct integration, moments method and FFT method.

- **Direct Integration Method**

The direct integration method is the simplest method to evaluate the convolution integral. The integral interval is equally divided into several subintervals and the integration is computed by summing the function to be integrated at each subintervals. The numerical accuracy of this method depends on the number of subintervals chosen, i.e. the number samples of $f(t-\tau)$ and $h_r(t)$ taken. Since $h_r(t)$ is a fast varying function, for better numerical accuracy one must use a simulation bandwidth of the order of 60-70 THz. But this leads to over-sampling of the relatively slowly varying function $f(t)$ and thereby decreases the numerical efficiency.

- **Moments Method**

The moments method can be used to get around the over-sampling of the relatively slowly varying $f(t)$. The moments method also brings down the computational time and the required simulation bandwidth. The Taylor series expansion of $f(t-\tau)$ gives

$$f(t-\tau) = f(t) - \tau \frac{\partial}{\partial t} f(t) + \frac{\tau^2}{2} \frac{\partial^2}{\partial t^2} f(t) - \text{........} \qquad \text{... (3.2.18)}$$

On substituting the above, equation 3.2.17 becomes

$$\int_0^\infty f(t-\tau) h_r(\tau) d\tau = f(t) \int_0^\infty h_r(\tau) d\tau - \frac{\partial}{\partial t} f(t) \int_0^\infty \tau h_r(\tau) d\tau + \frac{1}{2} \frac{\partial^2}{\partial t^2} f(t) \int_0^\infty \tau^2 h_r(\tau) d\tau - \text{.....}$$

$$\text{... (3.2.19)}$$

The above integrals can be computed easily, because the Raman response function has a temporal variation only in $0 < t < 1$ picoseconds range, as seen from figure 2.5. Defining

$$\tau_R^1 = \int_0^\infty \tau h_r(\tau) d\tau \qquad \text{- First order moment of the nonlinear response function}$$

$$\tau_R^2 = \int_0^\infty \tau^2 h_r(\tau) d\tau \qquad \text{- Second order moment of the nonlinear response}$$

function

and similarly for the higher order moments, equation 3.2.19 can be represented as

$$\int_0^\infty f(t-\tau) h_r(\tau) d\tau = f(t) \int_0^\infty h_r(\tau) d\tau - \tau_R^1 \frac{\partial}{\partial t} f(t) + \frac{1}{2} \tau_R^2 \frac{\partial^2}{\partial t^2} f(t) - \text{.....}$$

$$\text{... (3.2.20)}$$

The numerical accuracy of this method depends on the number of terms included in the Taylor expansion of $f(t-\tau)$ and on the accuracy of calculation of the derivatives. The derivatives can be calculated with a 5 points resolution using

$$\frac{df(t)}{dt} = \frac{1}{dt}\frac{\{f(t-2)-8f(t-1)+8f(t+1)-f(t+2)\}}{12} \qquad \text{... (3.2.21)}$$

$$\frac{d^2f(t)}{dt^2} = \frac{1}{(dt)^2}\frac{\{-f(t-2)+8f(t-1)-14f(t)+8f(t+1)-f(t+2)\}}{4} \qquad \text{... (3.2.22)}$$

If the signal envelope has a bandwidth that is within the linear range of Raman gain curve (< 4 THz), first order moment is sufficient to give reasonable results. But if the signal bandwidth extends beyond the linear range of Raman gain curve, higher order moments (2nd & 3rd order) should also be included.

- **FFT Method**

The FFT method makes use of the property that convolution in time domain is equivalent to multiplication in frequency domain. This can represented as

$$\int_0^\infty f(t-\tau)h_r(\tau)\,d\tau = FFT^{-1}\{F(\omega)\,H_r(\omega)\} \qquad \text{... (3.2.23)}$$

where $F(\omega)$ and $H_r(\omega)$ are the Fourier transform of $f(t)$ and $h_r(t)$ respectively.

As $h_r(t)$ is defined only for $t > 0$, it can be written as

$$h_r(t) = A\sin\left(\frac{t}{\tau_1}\right)\exp\left(-\frac{t}{\tau_2}\right)u(t) \qquad \text{where } A = \frac{\tau_1^2 + \tau_2^2}{\tau_1\,\tau_2^2} \qquad \text{... (3.2.24)}$$

Hence the spectrum of $h_r(t)$ is given by

$$H_r(\omega) = \frac{A/2}{\left(\dfrac{1}{\tau_1} - \omega\right) + \dfrac{j}{\tau_2}} - \frac{A/2}{\left(-\dfrac{1}{\tau_1} - \omega\right) + \dfrac{j}{\tau_2}} \qquad \text{... (3.2.25)}$$

$F(\omega)$ can be obtained using the Fast Fourier Transform of $f(t)$. Though the bandwidth of $H_r(\omega)$ is normally several times that of $F(\omega)$, the bandwidth of their multiplication is solely determined by the bandwidth of $F(\omega)$. Hence it is sufficient to calculate only the spectrum of $H_r(\omega)$ that falls within the signal bandwidth, and use it in equation 3.2.23. Since the simulation bandwidth is determined by the signal bandwidth, rather than the large bandwidth of $H_r(\omega)$, the computational efficiency of FFT method is much better than that of the direct integration method.

After the nonlinearities are evaluated using any of the three methods discussed above, they are applied to the signal envelope $A(t)$ as follows. From the propagation equation 2.3.17, it can be seen that the instantaneous SPM, instantaneous XPM, delayed self-polarization modulation and delayed cross-polarization modulation terms are functions of A_i, while the other nonlinearity terms are independent of A_i. Hence considering only nonlinearities the propagation equation can be expressed as

$$\frac{\partial A}{\partial z} = jkA + jg \qquad \text{... (3.2.26)}$$

where k and g can be evaluated numerically using any of the three methods mentioned earlier in this section. The solution for the above equation is of the form

$$A(z_0 + \Delta z) = A(z_0)\exp\{jk\Delta z\} + jg\Delta z \qquad \ldots (3.2.27)$$

3.3.7. Optical Amplifiers

Optical amplifiers are important components in the fiber-optic links. They are used to compensate the attenuation in fibers. In WDM systems, amplification is usually achieved using either Erbium-doped fiber amplifiers (EDFA) or Raman amplifiers. The noise arising from the amplifiers (both EDFAs and Raman amplifiers) propagate through a WDM system and are one of the factors for system degradation.

The EDFA model in FiberSim is a flat gain amplifier that uses the Equivalent noise bandwidth model. In equivalent noise bandwidth model, the spectrum of the amplified spontaneous emission (ASE) noise is assumed to be flat. The ASE noise is the major noise source from an optical amplifier. The noise parameter of an EDFA is expressed in terms of the noise figure of the EDFA in FiberSim. The evaluation of the values of various noises originating from EDFA, using the noise figure, is discussed in section 3.4.

An EDFA of gain G dB increases the optical power of the input signal by G dB, and its relationship to the optical signal envelope $A(t)$ is given by

$$A_{out}(t) = A_{in}(t) \sqrt{10^{\frac{G}{10}}} \qquad \qquad \text{... (3.2.28)}$$

Raman amplifiers can be modeled as distributed or lumped amplifiers, with backward flowing Raman pumps. They make use of the SRS phenomenon discussed in section 2.2.5 for optical amplification. The modeling of Raman amplified fibers in FiberSim uses an iterative approach in which, initially a pump power profile across the fiber is considered by just taking into account the fiber attenuation. During the next iteration, the SRS effect is taken into account to change the pump profile and is repeated till the pump profile stabilizes. Also, an equivalent noise figure value is evaluated from the pump powers, fiber attenuation, length of the fiber and Raman gain coefficient, and is explained in appendix-B. This equivalent noise figure value is then used to evaluate the values of various noises as discussed in section 3.4.

3.3.8. Optical Filters and Optical Demultiplexers

An optical filter is used in an optical link to separate the different channels or to suppress the ASE noise. The optical filter types available in FiberSim are Ideal, Bessel, Butterworth and Notch filters. The Bessel filter is most commonly used as it has a linear phase response. The bandwidth of the optical filter is usually chosen to be several times larger than the bandwidth depending on the channel spacing.

An optical demultiplexer is used in FiberSim to bring the optical carrier back to the baseband frequency. An optical demultiplexer basically filters out the optical channel from the higher frequency and shifts it to the baseband. The action performed by the optical demultiplexer in FiberSim can be diagrammatically represented as shown in figure 3.10.
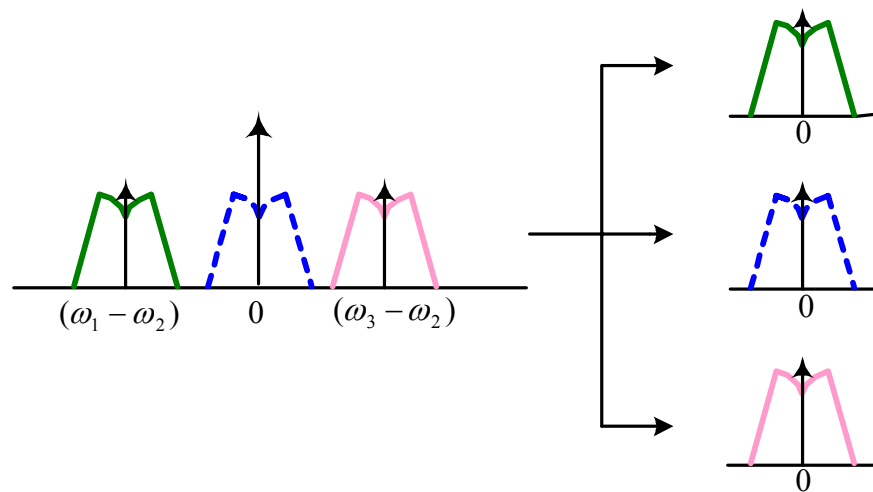
Figure 3.10: Optical demultiplexing in FiberSim

3.3.9. Optical Detectors

An optical detector is used to convert the optical signal back to electrical signal. In WDM systems, a photodetector is typically used as optical detector. In FiberSim, the parameter that is used to characterize the photodetector is the Quantum efficiency η, which is the number of current contributing electron-hole pairs generated per incident photon.

The responsivity of the photodetector is given by

$$R \; = \; \frac{I_p}{P_0} \; = \; \frac{\eta q}{h\nu} \qquad\qquad \text{... (3.2.29)}$$

where I_p is the electric current produced by the incident optical power P_0, q is the electric charge, $h\nu$ is the energy per photon and η is the quantum efficiency. The detector output is proportional to the modulus square of signal envelope,

$$y_i(t) \propto \left| A_i(t) \right|^2 \qquad\qquad \text{... (3.2.30)}$$

3.4.   BER and Q Calculation in FiberSim

Bit error rate (BER) is the percentage of bits that have errors relative to the total number of bits received in a transmission. In numerical simulation models like FiberSim, BER cannot be directly calculated by counting the number of error bits. This is because, FiberSim being a numerical simulation model, cannot model long data sequences, due to limited computer speed and memory. The number of bits used in the input signals is usually limited to a few hundred. As BER values in fiber optic communication links are generally less than 10^{-9}, hundreds of bits in simulation cannot be used to directly calculate the BER by counting the error bits.

In FiberSim, the BER is calculated from a parameter known as Q-factor. The BER is related to Q-factor by

$$BER = \frac{1}{2} erfc\left(\frac{Q}{\sqrt{2}}\right) \approx \frac{1}{\sqrt{2\pi}} \frac{\exp(-Q^2)}{Q} \qquad \text{... (3.3.1)}$$

where the Q-factor is calculated from the following expression [Ref. 7]

$$Q = \frac{I_1 - I_0}{\sqrt{\sigma_1^2} + \sqrt{\sigma_0^2}} \qquad \text{... (3.3.2)}$$

where I_1 and I_0 are the detector current levels for a '1' and '0'. σ_1^2 *and* σ_0^2 are respectively the variances of the detector noise currents when a '1' and '0' are being received. The detector current levels are given by

$$I_1 = RP_1 \text{ and } I_0 = RP_0 \qquad \text{... (3.3.3)}$$

where P_1 and P_0 are the optical power levels of the lowest '1' and the highest '0' respectively and R is the responsivity of the photodetector.

In FiberSim, the noise characteristics of EDFAs are calculated in the following manner. An EDFA of gain G and noise figure NF has a noise power spectral density given by

$$S_{sp} = \frac{NF}{2} Ghv \qquad \text{... (3.3.4)}$$

where h is the Planck's constant and v is the optical carrier frequency. For a WDM system with M EDFAs, the noise spectral density at the end of Nth EDFA (where $M > N$) is given by

$$S_{sp} = \frac{1}{2} hv \sum_{i=1}^{N} (NF_i) G_i L_i \qquad \text{... (3.3.5)}$$

where NF_i and G_i are the noise figure and gain of the ith amplifier. L_i is the net gain (or loss) from the output of the ith amplifier to the detector.

The major noise sources in a WDM system are the spontaneous emission noise from the amplifier, the shot noise and thermal noise from the photodetector. Along with these are the beating noise sources resulting from the beating of shot noise with spontaneous emission noise (shot-spontaneous noise), spontaneous emission noise with itself (spontaneous-spontaneous noise) and the signal with spontaneous emission noise (signal-spontaneous noise).

The variance σ_0^2 can be obtained by summing the variances of various noise sources generated while transmitting a '0', which gives

$$\sigma_0^2 = \sigma_T^2 + \sigma_{sp-sp}^2 + \sigma_{s-sp}^2 + \sigma_{s0}^2 \qquad \qquad .... (3.3.6)$$

where [Ref. 4] ,

Thermal noise variance $\qquad \qquad \sigma_T^2 = \dfrac{4k_B T}{R_L}\Delta f \qquad \qquad ... \ (3.3.7)$

Spontaneous-spontaneous noise $\qquad \sigma_{sp-sp}^2 = 4R^2 S_{sp}\Delta v_{opt}\Delta f \ ... (3.3.8)$

Shot-spontaneous noise variance $\qquad \sigma_{s-sp}^2 = 4qRS_{sp}\Delta v_{opt}\Delta f \qquad ... (3.3.9)$

Shot noise variance (for '0') $\qquad \sigma_{s0}^2 = 2qRS_{sp}\Delta v_{opt}\Delta f \qquad ... (3.3.10)$

where K_B is the Boltzman constant, T is the operating temperature, R_L is the receiver load resistance, Δf is the receiver bandwidth, R is the responsivity of the photodetector, Δv_{opt} is the optical bandwidth and q is the charge of an electron.

Similarly the variance σ_1^2 can be found to be

$$\sigma_1^2 = \sigma_T^2 + \sigma_{sp-sp}^2 + \sigma_{s-sp}^2 + \sigma_{s1}^2 + \sigma_{sig-sp}^2 \qquad ... (3.3.11)$$

where [Ref. 4],

Signal-spontaneous noise variance $\quad \sigma_{sig-sp}^2 = 4R^2 P_1 S_{sp} \Delta f \qquad ... (3.3.12)$

Shot noise variance (for '1') $\quad \sigma_{s1}^2 = 2qR\left(P_1 + S_{sp}\Delta v_{opt}\right)\Delta f \; ...$

(3.3.13)

where P_1 is the power level of the lowest received '1'.

4. Modulation Techniques for Increasing Spectral Efficiency in WDM Systems

There is a growing demand for increasing capacity and efficiency in fiber-optic networks due to the explosion of internet-based services and explosion of communication traffic. This demand can be addressed by designing WDM systems with multi-terabit capacity over 1000s of kilometers. Multi-terabit capacity can be achieved by increasing the utilized bandwidth and/or by the spectral efficiency. Figure 4.1 shows the directions for better system performance. The vertical and horizontal axes give the techniques that can be used for increasing the spectral efficiency and the utilized bandwidth respectively. The outward axis gives the techniques that can be used to increase the transmission distance.

Spectral Efficiency

➤ Polarization Interleave Multiplexing
➤ Modulation format (Duobinary, VSB ..)

➤ Gain shifted TDFA for S-band

Utilized Bandwidth

➤ Dispersion Management
➤ Distributed Raman Amplification
➤ Forward Error correction (FEC)

Transmission Distance
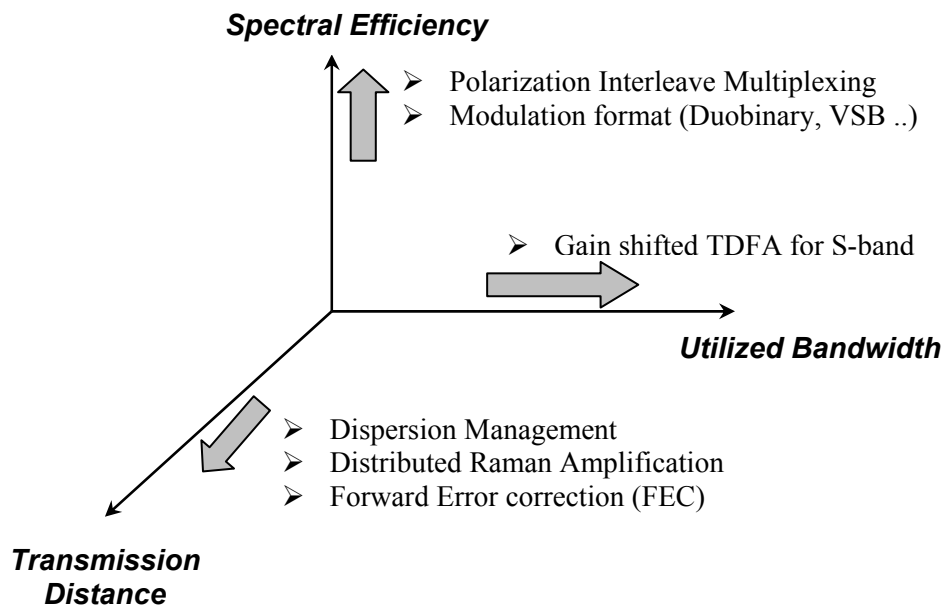
Figure 4.1: Techniques for improving the transmission capacity in WDM systems [Ref. 9]

The transmission distance of multi-terabit capacity WDM systems can be increased by employing proper dispersion management, distributed Raman amplification, and forward error correction (FEC). The effects of dispersion can be minimized by using dispersion-shifted fiber, which has smaller dispersion value at 1550 nm and also smaller dispersion slope value. Dispersion slope compensation, which offers identical dispersion compensation for all the channels, also helps in reducing the effects of dispersion in multi-terabit capacity WDM systems. The advantage of using dispersion slope compensation is explained in section 5.2.2. The attenuation in the fiber can be overcome using distributed Raman amplification that has lower noise characteristics when compared to EDFAs. The lower noise characteristic of Raman amplifiers help to increase the transmission distance. Also FEC, which is essentially the incorporation of a suitable code into a data stream for the detection and correction of data errors, helps us to increase the transmission distance [Ref. 10]. Some of the FEC codes that have been reportedly used in optical transmission system are Reed Solomon (RS) code and Veterbi convolution code. FEC-coded transmission can tolerate lower optical SNR, which in turn reduces impairments induced by nonlinearity, with the net effect being an increase in the Q-factor when signal power is reduced. The use of FEC leads to an increase in Q value by 4 dB.

An effective way to achieve a wide bandwidth is to use a 1.46 μm band (S-band) thulium-doped fiber amplifier (TDFA) in addition to the 1.55 μm (C-band)

EDFA and 1.58 μm (L-band) EDFA. This helps us to raise the utilized bandwidth to more than 100 nm. To utilize a wavelength region with lower fiber loss than at the 1.46 μm band, a gain-shifted thulium-doped fiber amplifier (GS-TDFA) operating in the 1.49 μm band can be used. Figure 4.2 shows the gain and noise characteristics of a GS-TDFA. One can achieve a gain of 25 dB and output power of +17 dBm [Ref. 9] using GS-TDFA. Thus, GS-TDFA opens up a new WDM window in the 1.48-1.51 μm region (S band), and the total WDM signal bandwidth is increased to over 100 nm with conventional EDFAs in C and L bands.
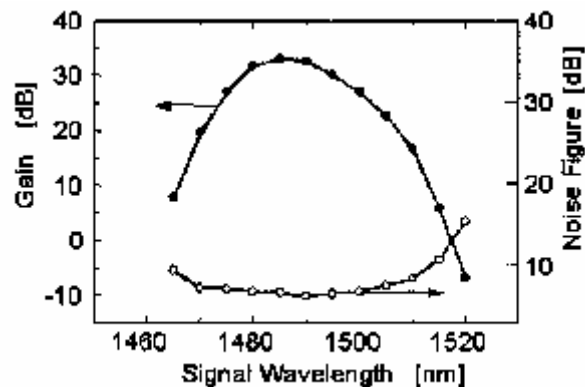
Figure 4.2: Gain and noise figure characteristics of GS-TDFA

The vertical axis of figure 4.1 deals with techniques to increase spectral efficiency. The spectral efficiency is the density of a WDM system and is the average channel capacity divided by the average channel spacing. From this definition of spectral efficiency, it can be seen that decreasing of channel spacing leads to increased spectral efficiency. The maximum spectral efficiency in

practical WDM systems with conventional binary signal is 0.4 bit/s/Hz, in which 40 Gbit/s optical signals are multiplexed with 100 GHz channel spacing [Ref. 9]. Different techniques are now being explored to increase the spectral efficiency of WDM system to reach 1 bit/s/Hz. In high spectral efficiency systems, due to the dense packing of channels, the cross talk between neighboring channels caused by nonlinear effects such as XPM and FWM becomes more pronounced. One of the techniques used for mitigating the impairments due to nonlinear effects such as XPM and FWM and hence mitigating the effects of cross talk between neighboring channels is polarization interleave multiplexing [Ref. 9].

In polarization interleave multiplexing, each channel is orthogonally polarized to the neighboring channels. This makes it necessary to have an automatic polarization-tracking control for the polarization demultiplexing in the receiver for stable operations. Polarization interleave multiplexing can be achieved by separately modulating the even and odd channels in a WDM transmitter and performing polarization-multiplexing using polarization beam splitters (PBS). Polarization demultiplexing can be achieved by using optical filters for separating the channels and using a PBS with polarization controller [Ref. 11]. But the performance of WDM system with polarization interleave multiplexing is degraded by the polarization dependency in the fiber. PMD degrades the orthogonality between the signal and neighboring channels.

Apart from using polarization interleave multiplexing, which helps to reduce the nonlinear effects of XPM and FWM in the densely packed WDM systems, spectral efficiency in WDM systems can be increased by using different modulation formats. In this chapter we will look into some of the modulation formats that can be used for increasing the spectral efficiency of WDM systems. As suggested earlier, decreasing the channel spacing can bring about the increase of spectral efficiency. Since the information carried on each channel occupies a certain bandwidth or spectrum, the channel spacing cannot be decreased beyond a certain limit as that would lead to overlapping of adjacent channel information. One method would, therefore be, to decrease the optical spectrum of a channel (without decreasing the amount of information or data carried) so that it can be placed more closely to its neighbor. The modulation formats that make use of this method to increase the spectral efficiency are *optical Duobinary signaling* and *differential quadrature phase-shift key* (DQPSK*) signaling*. The other method makes use of the fact that the complete information of a channel is contained in one half of its spectrum and that the other half of the spectrum is just redundant information, which can be ignored or can be reproduced from the first half of the spectrum. The modulation techniques that make use of this method to increase the spectral efficiency are *VSB-RZ signaling* and *VSB demultiplexing*.

4.1. Optical Duobinary Signaling

Optical duobinary signaling features three level coding, with correlation between these levels in order to reduce bandwidth. The principle of optical duobinary transmission system is as illustrated in figure 4.3 [Ref. 12]. Here, the three intermediate logical levels in duobinary signals are 0, 1 and −1 (obtained by an optical π-phase shift). The optical duobinary signal has two intensity levels "on" and "off" as shown in figure 4.3. The "on" state can have one of two optical phases, 0 and π. The two "on" states correspond to the logic states "1" and "-1" of the duobinary encoded signal and the "off" level corresponds to the logic state "0" of the duobinary encoded signal.
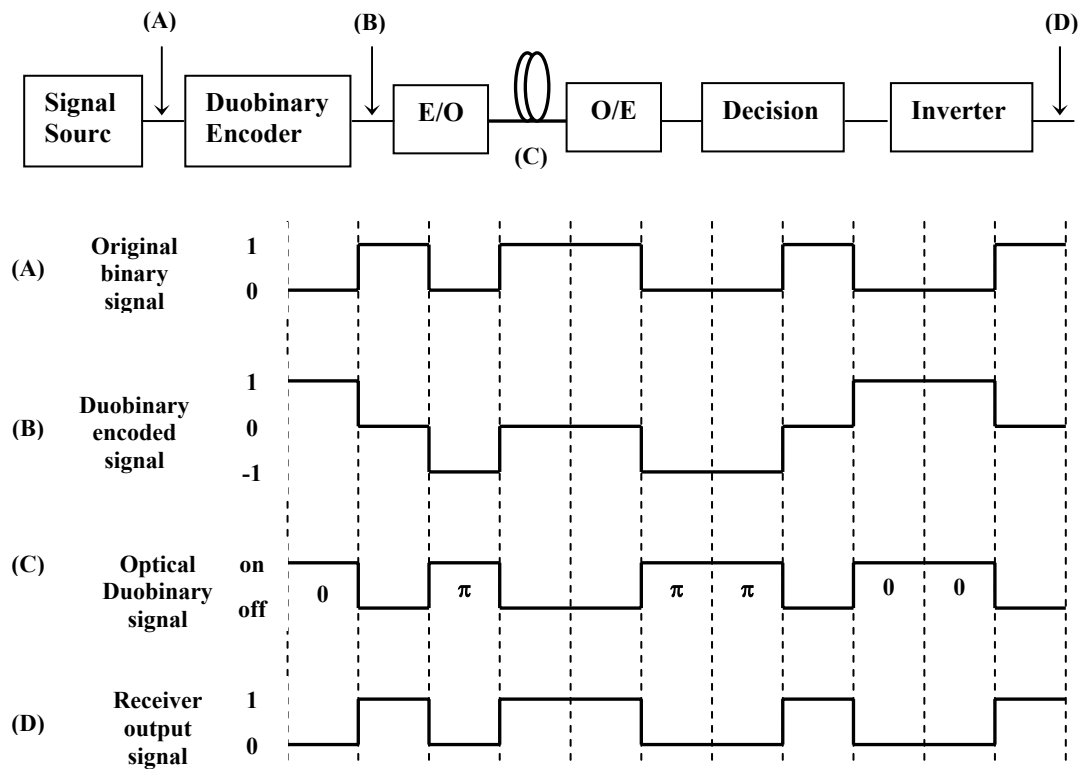
Figure 4.3: Principle of optical duobinary signaling [Ref. 12]

The two main advantages of this modulation format are increased tolerance to the effects of chromatic dispersion and an improved spectral efficiency. Both these advantages are attributed to the fact that the duobinary coding reduces the optical spectrum to half of that obtained using binary intensity modulates signals. The optical duobinary signals can be demodulated into a binary signal with a conventional direct detection type optical receiver and this is an important advantage in terms of ease of implementation.

Experimental systems with 0.6 bit/s/Hz have been demonstrated using optical duobinary signaling with 2.6 Tbit/s (20 Gbit/s x 132 channels) capacity [Ref. 11].

4.2. DQPSK Signaling

In optical differential quadrature phase-shift keying (DQPSK), information is encoded in the differential optical phase between successive bits $\Delta\phi$, where $\Delta\phi$ can take one of the four values [0, $\pi/2$, π, $3\pi/4$]. Since each symbol transmits 2 bits of information, the symbol rate is equal to half the total bit rate B. Since DQPSK format encodes two bits onto each symbol, its spectral efficiency is double that of on-off keying (OOK) format. The advantages of DQPSK format include improved receiver sensitivity (over OOK), high PMD and chromatic dispersion tolerance and large immunity to narrow optical filtering [Ref. 13].

The DQPSK signals can be formed using a digital precoder and optical encoder, as shown in figure 4.4 [Ref. 14]. The precoder function is required to provide a direct mapping of data from the input to the output. The four inputs to the precoder consist of two input data streams and the two time delayed precoder output and can be represented by equation 4.2.1. The encoder consists of a 3 dB optical power splitter, two MZMs, an optical phase shift and an optical power combiner. The decoding is performed using a pair of Mach-Zehnder interferometers, each with an optical delay τ equal to symbol period 2/B. The differential optical phase between interferometer arms is set to $\pi/4$ and $-\pi/4$ for upper and lower branches respectively. The outputs from the decoder are binary NRZ signals and hence conventional clock and data recovery can be used.

$$I_k = v_k \oplus \left(\bar{I}_{k-1} \bar{Q}_{k-1} \right) + u_k \oplus \left(I_{k-1} \bar{Q}_{k-1} \right)$$

$$\text{... (4.2.1)}$$

$$Q_k = u_k \oplus \left(\bar{I}_{k-1} \bar{Q}_{k-1} \right) + v_k \oplus \left(\bar{I}_{k-1} Q_{k-1} \right)$$
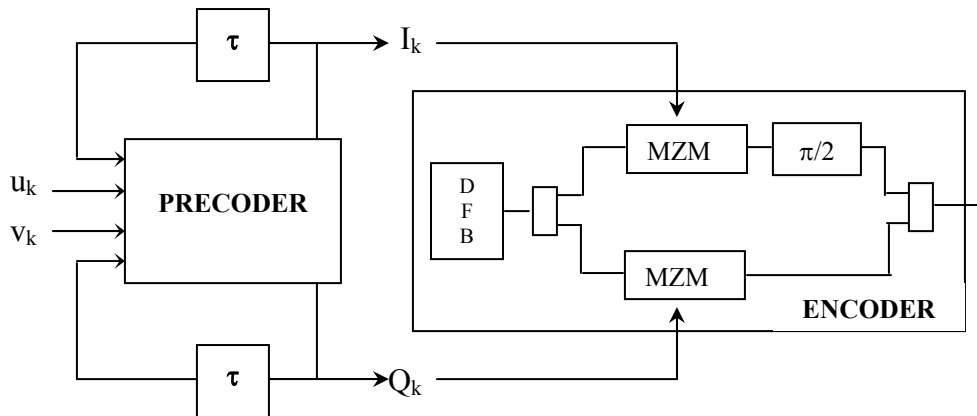
Figure 4.4: DQPSK signaling [Ref. 14]

Experimental system transmitting RZ-DQPSK format signals with 0.8 bit/s/Hz spectral efficiency over a distance of 100 km of SMF-28 fiber have been designed [Ref. 13]. Systems with spectral efficiency of 1.6 bits/s/Hz using RZ-DQPSK and polarization interleave multiplexing have also been reported [Ref. 15].

4.3. VSB – RZ Signaling

Vestigial side band (VSB) signals are obtained by partially removing one of the sideband spectra of the conventional double spectrum signal with a sharp optical filter. This leads to decrease of the channel spectrum, enabling a decrease in channel spacing, and hence an increase of spectral efficiency in WDM systems. Figure 4.5 shows the optical spectra of DSB-RZ and VSB-RZ signals.
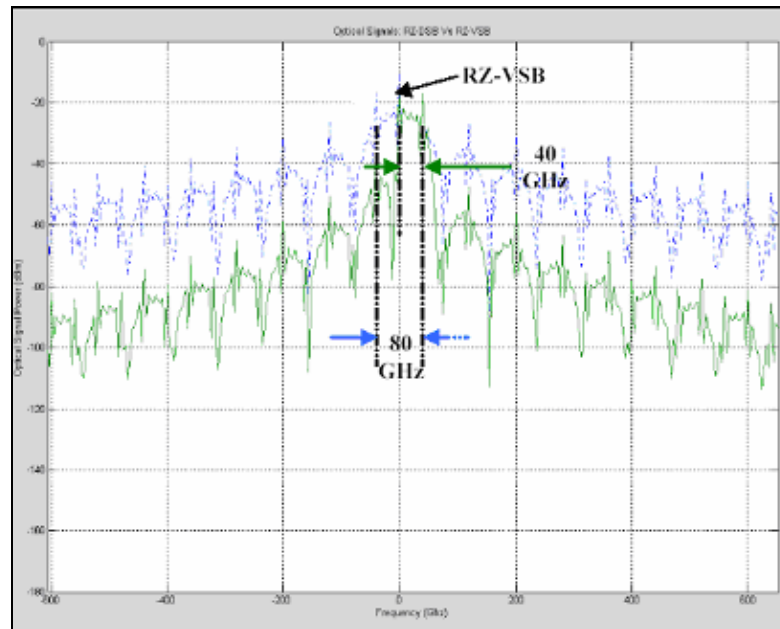
Figure 4.5: Optical spectra of DSB-RZ and VSB-RZ signals [Ref. 16]

For long distance transmission, the RZ format is considered a suitable signal format to overcome fiber nonlinearity [Ref. 17]. With spectral filtering at the transmitter to form VSB-RZ signals, the system is more tolerant to dispersion compensation error [Ref. 18]. Figure 4.6 shows 20 Gbit/s channels with VSB-RZ separated by 35 GHz channel spacing.
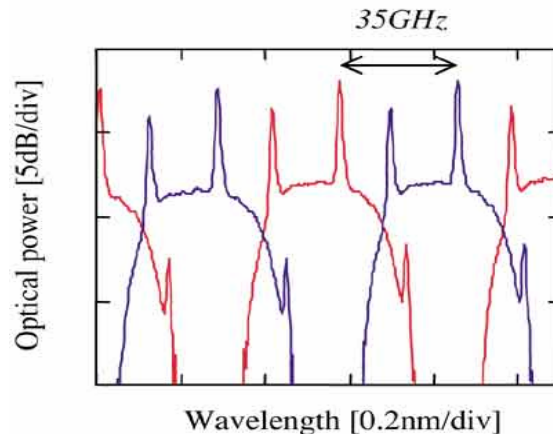
Figure 4.6: Spectra of 20 Gbit/s WDM signal with VSB-RZ format [Ref. 17]

A WDM system with 2 Tbit/s capacity (100 x 20 Gbit/s) using VSB-RZ and a spectral efficiency of 0.57 bit/s/Hz over a distance of 2700 km of fiber has been reported [Ref. 19]. 20 Gbit/s, 100 WDM over 4000 km transmission with a spectral efficiency of 0.6 bit/s/Hz using VBS-RZ has also been demonstrated [Ref 16].

4.4. VSB Demultiplexing

VSB demultiplexing also makes use of the fact that both optical sidebands of a NRZ modulated optical spectrum contain redundant information. It is difficult to implement VSB signals at the transmitter, because the suppressed sidebands are rapidly reconstructed during transmission due to fiber nonlinearities. Instead of performing VSB at the transmitter, we can use VSB filtering only at the receiver side in conjunction with a modified channel allocation scheme.

The approach followed for VSB demultiplexing is that the channels are spaced with alternating wider and narrower spacing as shown in figure 4.7. From the figure, it can be seen that one of the sideband spectrum of each channel is distorted by the sideband of the neighboring channel, whereas the other sideband of the channel is relatively unharmed. At the receiver, one can filter out the sideband, which experiences smallest overlap with adjacent channels and ignore the other sideband of the channel. Since a VSB-like filtering of the channel is performed at the demultiplexer, it is called as VSB demultiplexing.
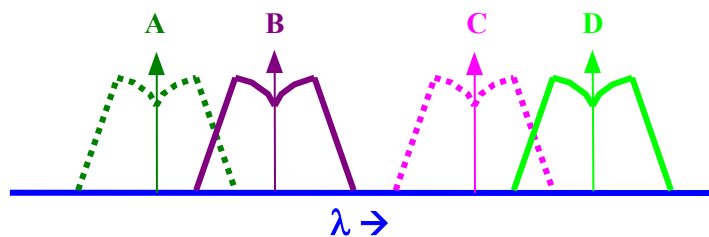
Figure 4.7: Channel spacing scheme for VSB demultiplexing

The VSB demultiplexing technique can be demonstrated further with the following example. The channel spacing and demultiplexer optical filter parameters that were reported for an experimental 40 Gbit/s WDM system that used VSB demultiplexing to achieve multi-terabit/s capacity [Ref. 20, 21] is discussed below. The channel spacing scheme used in a 40 Gbit/s experimental system is an alternatively spaced 75 GHz and 50 GHz channels [Ref. 20]. With an average spacing of 62.5 GHz for a 40 Gbit/s system, one can achieve a spectral efficiency of 0.64 bit/s/Hz. Figure 4.8 (a) gives the optical spectra of 40 Gbit/s channels spaced alternatively 75 GHz and 50 GHz apart. As explained earlier the sidebands within the 75 GHz spacing are demultiplexed, while the sidebands within the 50 GHz spacing is rejected as depicted in figure 4.8 (b) and (c).
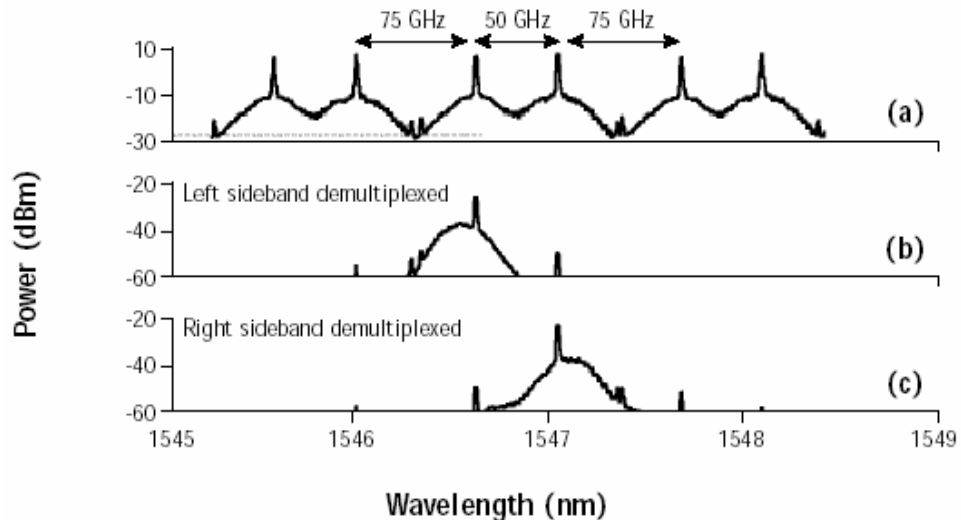
Figure 4.8: Optical spectra depicting channel allocation and demultiplexing [Ref. 20]

At the receiver, a very narrow optical filter demultiplexes the VSB of a given channel by detuning it off the channel central frequency towards the 75 GHz spaced neighboring channel. Thus, the sidebands experiencing the smallest overlap with adjacent channel are demultiplexed with a very low system penalty; VSBs within the 50 GHz spacing are rejected as shown in figure 4.9. For the 40 Gbit/s WDM system with 75 GHz and 50 GHz alternate spacing, the narrow optical filter used for demultiplexing the channels has an optical bandwidth of 60 GHz and an offset frequency of 20 GHz.
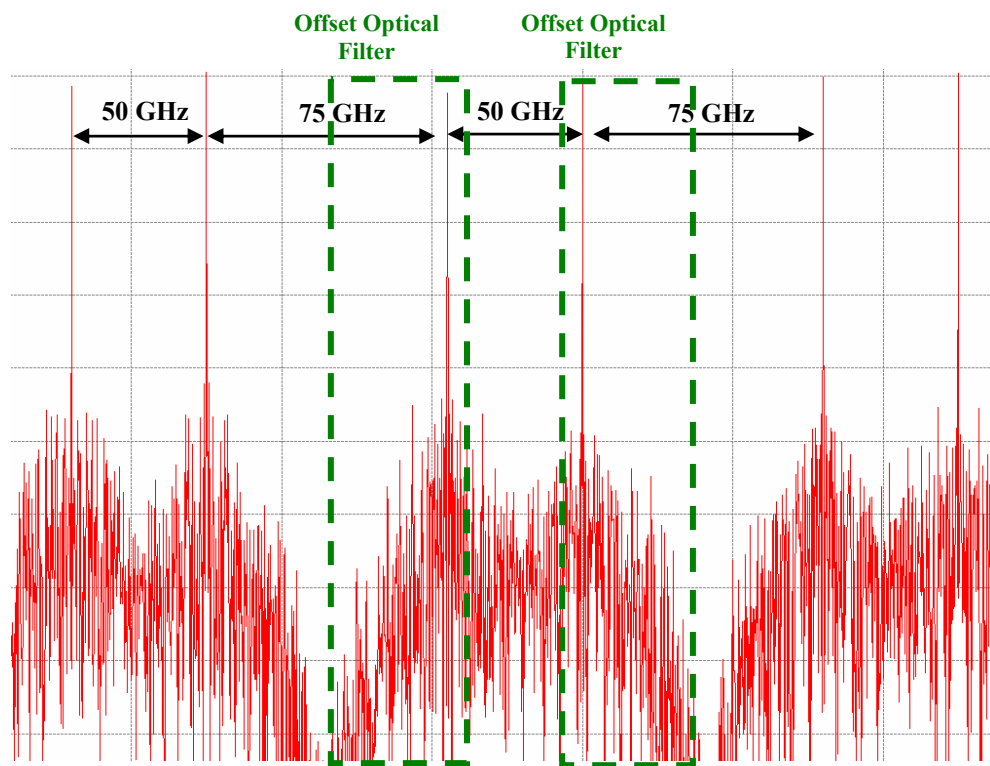
Figure 4.9: Offset optical filtering at demultiplexer

Transmission of 125 WDM channels at 42.7 Gbit/s over 12x100 km of Teralight Ultra fiber with a spectral efficiency of 0.64 bit/s/Hz using VBS demultiplexing and polarization interleave multiplexing has been demonstrated [Ref. 2]. Also, a 40 Gbit/s WDM system with total capacity of 5.12 Tbit/s using VBS demultiplexing and polarization interleave multiplexing over 300 km of Teralight fiber transmission and 1.28 bit/s/Hz spectral efficiency has been reported [Ref. 20].

5. Modeling and Analysis of an experimental VSB Demultiplexing system

The previous chapter mentioned the different techniques that can be used to increase the spectral efficiency of WDM system and described in detail the VSB demultiplexing technique. Of the described techniques, VSB demultiplexing is unique in that it utilizes conventional NRZ-modulated signals, which is used predominantly in the existing deployed WDM systems. Optical duobinary signaling and DQPSK signaling use new modulation formats, which require altering the transmitter and receiver equipments for deployment. VSB at the transmitter and the VSB demultiplexing seem more appropriate to achieve high spectral efficiency with the existing WDM systems.

Recently, a VSB system was reported by Alcatel that used VSB demultiplexing to achieve 5 Tbit/s capacity over 1200 km of Teralight Ultra fiber [Ref 2]. FiberSim is used to model this experimental system and analyze the effects of a number of parameters on system performance to get a better understanding of the experimental system.

In this chapter, the experimental system reported by Alcatel [Ref 2], which uses the VSB demultiplexing technique to achieve high spectral efficiency, is

described and compared with FiberSim model. The results obtained from this system are compared with that obtained from FiberSim simulation model.

5.1. Alcatel VSB Demultiplexing Experimental system

The vestigial side band demultiplexing technique has been used by Alcatel to achieve 5 Tbit/sec capacity over a distance of 1200 km. The experiment consisted of 125 WDM channels carrying electrically time division multiplexed (ETDM) data at effective rate of 40 Gbit/sec using regular NRZ format. The WDM channels are separated alternatively by 50 and 75 GHz to achieve a spectral efficiency of 0.64 bits/Hz and demultiplexed by optical vestigial side band filtering.

5.1.1. Experimental Setup

The WDM transmitter in the experiment consisted of 125 distributed feedback (DFB) lasers with wavelengths from 1529.94 nm to 1561.22 nm in the C-band and 1571.03 nm to 1602.53 nm in the L-band. To achieve the alternating 50 – 75 GHz spacing, two sets of 125 GHz spaced channels shifted with respect to each other by 50 GHz and corresponding to odd and even channels respectively, were combined using array-waveguide multiplexers in each band (C & L bands). The two sets of channels were modulated independently using Mach-Zehnder modulators fed using a 2^{31}-1 pseudo-random bit sequence (PRBS). In order to

provide effective decorrelation of the data carried by neighboring channels, PRBS were generated electrically using two separate pattern generators. Odd and even channels were interleaved with orthogonal polarization using polarization beam splitters (PBS), boosted using a pre-amplifier and sent into a loop via a 3 dB coupler. The channels had a launch power of -2 dB$_m$. The experimental set up of the recirculating loop is as shown in figure 5.1.
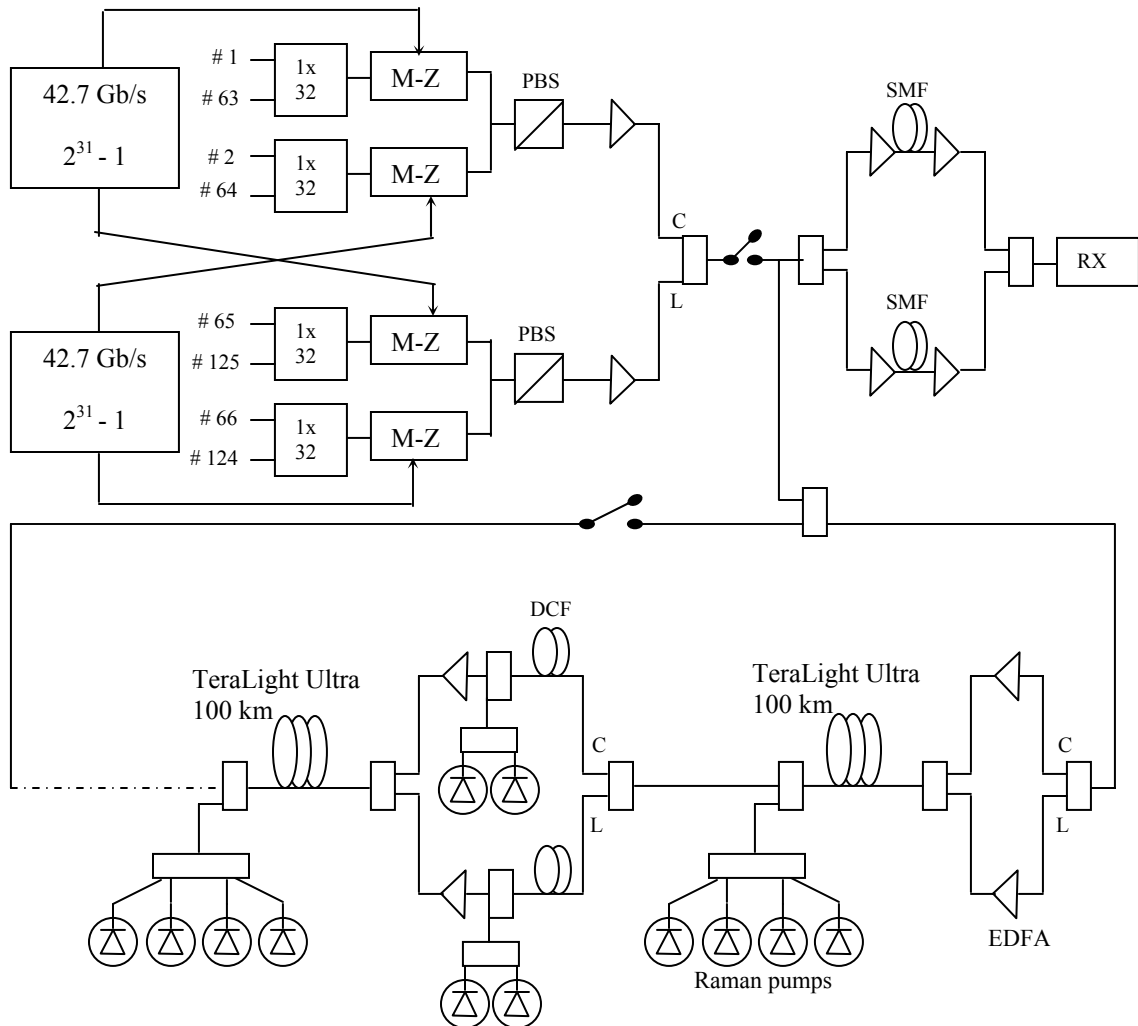
Figure 5.1: Experimental set-up [Ref. 2]

The recirculating loop consisted of three 100 km long section of TeraLight™ Ultra fiber. TeraLight™ Ultra is a non-zero dispersion-shifted fiber (NZ-DSF) with a loss of 0.20 dB/km, chromatic dispersion of 8.0 ps/nm.km and dispersion slope of 0.052 ps/nm².km at 1550 nm. It has a PMD value of 0.04 $ps/\sqrt{km}$ and effective core area of 63 μm². The dispersion was compensated using two sections of DCF for C and L bands, which were inserted within each repeater. DCF had a dispersion of −80.0 ps/nm.km and dispersion slope of −0.52 ps/nm².km at 1550nm. This provided full dispersion slope compensation and the accumulated dispersion was not made to exceed 20 ps/nm per span in the C band and 25 ps/nm per span in the L band. The fine-tuning of the residual dispersion was performed on channel-by-channel basis using a small spool of standard SMF within the receiver pre-amplifier, outside the loop.

The fiber attenuation and other power losses were compensated using Raman amplification and EDFAs. Each span consisted of dual-band EDFAs, providing a gain of 2 dB in C-band and 1 dB in L-band. The higher gain for the lower wavelength region was provided to mitigate self-induced SRS spectral distortion. Four sets of two polarization-multiplexed semiconductor pumps of wavelengths 1427 nm, 1439 nm, 1450 nm and 1485 nm were sent backwards into the fiber to provide amplification using SRS. The Raman gain provided by the four pumps was approximately 15 dB in each 100 km span of the TeraLight™ Ultra fiber.

The DCF loss was compensated by using four laser pumps, two in both bands, at wavelengths 1423 nm and 1455 nm in the C band and 1470 nm and 1500 nm in the L band. The Raman gain in DCFs was approximately 8 dB.

The receiver consisted of a narrow tunable filters used to select each channel. These filters, which had a bandwidth of 30 GHz at 3 dB, was used to perform VSB filtering by detuning the channel central frequency towards the 75 GHz spaced neighboring channel. Thus the part of the channel that had lesser interference from its neighbor is isolated and the other part is discarded.

5.1.2. Experimental Results

Figure 5.2 shows the optical SNR at the input of the pre-amplifier and the bit error rates (BERs) of all 125 channels at the end of 1200 km. The optical SNR varied within [22.1 dB, 26.0 dB] in the C-band and [22.7 dB, 27.6 dB] in the L-band. The measured BERs were always better than 1.4×10^{-4}, and with FEC, this would correspond to BER performance of better than 10^{-13}. It can be seen that the worst performing channels were the ones with relatively high SNR, limited by optical nonlinearities.
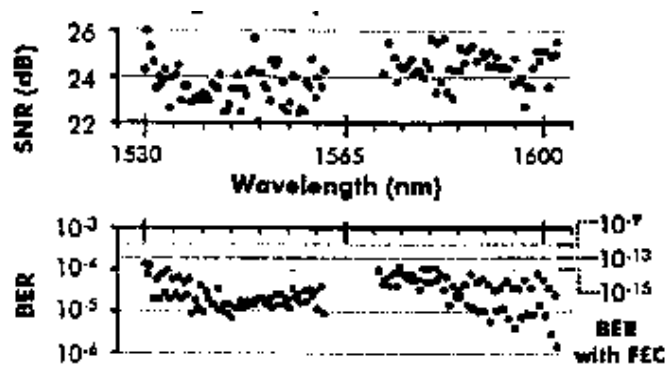
Figure 5.2: Optical SNR at the input of pre-amplifier and Q values at the
end of 1200 km [Ref. 2]

5.2. FiberSim VSB Demultiplexing Simulation Model

In this section, the modeling of the experimental system described in the previous section using the FiberSim simulator is carried out. All the characteristics of optical components used in an experimental system cannot be modeled in a simulator. This limits the extent to which an experimental system can be modeled using a simulator. For example, the loss due to fiber connectors and multiplexing losses cannot be exactly modeled using a simulator. Hence a practical approach is followed to make the simulation model as close as possible to the experimental system.

FiberSim has a Raman fiber module to model the SRS gain using Raman pumps. This utilizes the pump and signal interactions leading to SRS as discussed in section 2.2.5. Due to SRS and fiber attenuation, the high frequency Raman pumps decrease in power as they travel from the end of the fiber to its start in the

backward direction. The power loss due to SRS in turn amplifies the lower frequency signals (Stokes light). The SRS model in FiberSim uses an iterative approach in which, the initial pump power profile across the fiber is considered by just using the fiber attenuation. During the next iteration the SRS effect is taken into account to change the pump profile and is repeated till the pump profile stabilizes. In each iteration, the pump profile is changed as it propagates through the fiber in the backward direction and the signal profile is changed as it propagates in the forward direction interacting with the pump. This approach utilizes a significantly high amount of computer resources and time. For example, a single span (100 km length) of Raman fiber simulation takes more than 15 hours to complete. Since the experimental system being modeled requires 12 such spans, it would take days to complete. For this reason, an equivalent model for Raman amplified system was developed for reducing simulation time.

This equivalent model for Raman amplified system is discussed in Appendix-B. From the discussion in the appendix, it can be found that the gain characteristics of a Raman amplified fiber can be matched by breaking down the fiber into smaller sections, each with an effective attenuation parameter and the noise characteristics can be matched by using an EDFA with zero dB gain and a noise figure value equal to the equivalent Raman noise figure.

5.2.1. Simulation Model of Alcatel experimental system

The FiberSim simulation model uses a fiber-EDFA equivalent for the Raman amplified components of the experimental system. The 100 km Teralight Ultra with an attenuation parameter of 0.2 dB/km is replaced with 10 sections of 10 km each of Teralight Ultra fiber with an effective attenuation parameter. The effective attenuation parameters used are as given in Table B.1 in appendix B. The effective attenuation parameters are chosen such that a net effective loss of 4.995 dB exists in each 100 km span of Teralight Ultra fiber. Also according to figure B.1 the DCF must have a net gain of 3 dB. Since the length of the DCF is only 10 km, it can be used as a single section, instead of breaking it down into further sections as done with the Teralight Ultra fiber. Hence the simulation uses a DCF with attenuation parameter as – 0.3 dB/km to obtain a net gain of 3 dB. The equivalent noise figure of the Raman amplifier used in DCF is low compared to that of Teralight Ultra fiber and is therefore ignored. The simulation model can be depicted as given in figure 5.3.
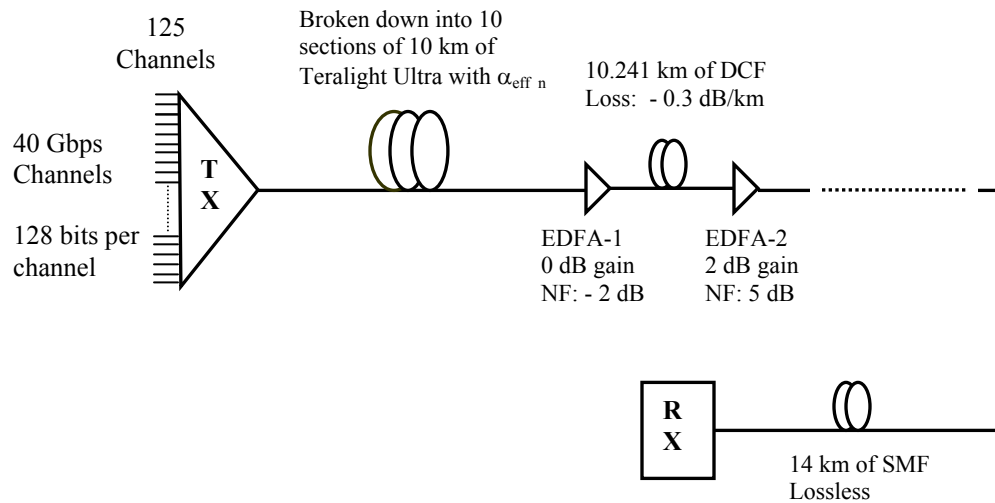
Figure 5.3: FiberSim simulation set-up

The transmitter consists of 125 channels from wavelengths 1529.94 nm to 1562.21 nm in the C-band, and 1573.06 nm to 1603.97 nm in the L-band. The channels are alternately spaced with 50 GHz and 75 GHz and have alternating 0 and 90 degree polarizations. The channel data input consists of 128 bits per channel generated randomly. Each span consists of 10 sections of 10 km of Teralight Ultra fiber each with dispersion of 8.0 ps/nm.km and dispersion slope of 0.052 ps/nm^2.km at 1550 nm. The Teralight Ultra fiber is followed by an EDFA with 0 dB gain and a noise figure value equal to the average Raman equivalent noise figure value of the experimental system, which is about –2.0 dB.

The DCF used has a dispersion of –80.0 ps/nm.km and dispersion slope of –0.52 ps/nm^2.km. The length of the DCF is chosen to be 10.241 km so that the accumulated dispersion per span does not exceed 20 ps/nm in the C-band and 25

ps/nm in the L-band. Also the DCF has an attenuation parameter of –0.3 dB/km and core effective area of 20 μm2. The DCF is followed by an EDFA with 2 dB gain and noise figure value of 5 dB. Since the experimental system used an EDFA with 2 dB gain in the C-band and 1 dB gain in the L-band, a gain tilted EDFA is used in the simulation model, so that the high frequency channels get higher gain than the low frequency channels.

At the end of 1200 km, a SMF of length 14.0 km with dispersion and dispersion slope of 16.7 ps/nm.km and 0.09 ps/nm^2.km respectively, is used for compensating the accumulated dispersion. The receiver consists of an optical filter with full optical bandwidth of 60 GHz and detuned by 20 GHz to select a particular channel.

5.2.2. Simulation Results

Due to the closely packed carriers, dispersion compensation schemes and signal power levels must be chosen carefully for optimal system performance. Also, the mitigation of SRS is necessary due to large number of carriers spread from 1529.9 nm to 1600.3 nm. In this section the dependence on the system performance on the amplifier gain tilt, dispersion compensation and launch power level are verified through simulations and the results are as discussed below.

Effects of Amplifier Gain Tilt

SRS leads to transfer of power from higher frequency channels to the lower frequency channels. The higher frequency or lower wavelength channels act as pumps to the lower frequency channels, which acts as stokes light. The EDFA following the DCF is used to compensate for this effect of SRS. Since the higher frequency channels lose power as they propagate through the fiber due to SRS, they can be given higher gain compared to the lower channels. This is achieved by using an EDFA with a tilted gain profile, such that the EDFA has a positive gain slope with respect to the frequency. Due to this positive gain slope the higher frequency channels will have more gain compared to the lower frequency channels. The required gain slope depends on the channel launch power and can be adjusted such that entire spectrum of channels have identical powers at the end of propagating through 1200 km of fiber.

Figure 5.4 shows the spectrum of the composite signal that is launched into the fiber. The composite signal consists of 125 channels with launch power of $-$ 4.56 dBm (i.e. 0.35 mW). Initially an EDFA of flat gain profile is used. The gain of the EDFA is 2 dB through the entire spectrum. Figure 5.5 gives the spectrum of the composite channel at the end of 1200 km of fiber. The effect of SRS is clearly evident from figure 5.5.
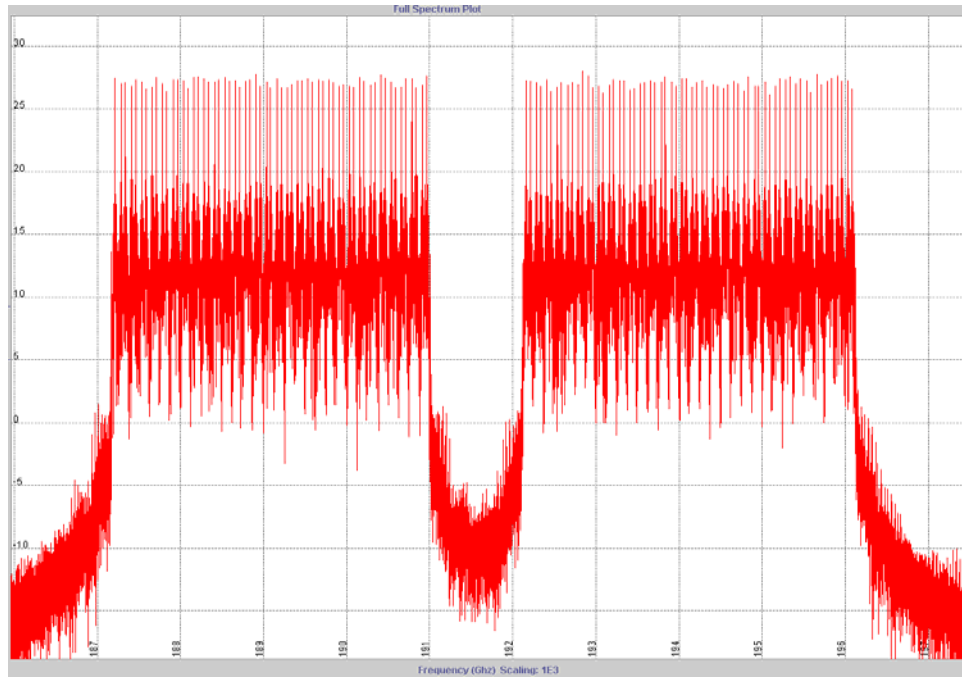
Figure 5.4: Signal spectrum at the launch
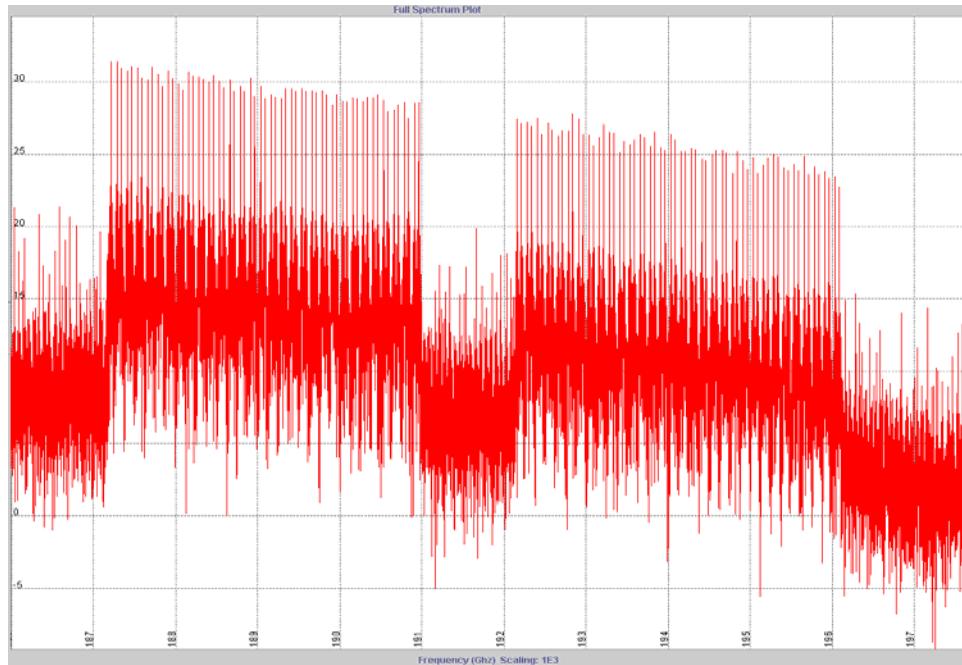
Figure 5.5: Signal spectrum at the end of 1200km of fiber using flat gain EDFA

The EDFA after the DCF is now modeled with a gain tilt (such that it has a positive gain slope with respect to the frequency). The optimal gain slope was found by running different simulations. The 2 dB amplifier gain is now considered to be the gain of the channels in the mid of the spectrum and then a gain slope value of 0.9 is applied across the spectrum. Figure 5.6 gives the signal spectrum at the end of 1200 km of fiber with an EDFA having a tilted gain profile.
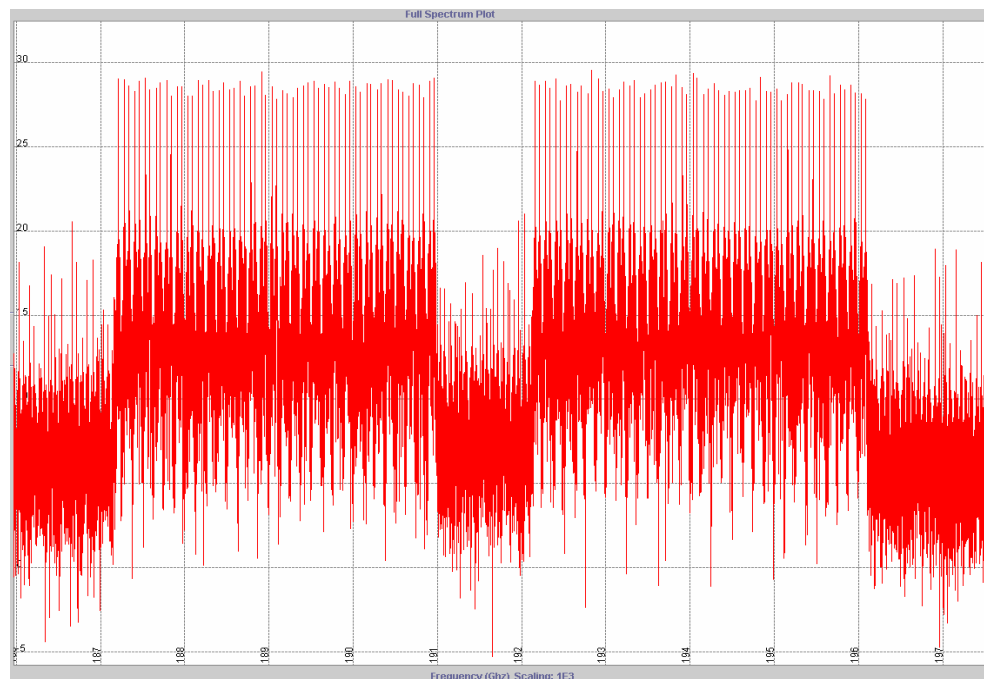
Figure 5.6: Signal spectrum at the end of 1200 km of fiber using a tilted gain profile EDFA

Figure 5.7 compares the average channel power of the 125 channels at the end of 1200 km of fiber with the amplifier gain tilt and with flat gain amplifier. It can

be seen that the average channel powers can be made uniform at the output by using a tilted gain profile amplifier.
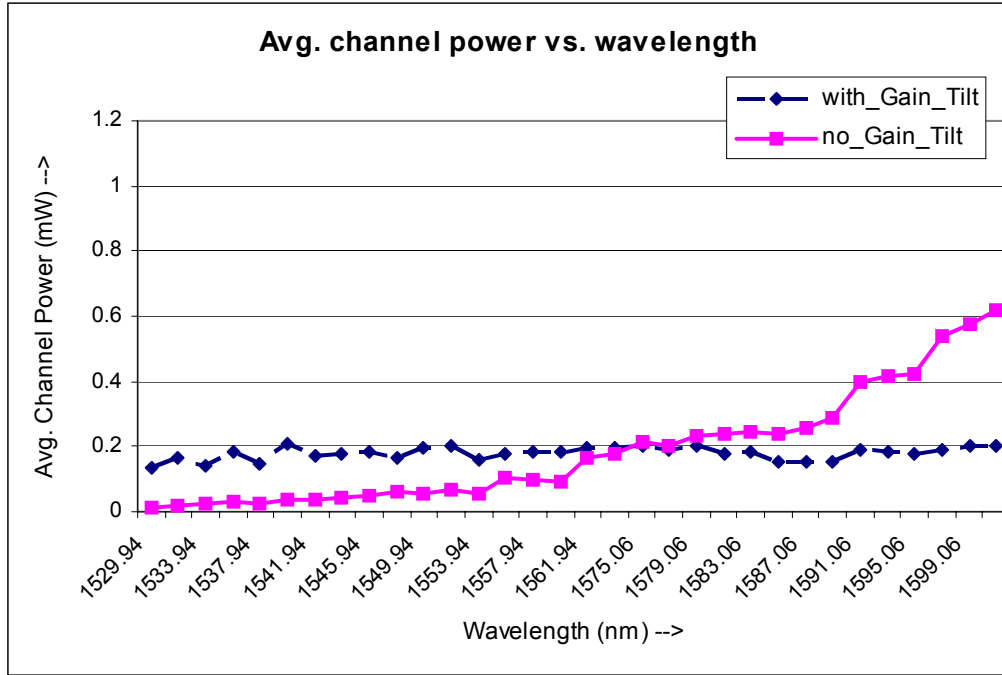
Figure 5.7: Average channel power vs. wavelength plot

Effects of Dispersion Slope Compensation

Dispersion becomes a major limitation when designing high spectral efficiency WDM systems. When a large number of channels are multiplexed, it is usually not possible to provide identical compensation for all the channels, as dispersion is dependent on wavelength. But the above problem can be overcome by performing dispersion slope compensation along with the dispersion compensation.

The dispersion slope compensation (DSC) value is evaluated as follows:

$$DSC = \dfrac{D_{Fiber}^{1550}\big/S_{Fiber}^{1550}}{D_{DCF}^{1550}\big/S_{DCF}^{1550}} = 1 \qquad\qquad ...\,(5.2.1)$$

where D_{Fiber}^{1550}, S_{Fiber}^{1550} are the dispersion and dispersion slope values of the fiber and D_{DCF}^{1550}, S_{DCF}^{1550} are the dispersion and dispersion slope values of the DCF. For perfect slope compensation the value of DSC should be equal to one.

The experimental system used Teralight fiber with dispersion and dispersion slope values of 8.0 ps/nm.km and 0.052 ps/nm^2.km respectively at 1550 nm wavelength. The DCF dispersion parameters were $-$ 80.0 ps/nm.km and $-$ 0.52 ps/nm^2.km at 1550 nm wavelength which leads to perfect dispersion slope compensation. For the simulation system, two cases are used, one with dispersion slope compensation and the other without the slope compensation. For the latter case the DCF was chosen with dispersion and dispersion slope values of -80.0 ps/nm.km and - 0.6 ps/nm^2.km. The channel Qs at the end of 1200 km for both these cases are as shown below. The channel launch power used is 0.35 mW.
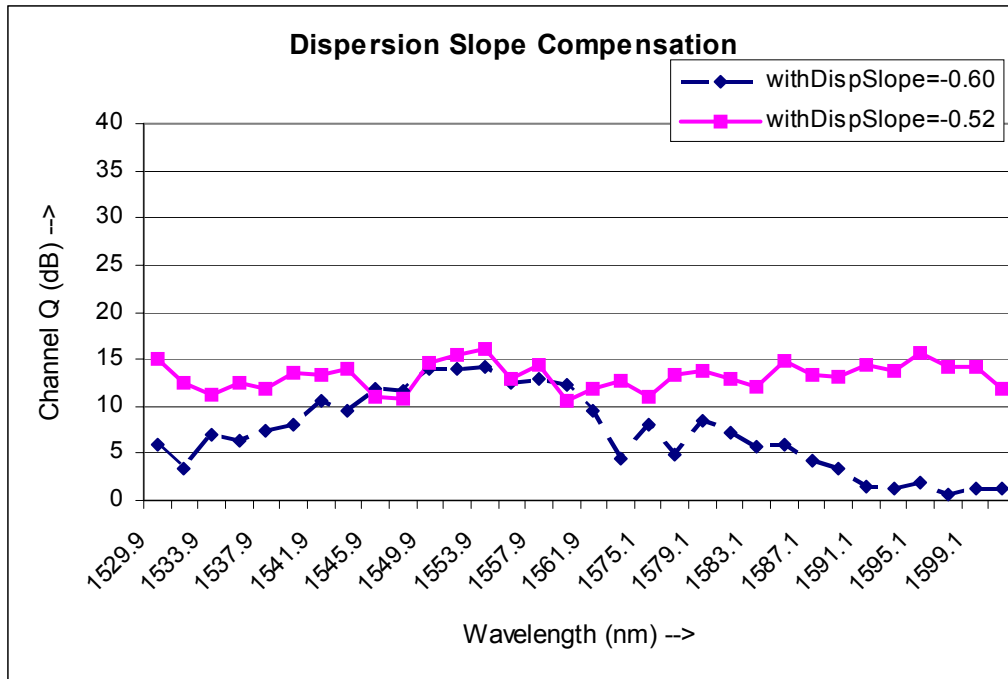
Figure 5.8: System performance with and without dispersion slope compensation

Effects of Residual dispersion per span

A residual dispersion per span is preferred compared to complete dispersion compensation as complete dispersion compensation enhances the effects of nonlinearities of fiber on the optical signal. Most WDM systems use positive residual dispersion per span, but the Alcatel experimental system used a net negative residual dispersion of −20 ps/nm in the C-band. This residual dispersion is compensated for by using a SMF at the end of 1200 km of transmission. A positive residual dispersion per span would lead to spreading of the channel spectrum. This is not acceptable in a high spectral efficient WDM system as the channels are very tightly packed. A negative residual dispersion per span, on the

other hand, would lead to compressed channel spectrums, which enhances the performance. Figure 5.9 shows the performance of two cases, one in which a positive residual dispersion per span not exceeding 20 ps/nm in the C-band was maintained and compensated with a DCF at the end of 1200 km of transmission, whereas the other used a negative residual dispersion per span not exceeding –20 ps/nm in the C-band. The channel launch power used in both these cases was 0.35 mW. We can see the system with net negative residual dispersion per span has better performance.
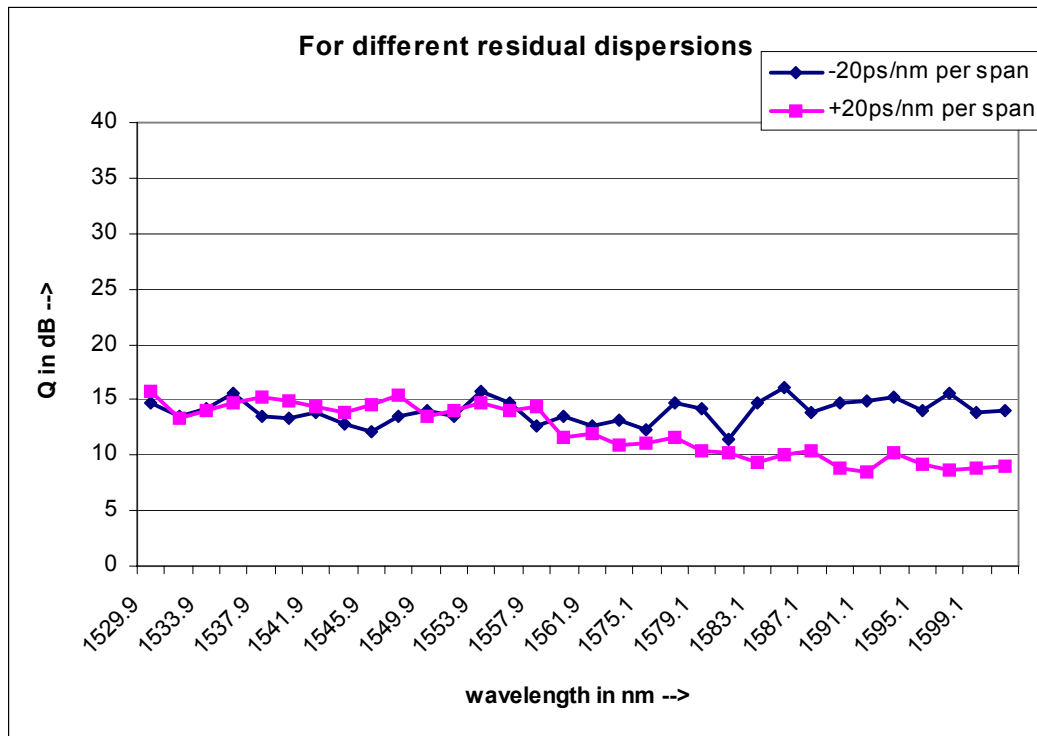
Figure 5.9: System performance for different residual dispersion schemes

Optimal Channel Launch Power

The channel launch power is also an important parameter in a WDM system. Higher channel powers can lead to increased nonlinearities in the fiber and lower launch powers can lead to diminishing of the signal due to attenuation. The WDM system simulated has an input of 125 channels with same launch powers. Simulations were run for different launch power levels and the results are as shown in figure 5.10.
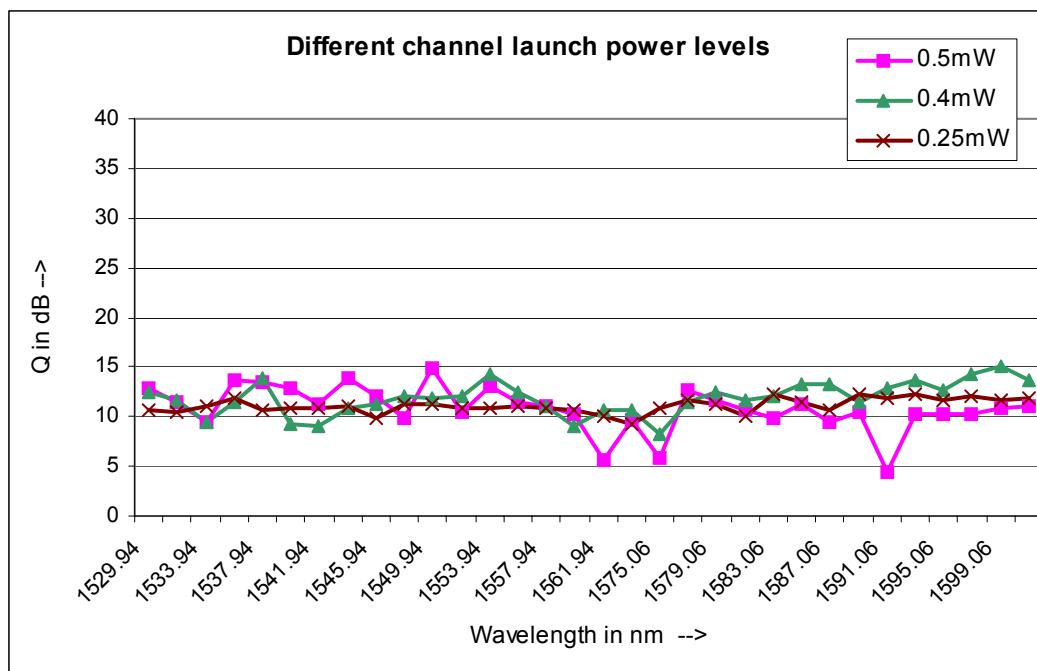
Figure 5.10: System performance for different channel launch powers

The optimal channel launch power is found to be around – 6.02 dBm (i.e. 0.25 mw).

5.3. Comparison of Experimental and FiberSim Model Results

The experimental system achieved an average BER of more than 10^{-13} with FEC, which corresponds to a Q value of 8 dB using equation 3.3.1. The use of FEC increases the Q values by as much as 4 dB. The channel launch power used in the experimental system was – 2 dBm i.e. 0.631 mW.

Figure 5.11 gives the Q values of all the 125 channels at the end of 1200 km transmission through Teralight Ultra fiber. The higher Q values of the simulated result compared the experimental result can be attributed to the fact that the simulation model is more of an idealistic system.
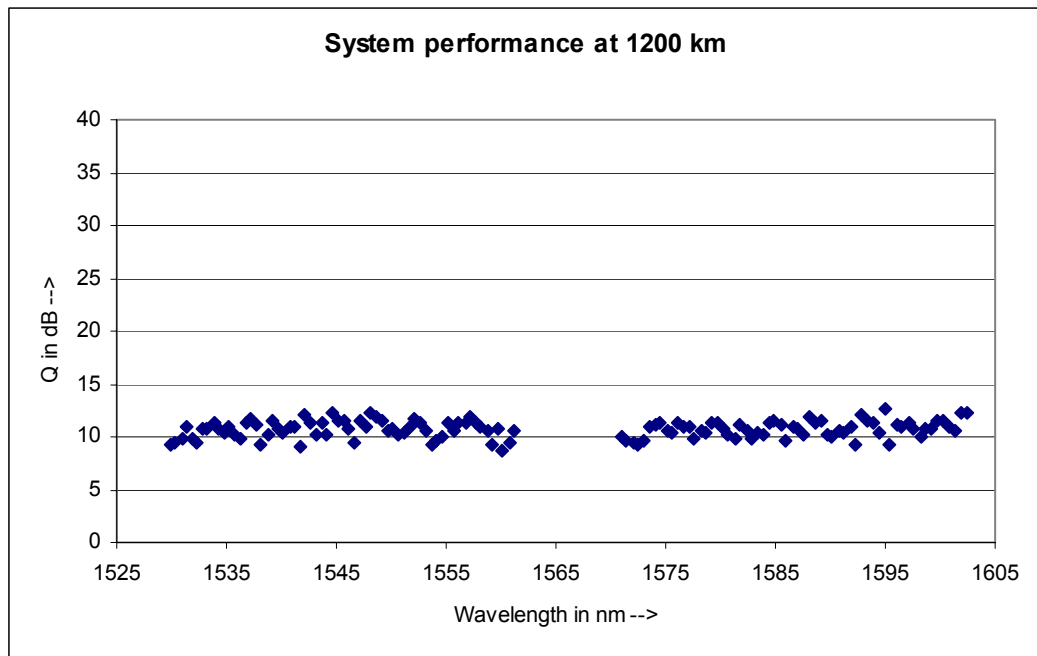
Figure 5.11: Q values of all the 125 channels at the end of 1200 km - simulated result

The optimal channel launch power is found out to be − 6.02 dBm i.e. 0.25 mW compared to the −2 dBm used in the experimental system. The 4 dB difference in the channel launch power can be due to the multiplexing and connector losses in the experimental system which are not taken into consideration during the simulation.

6. A VSB Demultiplexing system with 0.8 bit/s/Hz spectral efficiency

Chapter 3 discussed various techniques that can be used to achieve high spectral efficiency. Increasing the channel bit rates and reducing the channel spacing are two ways of improving the spectral efficiency of WDM systems. The use of high channel bit rates like 40 Gbit/s is considered cost effective because the number of terminals in transmitter and receiver is reduced compared to low bit rates systems like 10 Gbit/s, but at the same time the high bit rates introduce new problems. These include a reduction of dispersion tolerance, increased PMD and nonlinear effects, and need for more costly high frequency equipments [Ref. 15].

The dispersion problem due to high bit rates becomes more prominent when high dispersion fiber such as standard single mode fiber (SMF) is used for transmission. Many legacy systems use standard SMF for transmission and EDFAs for optical amplification. Given the problems of high bit rates in high dispersion fibers, an alternative approach is to use lower bit rate channels. To this end, a 10 Gbit/s WDM system using VSB demultiplexing with spectral efficiency as high as 0.8 bit/s/Hz over standard SMF was designed and is reported in this chapter. This designing of the 0.8 bit/s/Hz WDM system involved obtaining an optimal channel spacing scheme, with an average spacing of 12.5 GHz for a 10

Gbit/s system, and optical filter parameters for VSB demultiplexing at the receiver. The number of channels used for simulation was restricted to 12 in order to decrease the simulation time. Optical amplification was achieved using EDFAs instead of using Raman amplifiers so as to model the existing long haul networks, which are predominantly EDFA based. The fiber used in simulation is standard SMF. The system model for this design study is as shown in figure 6.1.
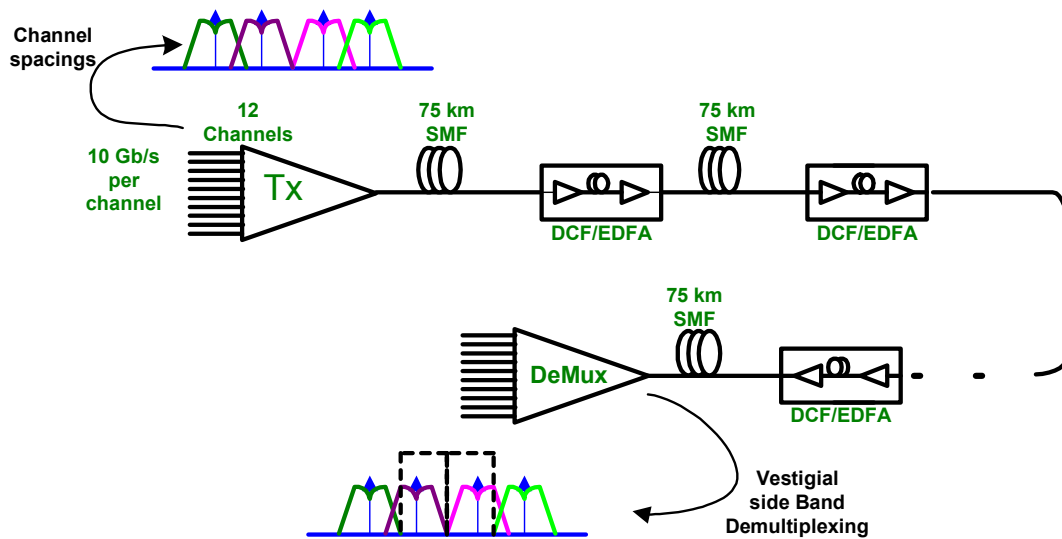
Figure 6.1: WDM system model

6.1. Simulation setup

The simulation set up used in FiberSim for optimizing the 10 Gbit/s, 0.8 bit/s/Hz spectral efficiency system is as shown in figure 6.2. The transmitter

consists of 12 NRZ modulated channels with starting wavelength as 1529 nm. Each channel is modulated at 10 Gbit/s, using standard on-off keying, with an electrical bandwidth of 7.5 GHz. Different channel spacing schemes and different launch powers are tried to optimize the results and are discussed in the later sections. The channel data input consists of 256 bits per channel generated pseudo randomly.

Each transmission span consists of 75 km of SMF, followed by a DCF and an EDFA. The SMF has an attenuation of 0.25 dB/km, with 16.7 ps/nm.km and 0.09 ps/nm^2.km dispersion and dispersion slope parameters at 1550 nm respectively, and an effective aperture of 83 μm^2. The DCF has a dispersion and dispersion slope of -104.5 ps/nm.km and -1.0 ps/nm^2.km respectively at 1550 nm and is assumed to be lossless. The length of the DCF used is 11.7 km, resulting in an accumulated dispersion of approximately 10 ps/cell for the lowest wavelength. The EDFA gain was chosen to exactly compensate for the SMF loss i.e. 18.75 dB, with a noise figure of 6.0 dB that accounted for the DCF loss.
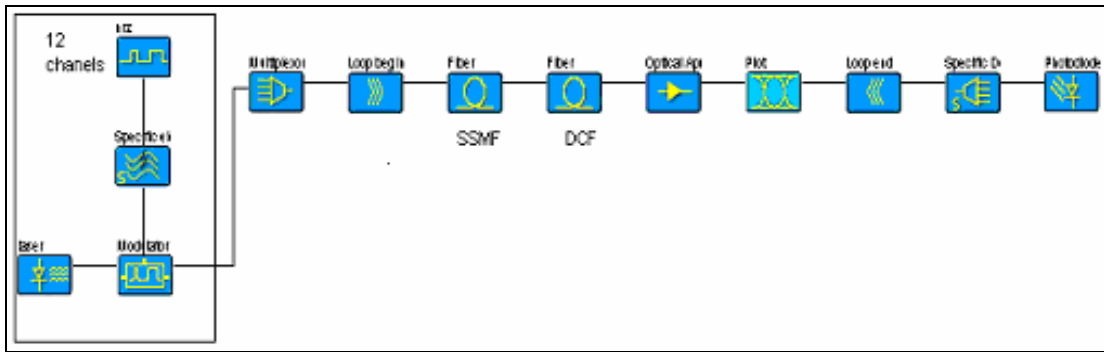
Figure 6.2: FiberSim simulation setup

At the receiver, the demultiplexing optical filter is detuned for the VSB demultiplexing. The amount of detuning and the optical BW of the filter are optimized for better system performance and their values are discussed in the next section. The electrical bandwidths of the detectors are set to 7.5 GHz.

6.2. Simulation Results

The WDM system designed here is optimized with respect to the channel spacing, launch power, polarization and demultiplexing optical filter parameters for better performance. In this section, the various simulation results that help us to find these optimized parameters are detailed.

6.2.1. Optimal Channel Spacing scheme

To obtain a 0.8 bit/s/Hz spectral efficiency for a 10 Gbit/s system, the channel spacing should be 12.5 GHz. For a constant 12.5 GHz spacing, the dispersion

limitation for the tightly spaced carriers is more pronounced and it limits the maximum distance without regeneration to less than 375 km. Hence the alternate wide and narrow spacing scheme explained in section 4.4 is used. For achieving an average spacing of 12.5 GHz, the carriers can be alternatively spaced at 10 GHz and 15 GHz or 11 GHz and 14 GHz or 11.5 GHz and 14.5 GHz etc.

The spacing schemes considered are alternating 9.5GHz-15.5GHz, 10.0GHz-15.0GHz, 10.5GHz-14.5GHz, 11.0GHz-14.0GHz, 11.5GHz-13.5GHz, and 12.0GHz-13.0GHz. The launch power used is 1.5 mW for all the channels and the channel performance at the end of 150 km is taken for reference. This distance was chosen as the signal undergoes sufficient amount of dispersion and nonlinearities by then. For each of these spacing schemes, the optimized demultiplexing optical filter parameters are found and are as shown in table 6.1. It is found out that the optimized optical filter for the different spacing schemes is a 3rd order Butterworth filter. The filter BW and offset are as tabulated in table 6.1.

Spacing Scheme (in GHz)	Demux. Filter offset (in GHz)	Demux. Filter BW (in GHz)	Max Channel Q at 150 km (in dB)
Alternating 9.5 – 15.5	1.3	10.1	11.65
Alternating 10.0 – 15.0	0.9	11.1	18.01
Alternating 10.5 – 14.5	0.8	10.7	17.16
Alternating 11.0 – 14.0	1.0	12.0	20.39
Alternating 11.5 – 13.5	0.9	9.9	19.08
Alternating 12.0 – 13.0	0.5	10.5	17.34

Table 6.1: System performance for different spacing schemes

The above study was based on the performance of channel 4 in the 12 channel WDM system, which was the worst affected channel. The plot for maximum achievable Q versus the various spacing schemes is as shown in figure 6.3. It can be seen that the optimized spacing scheme for a 10 Gbit/s WDM system with a spectral efficiency of 0.8 bit/s/Hz is the alternating 11 GHz and 14 GHz. The demultiplexer optical filter parameters used for the VSB demultiplexing of the channels in an 11 GHz – 14 GHz alternately spaced WDM system is discussed in the next section.
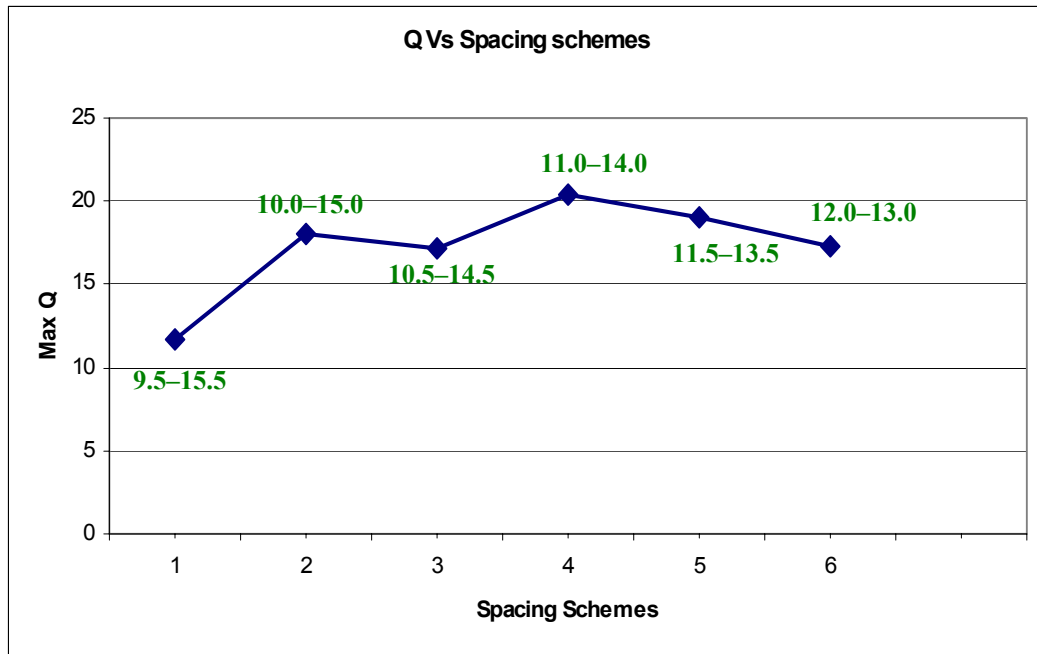
Figure 6.3: Performance of various channel spacing schemes

6.2.2. Optimal demultiplexing optical filter detuning and bandwidth

For VSB demultiplexing, the demultiplexing optical filter must detune the channel central frequency towards the further spaced neighboring channel, i.e. in the 11-14 GHz spacing scheme, towards the 14 GHz spaced neighboring channel. The amount of detuning depends on the spacing scheme used. In this section, the optimized detuning and bandwidth of the optical filter for the 11 –14 GHz spaced system is discussed.

As mentioned in the previous section, the system performance observation was based on the performance of channel 4 at the end of 150 km. The launch power used is 1.5 mW for all the channels. The demultiplexing filter was detuned

in small steps and for each detuning the optimal optical bandwidth for better performance was found. The optical filter was of the 3rd order Butterworth filter type. The optimized demultiplexer optical filter bandwidth and maximum achievable Q for various offset frequencies are as tabulated in table 6.2.

Demux. Filter Offset (in GHz)	Optimized Demux. Filter BW (in GHz)	Max. Channel Q at 150 km (in dB)
0.4	11.0	19.41
0.8	11.6	20.16
0.9	11.7	20.27
1.0	12.0	20.39
1.1	12.1	20.37
1.2	12.4	20.32
1.4	12.9	19.96
1.6	12.9	19.25

Table 6.2: Demux. Filter parameter for alternate 11-14GHz spaced WDM system

From the table 6.2 it can be seen that the optimized demultiplexer filter detuning for the alternate 11-14 GHz spaced WDM system is 1.0 GHz, with an optical bandwidth of 12.0 GHz for VSB demultiplexing. Figure 6.4 gives the plot for maximum achievable Q at 150 km versus the optical filter offset.

Max Q Vs Offset
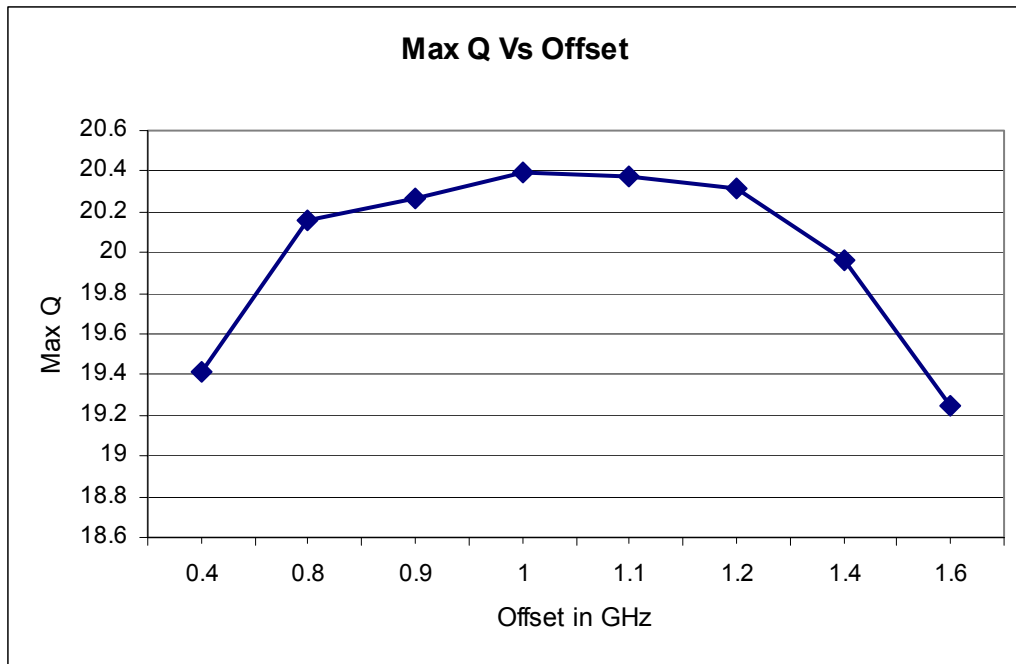
Figure 6.4: Maximum achievable channel Q at 150 km versus optical filter offset

6.2.3. Effects of Channel polarization

In a tightly spaced WDM system, along with dispersion, fiber nonlinearities such as XPM and FWM are the major system performance degradation factors. Though using low dispersion fibers reduces the problem of dispersion, it increases the effects of FWM. Using high dispersion fiber results in decreasing the effects

of XPM. Another technique that can be used for decreasing the effects of XPM is to use polarization interleave multiplexing, i.e. orthogonal polarizations between the neighboring channels. Figure 6.5 gives the comparison between VSB demultiplexed WDM system with constant zero degree polarization and alternating 0-90 degrees polarization.
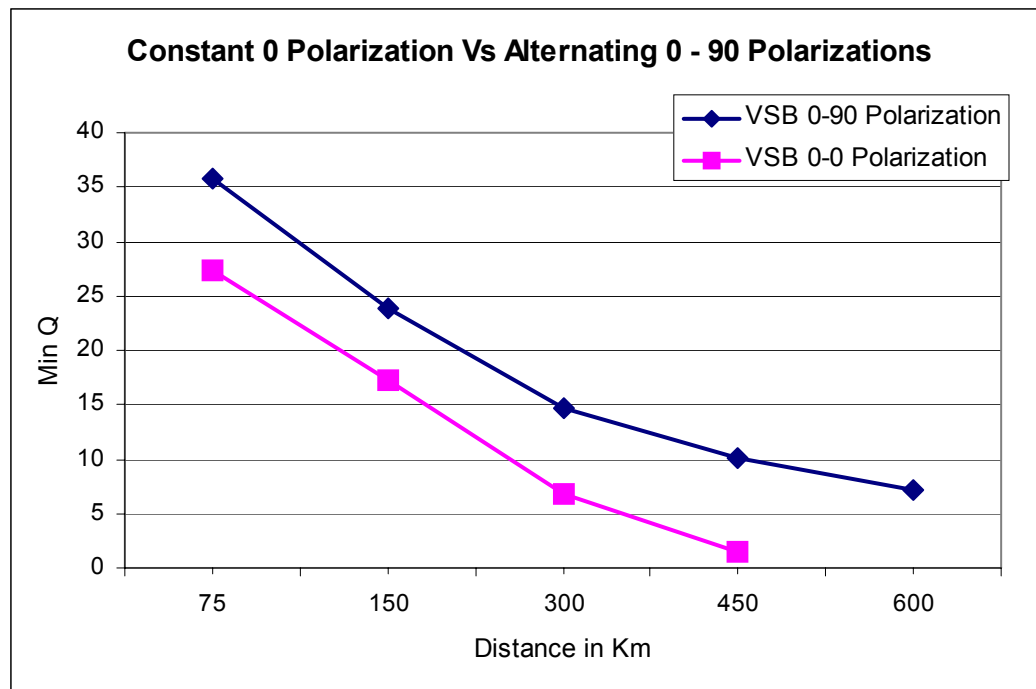
Figure 6.5: Performance comparison of constant zero polarization and alternating 0-90 degrees polarization

The 12 channel WDM system used for obtaining the above result had a launch power of 1.5 mW, with alternating 11-14 GHz spacing scheme. The *Q* value of the worst affected channel is plotted as a function of distance in figure 6.5. From the above figure it can be concluded that for high spectral efficiency WDM

system, polarization interleave multiplexing increases system performance significantly by decreasing the XPM in the transmitting fiber. It can also be seen that with the constant zero polarization for all the channels, the maximum distance reachable with a minimum BER of 10^{-12} is about 300 km. On the other hand, with polarization interleave multiplexing channels have a maximum reachable distance of about 600 km with a minimum BER of 10^{-12}, which corresponds to a *Q* value of about 7 dB.

6.2.4. Optimal Channel launch power

The 12 channels 10 Gbit/s WDM system with alternating 11 – 14 GHz channel spacing and alternating 0 – 90 degrees polarizations between the channels is run for different launch power for finding the optimized launch power. The worst affected channel *Q* for the various launch powers is plotted against distance as given in figure 6.6. The optimized channel launch power was found to be 1.5 mW i.e. 1.761 dBm.
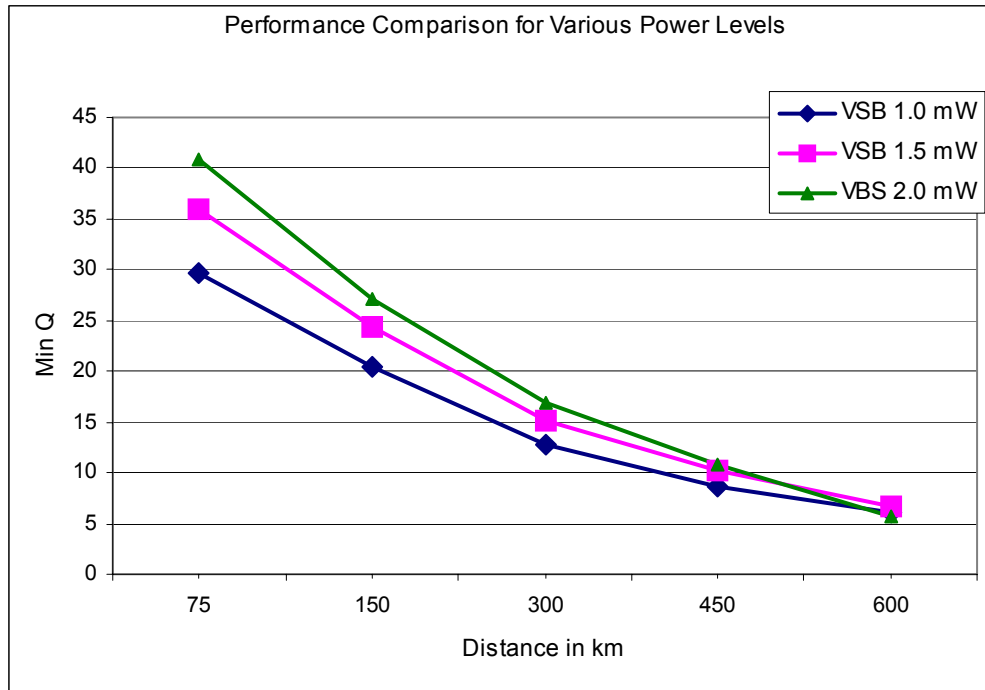
Figure 6.6: System performance for different launch powers

6.3. Comparison of alternating 11-14 GHz spaced VSB demultiplexed system with 25 GHz spaced DSB system

In this section, the performance of the alternating 11 GHz - 14 GHz spaced 10 Gbit/s VSB demultiplexed WDM system is compared with that of a 25 GHz spaced 10 Gbit/s double side band (DSB) system. The DSB system consisted of 12 channels with a launch power of 1.5 mW and having a constant 25 GHz spacing between the channels. The transmission span of both these systems consisted of 75 km of SMF, followed by DCF and an EDFA.

For the 25 GHz spaced DSB system, simulations were run for both constant zero polarization and polarization interleave multiplexing. It was found that the system performance of the DSB system does not improve significantly by going from the constant zero degree polarization to the alternating 0 - 90 degrees polarization as it is not as tightly spaced as the 12.5 GHz average spaced VSB demultiplexing system.

Figure 6.7 shows Q values of the worst affected channel at various distances for both the VSB demultiplexed and DSB systems. It should be noted that the 25 GHz based DSB system has a spectral efficiency of 0.4 bit/s/Hz, whereas the VSB demultiplexed system has twice the spectral efficiency at 0.8 bit/s/Hz. The maximum reachable distance for the DSB system is around 900 km with a minimum BER of about 10^{-12} and that for the VSB demultiplexed system is around 600 km. This comparison was performed to find if the maximum distance reached with the 0.8 bit/s/Hz VSB demultiplexed system is optimized. From the results, it is found that doubling the spectral efficiency reduced the transmission distance by only one-thirds.
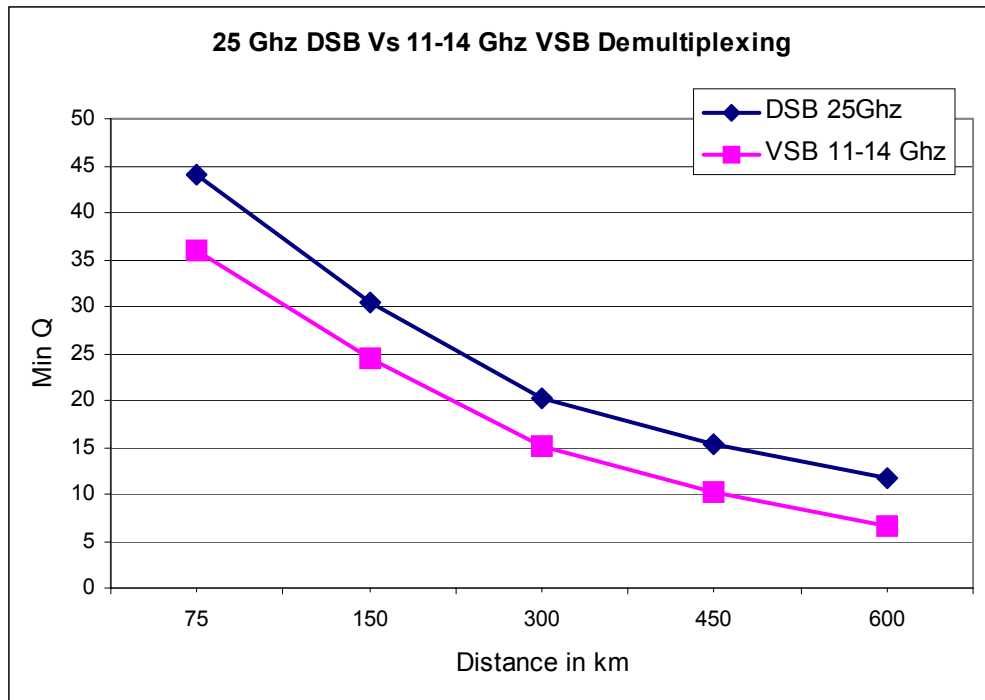
Figure 6.7: Comparison of VSB demultiplexed system with 25 GHz spaced DSB system

The VSB demultiplexed system with its 0.8 bit/s/Hz spectral efficiency can achieve twice the WDM capacity compared to the 0.4 bit/s/Hz DSB system. In addition, the maximum transmission distance achieved by VSB demultiplexed system is reduced only by one-thirds compared to the DSB system. From this it can be concluded that higher transmission capacity can be achieved by using the VSB demultiplexed system.

7. Summary, Conclusion and Future work

This final chapter summarizes the work performed, gives conclusions to this research effort and gives some pointers on the future work.

7.1. Summary and Conclusion

The current emphasis on WDM lightwave systems is on increasing the system capacity by transmitting more and more channels using the WDM technique. This can be achieved by increasing the spectral efficiency of WDM systems and/or by extending the wavelength range over which a WDM system can operate simultaneously. The techniques that are used for increasing spectral efficiency are polarization interleave multiplexing and modulation formats like vestigial side band demultiplexing.

This thesis has considered the design and modeling of two dense WDM systems that use VSB demultiplexing for achieving high spectral efficiency. We performed modeling and analysis of an experimental 40 Gbit/s WDM system reported by Alcatel. The 40 Gbit/s experimental system, presented in the European Conference on Optical Communications in 2001, used VSB demultiplexing and polarization interleave multiplexing to achieve 5 Tbit/s capacity and 0.64 bit/s/Hz spectral efficiency over 1200 km of Teralight Ultra

fiber. This paper reported one of the highest transmission capacities (i.e. bit rate and distance of transmission product) achieved in the recent past. The modeling was performed using FiberSim (the fiber optic simulator developed at Information and Telecommunication Technology Center, University of Kansas).

The Alcatel experimental system used distributed Raman amplification in its Teralight Ultra fiber and DCF spans. In order to reduce the simulation time of the experimental system model in FiberSim, we developed a fiber-EDFA equivalent model that matches the gain and noise characteristics of Raman amplified systems. In this fiber-EDFA equivalent model, the Raman amplified fiber is broken down into smaller sections of normal fiber, each with an effective attenuation parameter for matching the gain characteristics, followed by an EDFA with zero dB gain and a Raman equivalent noise figure value for matching the noise characteristics. The Raman equivalent noise figure value is a function of pump powers and wavelengths. The paper describing the Alcatel experimental system reported the pump wavelengths, but not the pump powers used. The Raman pump power values used in the experimental system were discovered through simulations using FiberSim. From simulations, the pump power values of Raman pumps at 1427 nm, 1439 nm, 1450 nm and 1485 nm wavelengths were found to be 60 mW, 60 mW, 55 mW and 55 mW respectively.

Through simulations it was found that the WDM system performance was greatly influenced by the amplifier gain tilt, the dispersion compensation scheme, and the launch power levels. The amplifier gain tilt is necessary to mitigate the effects of SRS, which would otherwise lead to degradation of lower wavelength channels. Dispersion slope compensation helps to achieve complete dispersion compensation through the entire spectrum of the WDM channels. The channel launch power should be optimized to balance the signal to noise ratio and the fiber nonlinearities.

The use of high channel bit rates, like 40 Gbit/s, introduces new problems, such as a reduction of dispersion tolerance, increased PMD and nonlinear effects etc. An alternative approach is to use lower bit rate channels. To investigate this approach, a 10 Gbit/s WDM system with a spectral efficiency of 0.8 bit/s/Hz was designed using FiberSim. We performed simulations to find the optimal channel spacing, demultiplexer optical filter parameters and channel launch powers. The fiber used in this WDM system was standard SMF, as used in most of the legacy systems, and amplification was achieved using EDFAs. The optimal channel spacing scheme for a 10 Gbit/s WDM system with 0.8 bit/s/Hz spectral efficiency using VSB demultiplexing was found to be alternating 11 – 14 GHz spacing. The optimal demultiplexer optical bandwidth found was 12 GHz with a detuning of 1 GHz. The optimal channel launch power was 1.5 mW i.e. 1.76 dBm. The 12

channels 10 Gbit/s WDM system reached a maximum distance of 600 km with a minimum BER of 10^{-12}.

The successful modeling of a complex experimental system using FiberSim shows the flexibility and resourcefulness of this simulator. From the agreement between the FiberSim simulation results and the reported experimental results, we conclude that the fiber module in the simulator models the dispersive, polarization and nonlinear characteristics of an actual fiber. The analyses on various simulation parameters to find their effect on system performance also validates that the simulator can be used to offer insights regarding which effects are significant and which are not in a particular system. FiberSim can be used to explore news schemes for system design, as proven by the 0.8 bit/s/Hz spectral efficiency 10 Gbit/s WDM system design. This thesis does not offer comprehensive tests to validate the simulator, but it does prove that complex WDM systems can be modeled using the FiberSim simulator.

This research effort concludes that VSB demultiplexing technique can be used for high spectral efficiency WDM systems. The effects of FWM and cross talk between the channels in the closely packed WDM system can be minimized be using polarization interleave multiplexing. The important parameters in densely packed high capacity WDM systems are dispersion slope compensation, residual dispersion per span, SRS mitigation by using EDFAs with higher gain in the C-

band compared to the L-band and channel launch power level. The optimization of the channel spacing scheme and optical filter at the Demultiplexer is significant in improving system performance in VSB demultiplexed WDM system.

7.2. Future Work

This section suggests possible enhancements and scope for future work to this research effort.

- ➢ A WDM system using VSB-RZ signaling at the transmitter to increase the spectral efficiency can be designed and compared with that of the VSB demultiplexing technique.

- ➢ The Raman fiber component in FiberSim can be made more time efficient so that it can be used in simulation rather than using a fiber-EDFA equivalent model.

- ➢ Dispersion slope compensation can be applied to the 10 Gbit/s WDM system with 0.8 bit/s/Hz spectral efficiency designed in chapter 6.

- ➢ We can compromise a bit on the spectral efficiency to increase the transmission distance of the 10 Gbit/s WDM system designed i.e. instead of 0.1 nm (12.5 GHz) average spacing we can go in for 0.12 nm (15 GHz), which would bring down the spectral efficiency to 0.667 bit/s/Hz.

- ➢ The use of other modulation formats like carrier-suppressed return-to-zero (CS-RZ) in increasing the spectral efficiency can also be investigated.

References:

1. G.P. Agrawal, *Fiber-optic Communication Systems*, Third Edition, John Wiley & Sons, New York, 2002.

2. S. Bigo, W. Idler, J.C. Antona, G. Charlet, C. Simonneau, M. Gorlier, M. Molina, S. Borne, C. de Barros, P. Sillard, P. Tran, R. Dischler, W. Poehlmann, P. Nouchi, and Y. Frignac, "Transmission of 125 WDM channels at 42.7 Gbit/s (5 Tbit/s capacity) over 12x100 km of Teralight^{TM} Ultra fibre", *European Conference on Optical Communication*, Vol. 6, pp. 2-3, 2001.

3. G. Keiser, *Optical Fiber Communications*, Third Edition, The McGraw-Hill Companies, 2000.

4. G.P. Agrawal, *Nonlinear Fiber Optics*, Second Edition, Academic Press, 1995.

5. E.A. Golovchenko, and A.N. Pilipetskii, "Unified analysis of four-photon mixing, modulation instability, and stimulated Raman scattering under various polarization conditions in fibers", *Journal of the Optical Society of America B: Optical Physics*, 11(1), pp. 92-101, 1994.

6. Craig D. Poole and Jonathan Nagel, *Polarization effects in Lightwave systems*, chapter 6 from the book titled, *Optical fiber telecommunications IIIA*, Edited by Ivan P. Kaminow and Thomas L.Koch, Academic Press, San Diego, 1997.

7. R. Hui, M. Vaziri, J. Zhou, and M. O'Sullivan, "Separation of Noise from Distortion for High Speed Optical Fiber System Link Budgeting", *IEEE Photonics Technology Letters*, 11(7), pp. 910-912, 1999

8. FiberSim User Manual , ITTC Technical Report ITTC-FY2004-TR-22737-01, University of Kansas.

9. T. Ono, "Wavelength-division-multiplexing terabit technologies with high spectral efficiency", *Optics and Photonics News*, 12(3), pp. 56-59, 2001.

10. N. Ramanujam, A.B. Puc, G. Lenner, H.D. Kidorf, C.R. Davidson, I. Hayee, J.-X. Cai, M. Nissov, A. Pilipetskii, C. Rivers, and N.S. Bergano, " Forward Error Correction (FEC) Techniques in Long-Haul Optical Transmission Systems", *Conf. Proc. of Lasers and Electro-Optics Society Annual Meeting*, Vol. 2, pp. 405-406, 2000.

11. T. Ono and Y. Yano, "Key Technologies for Terabit/second WDM Systems with High Spectral Efficiency of over 1 bit/s/Hz", *IEEE Journal of Quantum Electronics*, 34(11), pp. 2080-2088, 1998.

12. S. Kawanishi, "High bit rate transmission over 1 Tbit/s", *IEICE Transaction on Electronics*, Vol. E84-C, pp. 509-515, 2001.

13. H. Kim, and R.-J. Essiambre, "Transmission of 8 x 20 Gb/s DQPSK Signals over 310-km SMF with 0.8-bit/s/Hz Spectral Efficiency", *IEEE Photonics Technology Letters*, 15(5), pp. 769-771, 2003.

14. R.A. Griffin and A.C. Carter, "Optical Differential Quadrature Phase-Shift Key (oDQPSK) for High Capacity Optical Transmission", *Conference on Optical Fiber Communication*, Vol. 70, pp. 367-368, 2002.

15. C. Wree, N. Hecker-Denschlag, E. Gottwald, P. Krummrich, J. Leibrich, E.-D. Schmidt, B. Lankl, and W. Rosenkranz, "High Spectral Efficiency 1.6-b/s/Hz

Transmission (8x40 Gb/s with a 25-GHz Grid) over 200-km SSMF uing RZ-DQPSK and Polarization Multiplexing", *IEEE Photonics Technology Letters*, 15(9), pp. 1303-1305, 2003.

16. L.N. Binh, B. Pujji, and S.L. Leong, "Vestigial Side Band Modulation Formats for Ultra-High Capacity 40 Gb/s Optical Communication Systems", Technical Report, Monash University.

17. M. Suzuki, T. Tsuritani, and N. Edagawa, "Multi-Terabit Long Haul DWDM Transmission with High Spectral Efficiency", *LEOS Summer Tropical Meeting*, pp. 41-42, 2001.

18. T. Tsuritani, I. Morita and N. Edagawa, "Study on PMD and Dispersion Tolerance of 20 Gbit/s VSB-RZ Optical Signal", *Pacific Rim Conference on Lasers and Electro-Optics*, Vol. 2, pp. II552-II553, 2001.

19. T. Tsuritani, I. Morita and N. Edagawa, "Ultra Long Haul Transmission with Multi-Terabit Capacity", *Conf. Proc. of Lasers and Electro-Optics Society Annual Meeting*, Vol. 1, pp. 151-152, 2001.

20. W. Idler, and S. Bigo, "Design of 40 Gbit/s based Multi-Terabit/s Ultra-DWDM Systems ", *IEICE Transactions on Communications*, Vol. E85-B(2), pp. 394-402, 2002.

21. W. Idler, S. Bigo, Y. Frignac, B. Franz, and G. Veith, "Vestigial Side Band Demultiplexing for Ultra High Capacity (0.64 bit/s/Hz) Transmission of 128x40 Gb/s Channels", *Conference on Optical Fiber Communication*, 54(1), pp. MM3/1-MM3/3, 2001.

22. L.-A. Montmorillon, A. Bertania, P. Sillard, L Fleury, P. Nouchi, J.-F. Chariot, S. Bigo, and J._P. Hamaide, Technical Article on Eurowire.com titled "Optimised Fiber for Terabit Transmission", http://www.read-eurowire.com/alcatel.htm

23. S. Wang and C. Fan, "Distributed fiber Raman amplifiers: Analytical expression of noise characteristics under complex conditions", *Optics Communications*, 198(1-3), pp. 65-70, 2001.

Appendix – A: Mach-Zehnder Modulator
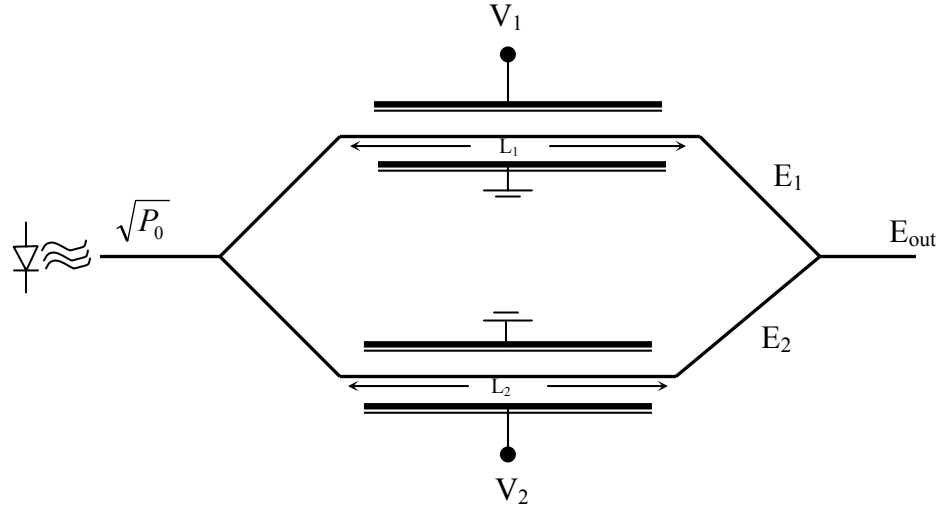
The E-field in the upper and lower arms of the modulator is given by

$$E_1 = \sqrt{\frac{P_0}{2}} \exp(-jk_1 L_1)$$

$$E_2 = \sqrt{\frac{P_0}{2}} \exp(-jk_2 L_2)$$

... (A.1)

where
$$L_1 = L_0 + \frac{h}{2}$$
$$L_2 = L_0 - \frac{h}{2}$$
and
$$k_1 = k_0 + \varepsilon V_1$$
$$k_2 = k_0 - \varepsilon V_2$$
... (A.2)

The output E-field is given by

$$E_{out} = \frac{\sqrt{P_0}}{2} \left\{ e^{-jk_1 L_1} + e^{-jk_2 L_2} \right\}$$

... (A.3)

On using the equations A.2.,

$$E_{out} = \sqrt{P_0}.e^{-jk_0L_0} e^{-j\frac{\varepsilon}{2}L_0(V_1-V_2)} e^{-j\frac{h\varepsilon}{2}L_0(V_1+V_2)} \cos\left[\frac{k_0h}{2} + \frac{h\varepsilon}{4}(V_1 - V_2) + \frac{\varepsilon L_0}{2}(V_1 + V_2)\right]$$

$$\text{... (A.4)}$$

For balanced operation, we have $V_1 = V_2 = V$, hence

$$E_{out} = \sqrt{P_0}.e^{-jk_0L_0} e^{-jh\varepsilon V} \cos\left[\frac{k_0h}{2} + \varepsilon L_0 V\right] \qquad \text{... (A.5)}$$

The applied voltage V is in practice sum of a dc bias voltage and the signal voltage, which can be expressed as

$$V = V_{dc} + V_s \qquad \text{... (A.6)}$$

The dc bias voltage and the differential length h of the arms of the Mach-Zehnder modulator determine the offset of the sinusoidal waveform. Treating the lumped effect of both of these to arise from a effective bias voltage V_{bias}, we have

$$E_{out} = \sqrt{P_0}.e^{-jk_0L_0} e^{-jh\varepsilon V} \cos\left[\varepsilon L_0(V_s + V_{bias})\right] \qquad \text{... (A.7)}$$

In convention the voltage swing that brings the output of a Mach-Zehnder modulator from full off to full on is denoted by V_π. Using the definition of V_π and ignoring the static delay $e^{-jk_0L_0}$ of the device, we have

$$E_{out} = \sqrt{P_0}.e^{-jh\varepsilon V} \sin\left[\frac{\pi}{2V_\pi}(V_s + V_{bias})\right] \qquad \text{... (A.8)}$$

The chirp introduced during modulation is determined from the electro-optic parameter ε and the differential length h. It is customary to represent the chirp in terms of chirp parameter α, which for an E-field of the form $E = \sqrt{P}e^{j\phi}$, is given by

$$\alpha = -\frac{\dfrac{d\phi}{dt}}{\dfrac{1}{2P}\dfrac{dP}{dt}} \qquad \text{... (A.9)}$$

For the Mach-Zehnder modulator we have

$$P = P_0 \sin^2\left[\frac{\pi}{2V_\pi}\left(V_s + V_{bias}\right)\right] \qquad \text{and} \qquad \phi = -h\varepsilon V \quad \text{... (A.10)}$$

Using the above in equation A.9., we get

$$\alpha = \frac{2\varepsilon h V_\pi}{\pi}\tan\left[\frac{\pi}{2V_\pi}\left(V_s + V_{bias}\right)\right] \qquad \text{... (A.11)}$$

For binary modulation formats such as NRZ, RZ and CS-RZ, the bias voltage V_{bias} is zero, which gives

$$\alpha = \frac{2\varepsilon h V_\pi}{\pi}\tan\left[\frac{\pi}{2V_\pi}V_s\right] \qquad \text{... (A.12)}$$

By convention, the chirp parameter α_0 for a Mach-Zehnder modulator is the chirp when the signal voltage equals the quadrature voltage $V_\pi/2$. Hence for $V_s = \dfrac{V_\pi}{2}$,

$$\alpha_0 = \frac{2\varepsilon h V\pi}{\pi} \qquad \text{... (A.13)}$$

Using the above in equation A.8. and with $V_{bias} = 0$, we get

$$E_{out} = \sqrt{P_0}\,.e^{-jV_s\frac{\pi\alpha_0}{2V_\pi}}\sin\left[\frac{\pi V_s}{2V_\pi}\right] \qquad \text{... (A.14)}$$

Appendix – B: Fiber-EDFA equivalent for a Raman amplified system

The Alcatel experimental system used Raman amplification for the Teralight Ultra fiber and the DCF with gains of 15 dB and 8 dB respectively. Along with Raman amplification an EDFA of 2 dB gain in the C-band was used in every span. The Teralight Ultra fiber has a loss of 0.2 dB/km and DCF can be considered to have a loss of 0.5 dB/km [Ref. 22]. Hence the net gain per component per span is as depicted in the figure below.

	100km of TeraLight Ultra Fiber Loss: 0.2 dB/km	10km of DCF Loss: 0.5 dB/km	EDFA
Loss per component:	20 dB [&]	5 dB [&]	
Gain per component:	15 dB**	8 dB**	2 dB
Net Gain per component:	-5 dB	3 dB	2 dB

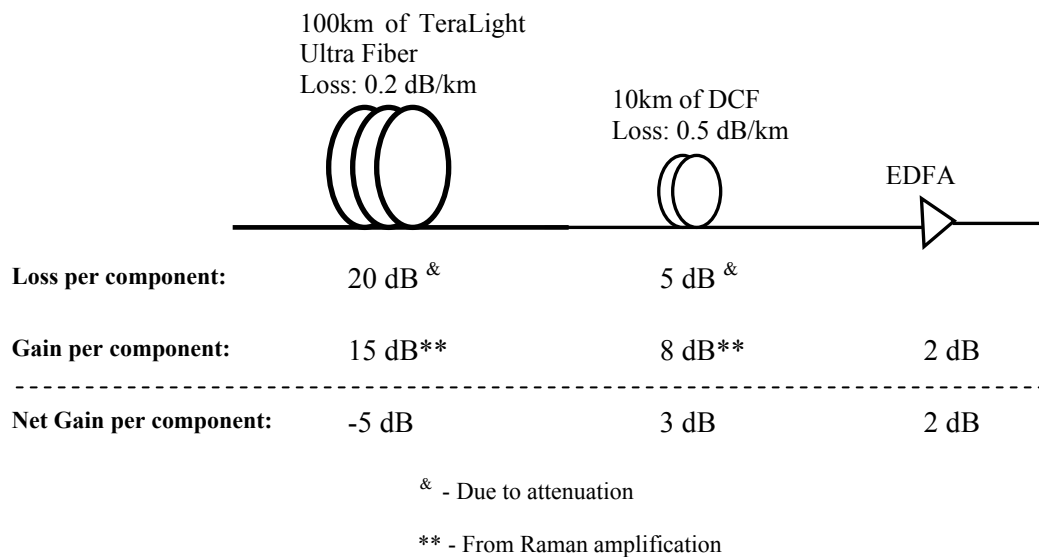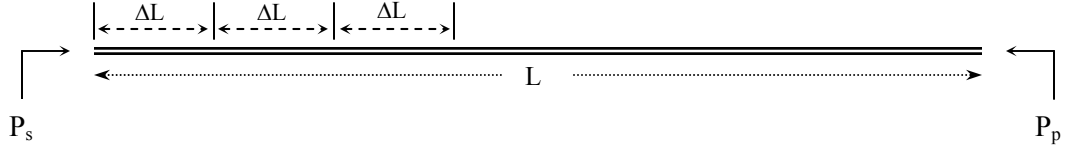[&] - Due to attenuation

** - From Raman amplification

Figure B.1: Gain and Loss per component per span

Thus there exists a 5 dB net loss in the 100 km of Teralight Ultra fiber and 3 dB net gain in the DCF. The simplest method to model the gain characteristics of 100 km fiber with 0.2 dB/km attenuation and 15 dB Raman amplification would

be to have a fiber with a net loss of 5 dB. This should be followed by representing the noise characteristics of the Raman amplifier. In FiberSim, the noise parameter is represented by the noise figure of the amplifier. So if NF_{raman} is the noise figure of the Raman amplifier used in the fiber, it can be modeled as EDFA with 0.0 dB gain and noise figure of NF_{raman}. The noise characterization is explained in more detail in the latter part of the appendix.

The 100 km of Teralight Ultra fiber with a net loss of 5 dB can be modeled as fiber with attenuation of 0.05 dB/km. This would lead to constant attenuation of the signal as it propagates through the fiber. But in a Raman amplified system, as the signal propagates through the fiber it interacts with the pump and experiences gain due to SRS. Since the pump is launched at the end of the fiber, the signal sees a weak pump at the beginning of the fiber and a very strong pump towards the end. Hence the signal experiences attenuation at the start of the fiber, as its interaction with weak pump does not induce SRS gain and amplification towards the end of the fiber. A constant attenuation of 0.05 dB/km cannot resemble this phenomenon of attenuation and amplification found in Raman amplified system. In this respect, the fiber can be broken down into a number of sections and the effect of pump on signal in each of these sections can be evaluated to see if the signal experiences attenuation or amplification. The solution to the coupled rate equations (equation 2.2.10) as given in equation 2.2.11 can be used to find the signal intensity at the end of each section. If the fiber is divided into n section of

equal lengths ΔL i.e. $L = n\Delta L$ as shown below, with P_s as the input channel power

and P_p as the pump power:

The signal intensity at the end of first section is given by [Ref. 4]

$$I_s(\Delta L) = I_s(0)\exp\{g_R I_0(\Delta L)L_{eff} - \alpha.\Delta L\}$$

where,
$$L_{eff} = \frac{1}{\alpha}[1 - \exp\{-\alpha.\Delta L\}]$$

... (B.1)

and
$$I_s(0) = \frac{P_s}{A_{eff}}$$

$$I_0(\Delta L) = \frac{P_p}{A_{eff}}\exp\{-\alpha.(L - \Delta L)\}$$

... (B.2)

where α is the fiber attenuation, A_{eff} is the effective core area of the fiber and g_R is

the Raman gain coefficient. Similarly we can find the signal intensity at the end of

second section with $I_s(\Delta L)$ as its input and $I_0(2.\Delta L)$ as the pump intensity in this

section and so on and so forth. Since the sections are of smaller lengths, the pump

depletion within these sections of fiber can be ignored without loss of much

accuracy. From these signal intensities we can find the effective loss or gain i.e.

α_{eff} experienced by the signal in each of these sections using

116

$$\alpha_{eff}(1) = \frac{I_s(\Delta L)}{I_s(0)}$$

.

.   ... (B.3)

.

$$\alpha_{eff}(n) = \frac{I_s(n\Delta L)}{I_s((n-1)\Delta L)}$$

For Teralight Ultra fiber, α is 0.2 dB/km and A_{eff} is 63 µm^2. Also from the above equations it can be seen that the α_{eff} is actually not dependent on the P_s value, but rather in the P_p value. The length of the fiber L is 100 km and the total number of sections is considered to be 10. The Raman gain coefficient value depends on the pump and signal frequency difference as shown in figure 2.4. The peak value of Raman gain coefficient is about 1.0×10^{-13} m/W. Using equations B.1 – B.3 and assuming the value of Raman gain coefficient to be about 0.9×10^{-13} m/W, the α_{eff} in the 10 sections of the fiber for various pump powers can be found to be as given in table B.1.

α_{eff} in dB/km in the 10 sections of 100km long fiber		
For Pp = 100mW	For Pp = 120mW	For Pp = 112.5mW
0.1921	0.1905	0.1911
0.1875	0.185	0.1859
0.1802	0.1762	0.1777
0.1686	0.1624	0.1647
0.1503	0.1403	0.1441
0.1212	0.1054	0.1113
0.0751	0.0501	0.0595
0.0021	-0.0375	-0.0227
-0.1137	-0.1765	-0.1529
-0.2972	-0.3966	-0.3593
Net loss over 100 km of fiber in dB: 6.662	3.995	4.995

Table B.1: Effective loss or gain in sections of fiber at different pump powers

The experimental system had a 100 km Teralight Ultra fiber with 5 dB net loss over its length using Raman amplification. From the above table it can be seen that for a pump power of 112.5 mW, we obtain an approximate net loss of 5 dB over the 100 km length and hence this set of α_{eff} values is used in the FiberSim simulation model. These values indicate that the signal undergoes attenuation in the beginning sections and amplification towards the latter sections of the fiber, which resembles the Raman amplified system.

The fiber-EDFA model should have the similar gain and noise characteristics as the Raman amplified system. The gain characteristics can be matched by breaking down the fiber into smaller section each with an effective attenuation parameter as discussed above. In order to match the noise characteristics, the noise figure of Raman amplifier should be evaluated and this requires the knowledge of pump powers used for Raman amplification. The experimental system [Ref. 2] gives the pump wavelengths and the required gain, but does not mention the pump powers. Pump powers are evaluated using FiberSim as described in appendix-C and from these pump powers the noise figure of Raman amplified system is evaluated as described below.

Raman Equivalent Noise Figure

In FiberSim, the noise parameter of the amplifier is expressed in terms of noise figure. Section 3.4 described the use of noise figure in the noise power spectral density calculation, which is then used to find the various noise variances for Q calculation. Noise figure in general is defined as ratio of the signal to noise (SNR) at the input to the SNR at the output of an amplifier.

In general Raman amplifiers have low noise characteristics when compared to EDFAs. And the equivalent noise figure of a Raman amplified system is given by [Ref. 23]

$$ENF = \frac{1 + N_{R_j}}{G_{R_j}} \qquad\qquad \text{... (B.5)}$$

where N_{Rj} is the photon number of the amplified spontaneous Raman scattering noise and G_{Rj} is the Raman on-off gain for the jth channel. The photon number and Raman on-off gain are given by

$$N_{R_j} = K\left\{ G_{R_j} \exp(-\alpha L) - 1 + \frac{K}{q_j}\left(G_{R_j} - 1\right)\right\} \qquad\qquad \text{... (B.6)}$$

$$G_{R_j} = \exp\left\{\frac{q_j}{K}\left[1 - \exp(-\alpha L)\right]\right\} \qquad\qquad \text{... (B.7)}$$

where α is the attenuation parameter, L is the length of the Raman fiber, K is the polarization factor and q_j is the weighted gain coefficient. The polarization factor takes the value one i.e. $K=1$, if the pump and signal have identical polarization states; $K= \infty$, if the pump and signal have orthogonal polarization states and $K=2$ denotes average result of totally scrambled polarization state. The weighted gain coefficient is given by

$$q_j = \sum_i \frac{g_{ij}P_{piL}}{\alpha} \qquad\qquad \text{... (B.8)}$$

where g_{ij} is the Raman gain coefficient corresponding to the ith pump and j^{th} signal, P_{piL} corresponds to the ith pump power at the end of the fiber i.e. the launch pump power.

Using the above equations the average ENF for the 120 channels, 4 Raman pumps system is found to be around –2.0 dB. And this value is used in the FiberSim simulation model.

Thus the fiber-EDFA equivalent for the Raman amplified system that is used in the FiberSim simulation model can be depicted as shown in figure B.2. The L km fiber is broken down into n sections of ΔL km fibers, each with an effective attenuation parameter and the noise characteristics is modeled using an EDFA with zero dB gain and a Raman equivalent noise figure value.
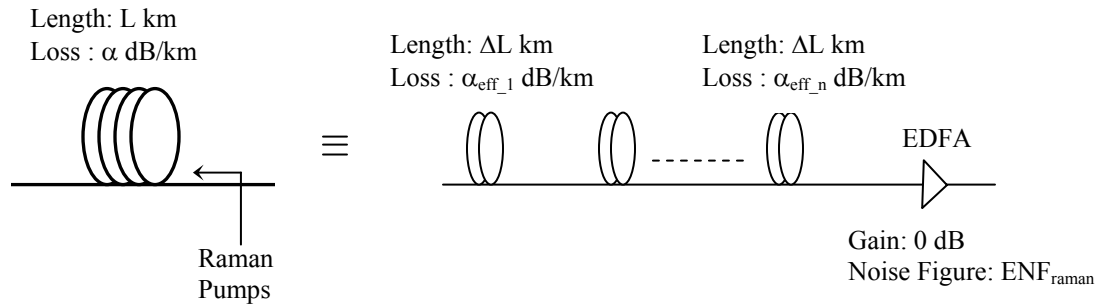

Figure B.2: Fiber-EDFA equivalent for Raman amplified fiber

Appendix – C : Raman Pump Powers Evaluation

FiberSim is used for finding the pump powers, which leads to a gain of 15 dB in the 100 km long Teralight Ultra fiber. For the purpose of evaluation of pump powers a simulation setup as depicted in figure C.1 is used.
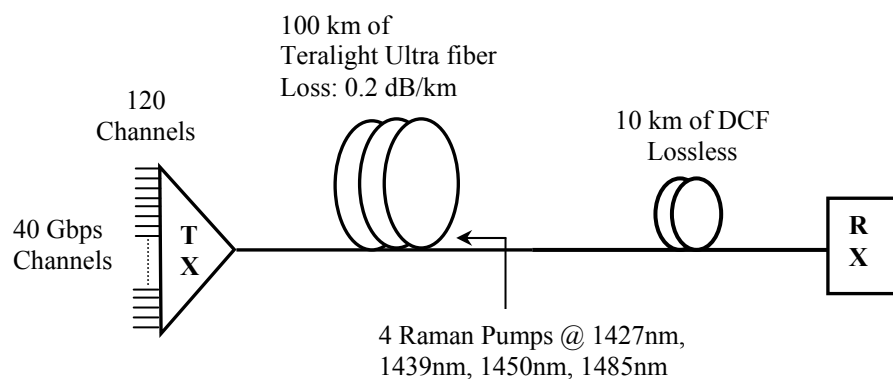

Figure C.1: Simulation set-up for Raman pump evaluation

The input consists of 120 channels separated by alternate 50 GHz and 75 GHz and having an alternate 0 and 90 degrees polarization. The 120 channels are spread over as 60 channels in the C-band and 60 channels in the L-band. The channels have a launch power of –2 dBm i.e. 0.631 mW. The simulation has a single span of 100 km long Teralight Ultra fiber with attenuation of 0.2 dB/km, dispersion of 8.0 ps/nm.km and dispersion slope of 0.052 ps/nm^2.km at 1550 nm. The core effective area of the fiber is defined to be 63μm^2. Four backward propagating Raman pumps at wavelengths 1427 nm, 1439 nm, 1450 nm and 1485 nm with different power levels are defined. The dispersion is compensated using a

DCF of 10 km with dispersion of −80.0 ps/nm.km and dispersion slope of −0.52 ps/nm^2.km at 1550 nm.

The simulation used 64 bits per channel. For evaluating the gain imparted by the pumps on the channels, initially the channels were modulated with all 1 bits except for some zero bits padded to the front and end i.e. channels had a bit sequence of the form 0011111…..111100. The pump powers were varied to obtain a 15 dB net gain across the channels. The net gain for a channel is calculated as

$$Net\_Gain(dB) = AttenuationParameter * Length + 10 * \log\left(\frac{P_{avg,out}}{P_{avg,in}}\right) \dots \text{(B.1)}$$

where attenuation parameter is in dB/km and Length is in km. $P_{avg,out}$ is the average channel power at the end of the fiber and $P_{avg,in}$ is the average input channel power.

Using the above described simulation, the pump powers that yields 15 dB gain are found to be 60 mW, 60 mW, 55 mW and 55 mW at 1427 nm, 1439 nm, 1450 nm and 1485 nm wavelengths respectively. Using the same pump profile, simulations were also run for channel input bits generated randomly rather than the 001111….111100 format. The simulation results are as shown in figure C.2.
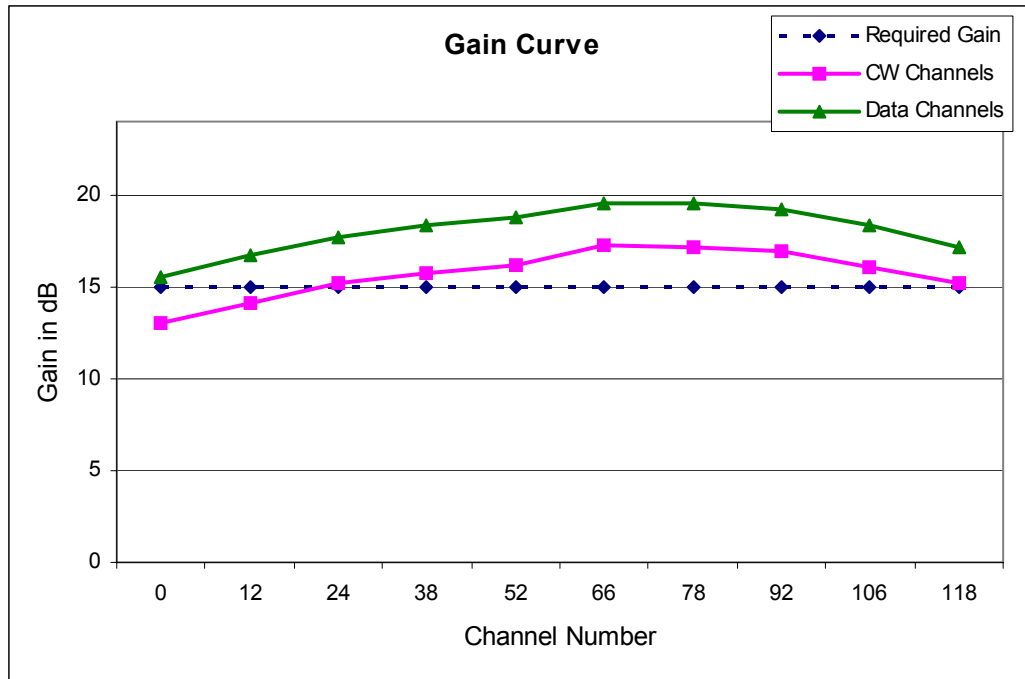
Figure C.2: Gain curves for different data inputs

In the above figure CW channels are the ones with input bits as 001111….111100 and Data channels are the ones with input bits generated randomly. The first channel at 1529.9 nm is represented as channel number 0 and channel numbers 0 – 59 represent the 60 channels in the C-band and the rest the channels in the L-band. Since the channels whose input bits are generated randomly have lower average power than the CW channels, their gain from Raman amplification would be higher and this agrees with the simulation result shown in figure C.2.

Simulations are also run using 100 km of SMF instead of Teralight Ultra fiber and using the same pump profile as above i.e. 60 mW, 60 mW, 55 mW and 55

mW at 1427 nm, 1439 nm, 1450 nm and 1485 nm wavelengths respectively. SMFs with an effective core area of 83 μm^2 are larger than the Teralight Ultra fiber and have a dispersion of 16.7 ps/nm.km and dispersion slope of 0.09 ps/nm^2.km at 1550 nm. The loss parameter of SMF is chosen same as Teralight Ultra i.e. 0.2 dB/km as the simulation is run for checking the effect of fiber core area on the gain. The DCF used has a dispersion of 104.5 ps/nm.km and dispersion slope of -1.0 ps/nm^2.km at 1550 nm. It can be predicted that since SMF has larger core area, its nonlinearities are not as pronounced as that of Teralight Ultra fiber. This would lead to lower SRS and eventually to lower gain and the simulation results agree with the above prediction. The gain curves for SMF and Teralight Ultra are as shown in figure C.3.
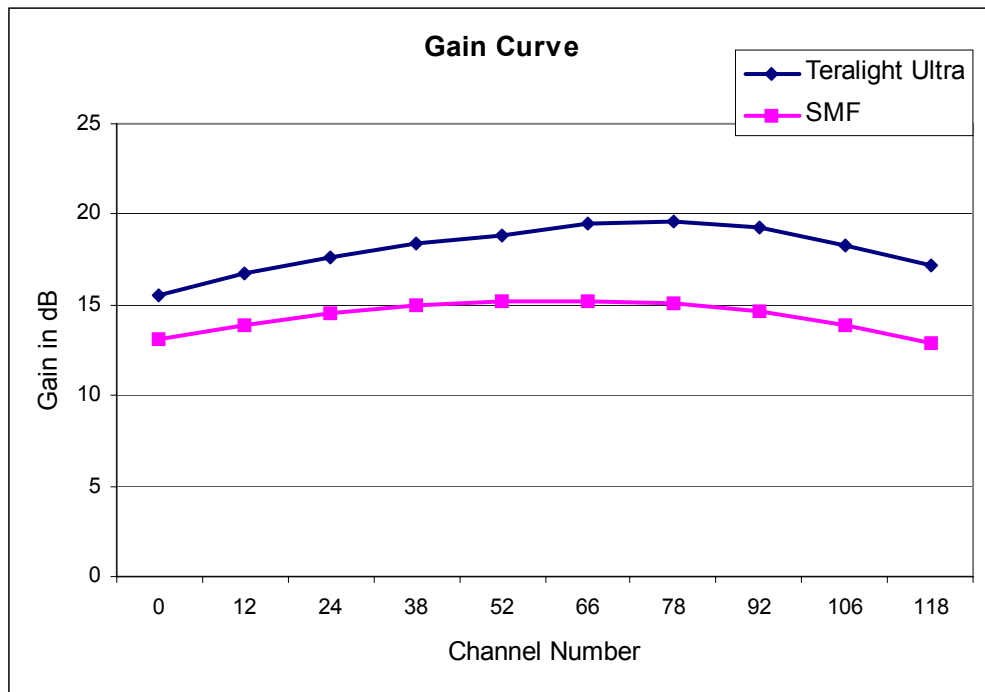

Figure C.3: Gain curves for SMF and Teralight Ultra fiber

From Table B.1 we have that for a 5 dB net loss over 100 km Teralight Ultra fiber, the equations B.1 – B.3 predict a pump power of around 112.5 mW. Since the SRS effect is maximum when the pump and signal frequency difference is around 13 THz and its effect is very low when the difference is less than 6 THz or greater than 16 THz, it can be said that in our 120 channels, 4 Raman pump system, for any given channel its gain is predominantly from the 2 adjacent pumps that are close to 13 THz from the channel. In this respect, from the simulation results for pump evaluation, any two adjacent pumps have a total power between 110mW - 120mW, which matches with the theoretical pump power of 112.5 mW.